

INSTITUTE FOR COMPUTATIONAL SCIENCE AT THE
UNIVERSITY OF ZURICH

MASTER THESIS

Direct Comparison of Satellite Formation in GI and CA disks

Author

Cassandra Inderbitzi

Supervisors

Prof. Dr. Judit Szulágyi
Prof. Dr. Aurel Schneider

October 19, 2021

Contents

1	Introduction	3
1.1	Solar System	3
1.1.1	Jupiter	3
1.1.2	Saturn	5
1.1.3	Uranus	7
1.1.4	Neptune	7
1.2	Star formation	8
1.3	Accretion & Planet formation	9
1.3.1	Dust growth	9
1.3.2	Terrestrial planets	11
1.3.3	Giant planets	16
1.4	Disk dispersion	17
1.4.1	Dispersal mechanisms and models	17
1.5	Migration	19
2	Model	22
2.1	Disk structure and evolution	22
2.1.1	Core Accretion Disk	22
2.1.2	Gravitational Instability	23
2.1.3	Evolution	23
2.2	Satellite formation and evolution	24
2.3	Migration	24
2.3.1	Type 1 Migration	24
2.3.2	Type 2 Migration	24
2.3.3	Resonant Capturing	25
2.4	Collision	25
2.5	Accretion	26
2.6	Dust depletion and refilling	26
2.7	Initial parameters	26
2.8	t-SNE algorithm	27
3	Results	29
3.1	Mass Distribution	29
3.1.1	All parameters random	29
3.1.2	One parameter set	31
3.2	Number of satellites	42
3.2.1	All Parameters random	42
3.2.2	One parameter set	42
3.3	Positions of orbit	47
3.3.1	All parameters random	47
3.3.2	One parameter set	49
3.4	Europa timescales	52
3.4.1	All parameters random	52
3.4.2	One parameter set	55
3.5	Formation temperature	58
3.5.1	All parameters random	58
3.5.2	One parameter set	60
3.6	Formation times	63
3.6.1	All parameters random	63
3.6.2	One parameter set	65
3.7	t-SNE visualization	68
4	Discussion	70

4.1	Model implications	70
4.2	Discussion Comparison	71
5	Conclusion	74
5.1	Outlook	75

1 Introduction

In the history of humanity, many people have looked to the stars for various reasons, be that due to scientific reasons (the urge to know more about the universe), spiritual or religious reasons or just purely aesthetic reasons. The earliest that we know of, the Babylonians identified the inner 6 planets as early as the second millennium BC ([Sachs 1974]) through observations done by eye. As technology advanced, so did the methods of observation. Galileo Galilei used a small telescope in the 17th century to observe the first satellites around another body than the Earth with the primary satellites of Jupiter ([Galilei 1610]), which were hence named after him. Over a century later, Frederick William Herschel observed Uranus ([Herschel 1787]) and shortly after that Giuseppe Piazzi observed Neptune ([Piazzi 1846]). It took until the beginning of the 20th century for Clyde William Tombaugh to observe Pluto ([Tombaugh 1946]).

As technology advanced even further, and allowed the study of Solar System objects via probes, the focus of observation shifted further out, until in 1992 the first exoplanet was discovered around the pulsar PSR B1257+12 ([Wolszczan 1992]). Since then we have discovered more than 3000 other exoplanets, a number which is steadily climbing, and in 2018 we discovered the first exomoon candidate ([Vanderburg et al. 2018]). It remains hard to resolve the effects of exomoons on the planets we can observe, but especially with advances in machine learning (e.g. [Teachey & Kipping 2021]), the difficulty lowers steadily.

But what defines a "planet" or even a "satellite"? The International Astronomical Union defines the objects we can observe in our Solar System as follows [IAU 2006]:

1. "A "planet" is a celestial body that (a) is in orbit around the Sun, (b) has sufficient mass for its self-gravity to overcome rigid body forces so that it assumes a hydrostatic equilibrium (nearly round) shape, and (c) has cleared the neighbourhood around its orbit."
2. "A "dwarf planet" is a celestial body that (a) is in orbit around the Sun, (b) has sufficient mass for its self-gravity to overcome rigid body forces so that it assumes a hydrostatic equilibrium (nearly round) shape, (c) has not cleared the neighbourhood around its orbit, and (d) is not a satellite."
3. "All other objects, except satellites, orbiting the Sun shall be referred to collectively as 'Small Solar-System Bodies'."
4. Satellites are then the objects that orbit not the sun but any other body in a solar system.

As per this definition there are then 8 planets (from Mercury to Neptune), a handful of dwarf planets (such as Pluto and Ceres) and a whole host of small Solar System bodies. These are however not perfect definitions: they are mostly geared toward our Solar System, which is not necessarily an "average" system, they leave satellites as a category, which in itself may at some point require further discrimination, and it categorizes Ceres and Pluto as the same bodies but neglects that Pluto and Charon, its moon, orbit a barycentre outside either body.

1.1 Solar System

1.1.1 Jupiter

Jupiter is the second largest (in both radius and mass) body in the Solar System (the sun being the biggest), where the radius is 10.97 times that of the earth and the mass is 318 times that of the earth. That makes it heavy enough that the Sun and Jupiter are orbiting around a common point (the barycentre) which lies slightly outside the Sun. It is made up almost entirely of hydrogen ($\approx 90\%$) with about 10% helium and some heavier molecules like methane, ammonia and water (in descending order of abundance). These are however not constant throughout the planet; the upper atmosphere is richer in the lighter elements (mostly hydrogen) but as one goes deeper the heavier ones take up a higher fraction.

Older models assumed either a solid core surrounded by liquid metallic hydrogen and an

atmosphere that is mostly molecular hydrogen or a progressively denser and denser fluid all the way to the core ([Smoluchowski 1971], [Guillot et al. 2004]). The Juno mission ([Bolton 2017a]) was launched with the primary goal of probing deep into Jupiter’s interior and ultimately determine whether there is a solid core or not. Its results however were surprising: Jupiter’s core is not truly either of those things. The core seems to be partially mixing with the surrounding mantle up to a almost half the radius, where heavy elements mass between 7 and 25 M_{Earth} in total ([Bolton 2017b]). The current model suggest that this diffusion happened as the result of a giant impact of a massive planetesimal with a nascent Jupiter’s solid core ([Liu et al. 2019], [Guillot 2019]). This also means that it is likely that Jupiter formed via the core accretion model (see 1.3.3) which could have implications on satellite formation and their resulting configuration.

Jupiter currently has 79 confirmed satellites ([Sheppard 2018]). They are dominated by the four so-called Galilean satellites, which make up around 99.99 % of the mass of the entire satellite system around Jupiter ([Williams 1995]). 1 shows an overview of the physical parameters.

Table 1: Physical properties of Jupiter’s major moons

Name	Mass [M_{Jup}]	Radius [km]	Semi-major axis [R_{Jup}]	Period [d]	Inclination [$^{\circ}$]
Io	$4.705 \cdot 10^{-5}$	1821.6	5.91	+1.769	0.04
Europa	$2.529 \cdot 10^{-5}$	1560.8	9.40	+3.551	0.4
Ganymede	$7.808 \cdot 10^{-5}$	2631.2	14.97	+7.155	0.18
Callisto	$5.667 \cdot 10^{-5}$	2410.3	26.33	+16.69	0.19

Io Io is the innermost Galilean satellite and slightly larger in both mass and radius than Earth’s moon. It is in a 1:2:4 resonance with Europa and Ganymede. This resonance is fundamental in shaping the characteristics of Io: it keeps its orbit, which is slightly eccentric, from becoming more circular due to tidal dissipation ([Yoder 1979]). This eccentricity, together with Jupiter’s high mass, which makes Io ovoid towards it, leads to constant internal stress as its form is constantly distorted. This process is called tidal heating and is seen as the driver of Io’s very active volcanism ([Peale, Cassenand & Reynolds 1979]) with over 400 active volcanoes, which makes it the most geologically active body in the Solar System ([Lopes et al. 2004]). Ever since the first images of Io, its impact crater density was a lot lower than expected ([Smith et al 1979]), which is a consequence of the volcanic lava flows ([Strom et al 1979]) burying the craters as they are produced. This makes Io’s surface geologically very young. According to measurements taken by the *Voyager* and *Galileo* probes, the interior seems to be completely differentiated between an iron/iron-sulfide core and a silicate rich crust, not unlike the inner system’s terrestrial planets ([Anderson et al 1996]). Later analysis of this data gives evidence for a sub-surface magma ocean ([Kerr 2010]).

Europa While being the smallest Galilean satellite, Europa is still bigger than all of the smaller satellites in the Solar System combined. Its most striking feature is its surface, which is not only smoother than any other in the Solar System ([JPL 2001]) and has a high albedo of 0.64 ([JPL 1996]), but is also crisscrossed by dark streaks. These "lineae" are thought to have been formed by eruptions of warm ice through cracks formed by tidal interaction with Jupiter. However, this would mean they would have a uniform orientation towards it, which is only true for the youngest cracks. Older ones have increasingly different orientations, a possible explanation of which is that the surface is decoupled from the interior and rotates at a different speed, which could be explained by a sub-surface ocean, and thus such an ocean was theorized in [Geissler et al. 1998], [Figueredo & Greeley 2004] and [Hurford, Sarid & Greenberg 2007]. Later, the *Galileo* team argued for it by analyzing images from both the *Galileo* and *Voyager* probes and further evidence is given by the fact that Jupiter induces a magnetic moment in Europa, which would require a heavily conductive layer within Europa (a sub-surface ocean could fulfill this requirement) ([Kivelson et al. 2000]). It is thought that, similar to Io, tidal heating allows for this ocean to remain liquid, and this theory has become scientific consensus ([Greenberg

2005]), especially after evidence was found of an expelled water plume ([Jia et al. 2018]). Europa seems to be made up of mostly silicate rocks with solid iron core, but it does contain significant amounts of water/ice (as seen in the surface and sub-surface ocean) ([Kargel et al 2000], [Bhatia & Sahijpal 2017]).

Ganymede As opposed to Io and Europa, Ganymede’s average density (50-60 % lower) seems to suggest that it is made up about equally of silicate rocks and water ices, where near-infrared spectroscopy suggests the surface is highly enriched in water ices ([Showman & Malhotra 1999], [Delitsky & Lane 1998]). Ganymede appears to be fully differentiated, with a liquid iron/iron-sulfide core surrounded by a silicate mantle with layers of liquid water and water ices on the outside (which would explain the water ice rich surface), where the precise thickness of the layers depends on certain assumptions like for example the sulfur content of the core ([Kivelson et al. 2002], [Bhatia & Sahijpal 2017], [Kuskov, Kronrod & Zhidikova 2005]). Remarkably, Ganymede is the only satellite that has a magnetic field, which is very likely generated by a liquid core, much in the same way as Earth’s magnetosphere, and the moving conductive material that comes with it ([Hauck, Aurnou & Dombard 2006]). There are some problems with this though in that Ganymede is still small enough that it should have cooled enough by now that the core would not be liquid anymore, some of which could be explained by tidal heating ([Bland, Showman & Tobie 2007]). First indications of a sub-surface ocean came with the *Galileo* probe ([Showman & Malhotra 1999]) and the theory was proposed that Ganymede had several ocean layers separated by ice phases ([Vance et al 2014]). Further evidence of this is given by the movement of the aurorae, which is different from how it should be due to the possibly salt-water ocean influencing Ganymede’s magnetic field ([Saur et al 2015]).

Callisto Callisto is very similar in composition to Ganymede, approximately 50/50 rocky material and water ice, although the surface does not seem to be as enriched in ice ([Kuskov & Kronrod 2005], [Showman & Malhotra 1999]). Its surface is remarkable in that it seems to be one of the oldest in the Solar System and thus being one of the most heavily cratered. Thus, there are no other distinctive features other than craters, which are so numerous that essentially every newly created crater erases an old one ([Zahnle, Dones & Levison 1998]). Its interior does not seem to be clearly differentiated, so that apart from a sub-surface ocean and an iron-silicate core it seems to be made up of a rock-ice mixture ([Spohn & Schubert 2003]). A possible explanation for this is that Callisto formed very slowly and thus never fully melted to allow differentiation ([Canup & Ward 2002]). Studies of how Callisto reacts to Jupiter’s magnetic field have shown that it behaves like a perfectly conducting sphere which could be explained by a thick layer of saltwater under the surface ([Zimmer, Khurana & Kivelson 2000]). This ocean does speak against an undifferentiated interior and recent studies have shown that it is more likely that the interior is more differentiated than previously thought ([Monteux et al. 2014]).

1.1.2 Saturn

Saturn is the third largest body in the Solar System and often considered a smaller Jupiter. Its mass is 95 times that of Earth and its radius 9.45 times that of Earth, which makes it the only planet that has an average density less than that of water ([Williams 1995]). Like Jupiter, it is made up by and large of molecular hydrogen, helium, methane, ammonia and water, but it is enriched in hydrogen (96% in Saturn as opposed to 90% in Jupiter). It also seems to have a higher metallicity than Jupiter, by about a factor of 2-3 ([Fletcher et al. 2009]).

The standard model for the internal structure has long been a three layered model: a dense core, a helium rich inner and a helium poor outer envelope. Core masses have been estimated to be 10-25 M_{Earth} with a total metallicity of 13-28 M_{Earth} or 0-20 M_{Earth} with a total metallicity of 20-30 M_{Earth} ([Saumon & Guillot 2004]). However, recent studies on Saturn’s rings have shown unexplained waves in certain regions of the rings (e.g. [French et al. 2019], [Hedman, Nicholson & French 2019]), which can be used to seismically study the interior (e.g [Fuller 2014], [Mankovich et al. 2019]). Having done exactly that, ([Mankovich & Fuller 2021]) predict a much more diffuse

core, although whether that is due to how it originally accreted, an impact on a dense core or erosion of one such is an open question, although it does support recent models on core-accretion ([Ormel, Vazan & Brouwers 2021]).

Saturn’s most striking feature are its rings. They have a distinct band-like structures and can loosely be grouped into the ”main rings”, which extent to about 140’000 km from Saturn’s center, which mainly consists of particles in the range of 1 *cm* to 1 *m* ([Zebker et al 1985]), and the ”dusty ring” which extend all the way up to Titan and consist mostly of particles in the μm range. There is not enough data on the rings to get a definitive read on their mass, but the data from the *Voyager 11* probe gives an upper value of about $10^{-6} M_{\text{Saturn}}$ ([Null et al. 1981]), while models based on density waves in the rings give a lower limit of about $10^{-8} M_{\text{Saturn}}$ ([Esposito, O’Callaghan & West 1983]). Both regions consist mainly of water ice ([Nicholson et al. 2008]). Their origin is equally uncertain ([Charnoz et al 2009b]):

1. Remnants of the CPD: [Pollack et al 1976] theorized the rings might be leftover material from the CPD within which the satellites formed, which would explain why they are in the same plane as them. However, how this material could survive past the dispersion of the CPD without falling into the planet is unclear and the fact that it is made up almost solely of water ice whereas the disk has a definite silicate component speaks against it as well.
2. A destroyed satellite: As the mass of the rings roughly equals one of Saturn’s smaller moons, the theory has been proposed that the rings once were a satellite that, due to type 1 migration (section 2.3), migrated into the Roche zone (the zone where tidal forces would destroy it). There, it would have needed to be destroyed by an impactor, to explain the small size of the particles, which has been shown to be possible to happen ([Charnoz et al. 2009a]), although that would still mean that there should be silicates in them.
3. Tidally split comet: [Dones, Agnor & Asphaug 2007] proposed that a comet could have been destroyed by tidal forces due to a close pass. This could explain that the rings are mainly water ice if the comet’s composition was like that. It has the problem that a comet of necessary size passing this close to Saturn would be a very rare occurrence ([Charnoz et al. 2009a]).

Saturn has currently 82 confirmed satellites, making it the planet with the most moons ([Sheppard 2019]), which are heavily dominated by Titan that is almost two orders of magnitude bigger than the next smaller one.

Table 2: Physical properties of Saturn’s major moons

Name	Mass [M_{Sat}]	Radius [<i>km</i>]	Semi-major axis [R_{Sat}]	Period [<i>d</i>]	Inclination [$^{\circ}$]
Mimas	$7.03 \cdot 10^{-8}$	198	3.08	+0.94	1.53
Enceladus	$1.94 \cdot 10^{-7}$	252	3.95	+1.37	0.00
Thetys	$1.09 \cdot 10^{-6}$	531	4.89	+1.89	1.86
Dione	$1.94 \cdot 10^{-6}$	561.5	6.26	+2.74	0.02
Rhea	$4.05 \cdot 10^{-6}$	763	8.75	+4.51	0.35
Titan	$2.38 \cdot 10^{-4}$	2575	20.27	+15.95	0.33
Iapetus	$3.17 \cdot 10^{-6}$	735	59.10	+79.33	14.72

Enceladus Enceladus is one of Titan’s smaller moons orbiting within the outermost ring structure, the so called E-ring. The *Voyager* program’s original mass estimates suggested it was made up mostly of water ice, however *Cassini* later measure its gravity and showed that the density is too high for that, so it has an appreciable amount of silicates and iron in it ([Rothery 1999], [Brown et al. 2006]). Its very reflective surface coupled with a low amount of impact craters suggests that it could have had a relatively active ”water volcanism” recently ([Thompson 2017]). This is supported by the fact that *Cassini* observed a plume of icy particles ([Porco et al. 2006]) and even flew through them ([Perry et al. 2016]), which means there are active

cryovolcanoes on Enceladus, which are also thought to sustain the E-ring ([Porco et al. 2006]). Further, this makes Enceladus the only confirmed body (other than Earth) to contain (at least pockets) of liquid water. Gravimetric data from *Cassini* also suggests that there is a sub-surface ocean on Enceladus ([Iess et al 2014]) and that the icy crust is fully detached from the rocky core ([Thomas et al 2016]), which would explain some of the tectonic features its surface shows.

Titan Titan is by far the largest of Saturn’s satellites and is likely differentiated into a rocky core surrounded by ice layers, a subsurface ocean of ammonium rich liquid water (where the ammonium would raise the freezing point enough for it to remain liquid) and an icy crust ([Brown et al. 2009], [Tobie et al. 2005]). Evidence for a sub-surface ocean includes observation of shifting surface features (which hints at a decoupled surface) ([Lorentz et al 2008]) and variation of its gravitational field as it orbits ([Iess et al 2012]). Its most remarkable feature is the existence of liquids on its surface. Hydrocarbon lakes have long been theorized to exist and were finally confirmed by the *Cassini – Huygens* mission ([Stofan et al 2007]), making it the only body in the Solar System (except Earth) that contains liquids on its surface, albeit not water but hydrocarbons. It has been theorized that these lakes may be possible locations for life to exist ([Fortes 2000]).

1.1.3 Uranus

Uranus is one of the two so-called "ice giants" in the Solar system. While they have an appreciable gas envelope similar to Jupiter/Saturn, its mass is dominated by ices, hence the name. The standard model of Uranus gives it a small silicate/iron core of about $0.55 M_{\text{Earth}}$, an ice mantle of about $13.4 M_{\text{Earth}}$ (which is the bulk of the mass) and a hydrogen/helium gas envelope of about $0.5 M_{\text{Earth}}$, where the fraction is roughly 85/15 % ([Faure & Mensing 2007], [Herbert et al 1987]).

Uranus has the highest axial tilt in the Solar System with 97.77 degrees, its rotation axis almost lining up with the orbital plane. The most popular theory for this tilt is a giant impact that knocked Uranus on its side ([Bergstrahl, Miner & Matthews 1991]), but there are theories that could help the original CPD tilt, if not necessarily to the current degree ([Millholland & Batygin 2019]). [Woo et al. 2021] suggest a model for the formation of the satellites system due to a giant impact, which would explain both the tilt and the fact that the satellite orbits show the same tilt as Uranus.

Table 3: Physical properties of Urnaus’ major moons

Name	Mass [M_{Ur}]	Radius [km]	Semi-major axis [R_{Ur}]	Period [d]	Inclination [$^{\circ}$]
Miranda	$7.60 \cdot 10^{-7}$	236	5.82	+1.41	4.34
Ariel	$1.49 \cdot 10^{-5}$	579	37.47	+2.52	0.04
Umbriel	$1.40 \cdot 10^{-5}$	584.7	10.41	+4.14	0.13
Titania	$3.94 \cdot 10^{-5}$	788.9	17.07	+8.71	0.08
Oberon	$3.31 \cdot 10^{-5}$	761.4	22.83	+13.46	0.07

1.1.4 Neptune

Neptune is slightly smaller than Uranus with a similar tilt as the other planets. Its composition is very similar as well, a silicate/iron core (roughly 5-10 % of the mass), a hydrogen/helium atmosphere (also roughly 5-10% of the mass, about an 80/20 % split) and an icy mantle making up the bulk of the mass ([Hubbard 1997]). Neptune’s most remarkable feature is that it boasts the only major satellite in a retrograde orbit, Triton.

Triton While there are satellites in a retrograde orbit around the other gas giants too, all of them are very small and on large orbits. Triton on the other hand is one of the seven largest moons in absolute terms and the second largest relative to its host. It likely has a core of

Table 4: Physical properties of Neptune’s major moons

Name	Mass [M_{Nep}]	Radius [km]	Semi-major axis [R_{Nep}]	Period [d]	Inclination [$^{\circ}$]
Triton	$2.09 \cdot 10^{-4}$	1,353.4	14.33	-5.88	157.345

silicate/iron, which makes up around 2/3 of its mass and an icy mantle and crust making up the rest of the mass ([McKinnon & Kirk 2014]). As it orbits retrograde, it cannot have formed in a CPD around the planet. As such, the leading theory is that it is a captured object from the Kuiper belt ([Agnor & Hamilton 2006]), which is substantiated by the similarity in size and composition to Pluto ([Cruikshank 2004], [McKinnon & Kirk 2014]).

1.2 Star formation

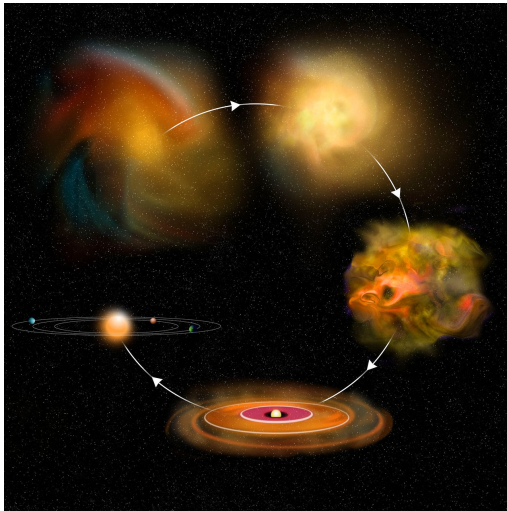


Figure 1: Schematic of the process of star formation: A big molecular cloud, mainly made up of hydrogen and helium, starts to contract under gravity and due to radiative cooling. As it contracts, some regions may become gravitationally unstable on collapse even faster, forming proto-stars. Due to rotation, angular momentum conservation and vertical settling a disk, which is commonly called a CSD (circumstellar disk), will form around the nascent star. Parts of this disk will be accreted onto the star, while other parts will be ejected due to mechanisms such as photoevaporation and the heavier elements will form into planetesimals and eventually planets. The disk will slowly disperse until only the formed star and any potential planets are left over. Credit: [Saxton 2016], taken from ESO Supernova

Stellar formation is a product of the lifecycle of molecular clouds. Those are large, turbulent structures, comprised mostly of Hydrogen and Helium ([Draine 2010]), which form out of the gas and dust that makes up interstellar space. They have typical extents of about 10 to 50 pc and masses of around 10^2 to 10^6 solar masses and have a very turbulent structure ([Miville-Deschênes, Murray & Lee 2017]). They are not homogeneous, so parts of the clouds are hotter than others or less dense than others or even more ionized than others. As this cloud cools and contracts it will eventually fragment into smaller pieces, the resulting masses and sizes of these clumps are the result of processes like gravitational instability, rotation, magnetic fields and turbulence. As in principle many such regions can undergo this fragmentation process (and in fact the clumps themselves might fragment further), many stars will form in groups rather than isolated (which we see in our galaxy in say the Pillars of Creation or the Taurus cluster) ([Lada & Lada 2003], [Bressert et al. 2010], [Kruijssen 2012]), so called star forming clusters. This gravitational instability only really sets the seed of a star, its mass will be much more influenced by the surrounding material it can accrete. For high-mass stars there are two general models that can be seen in numerical simulations: As star clusters form, some of the infalling gas can fragment

further, which will lead to these newly formed stars accreting material that then cannot reach the inner stars, leaving them starved of material. This is the so-called fragmentation induced starvation model (e.g. [Longmore et al. 2014], [Krumholz, Mckee & Bland 2019], [Ward, Kruijssen & Rix 2020]). On the flip side of this is the competitive accretion model ([Bonnell et al. 2001]), in which case the gas is funneled to the center of the cluster by gravity and thus favourably accreted by stars in the center. Whichever model is applicable depends on numerous processes, like the precise gas flow and distribution or turbulence, but also on feedback due to the formation of (proto-)stars and stellar activity. Among those feedback processes are:

1. Proto-stellar outflows: the accretion of mass onto a proto-star also results in mass being ejected via magnetic fields which are wound up by rotating gas. This outflow influences how efficient star formation in a molecular cloud is (e.g. [Federrath et al. 2014], [Tanaka, Tan & Zhang 2017]), it drives turbulence both locally and globally (e.g. [Hansen et al. 2012], [Offner & Chaban 2017]) and is a way to transport momentum ([Bai et al. 2016])
2. Radiation: Accretion leads to the conversion of gas kinetic energy to heat, namely by accretion shocks, which will be radiated away. Proto-stars also heat up as they contract towards the main sequence, given by both liberation of gravitational energy as well as other internal processes. High mass proto-stars may also start the fusion process while still heavily accreting, which in itself will also emit radiation. All this radiation combined will heat up the surrounding gas and, if strong enough, can also drive some dynamics via radiation pressure or even ionization.
3. Stellar winds: Mass can also be ejected from the star by gas pressure, radiation pressure (for high mass stars) or magnetic fields.

By and large molecular clouds will disperse on timescales of 10-30 Myr (e.g. [Kruijssen et al. 2019], [Chevance et al. 2020]). As this cloud collapses, it will inevitably (due to the angular momentum that it has) start to rotate around a common axis, upon which, due to a combination of vertical settling due to gravity, as the gas pressure gradient in this direction would be much smaller than in the radial direction, and thermal escape the whole cloud will collapse towards a disk shape. This is then called a circumstellar disk or CSD for short, in which eventually planets will form.

1.3 Accretion & Planet formation

1.3.1 Dust growth

In CSDs, the components that eventually become planets starts out as sub-micron particles, called "dust" and so they have to grow around 12 orders of magnitude at the very least, and have to do so fast enough that gas giants have enough time to accumulate a gas envelope (see section 1.3.3). As dust particles are not supported by a pressure like the gas is, they are modeled as starting on Keplerian orbits and being subjected to a gas drag. This drag force together with gravity and any turbulence will determine the dust particle dynamics and how they grow, because the basic assumption is that particles grow by colliding with other particles, so the dynamics will have a huge influence on growth rates.

As the dust is not supported by a pressure, gravity works towards settling the dust particles in the mid plane. This is beneficial to dust growth, because it increases the dust density, which should lead to easier growth. Assuming at first that there is no turbulence, the timescale on which dust settles can be approximated by calculating a settling velocity. This is simply given by the terminal velocity, which we can get by equating gas drag and gravitational force (in the vertical direction, which we can assume as the dust is small enough to be well coupled), which results in a settling timescale

$$t_{\text{settle}} = \frac{2}{\pi} \frac{\Sigma}{\Omega_K \rho_d r_d} \quad (1)$$

where r_d is the particle radius, z is the height above the mid-plane, h is a scale height and assuming a gas density profile $\rho(z) = \frac{\Sigma}{h\sqrt{2\pi}}e^{-z^2/2h^2}$. This usually leads to settling timescales much lower than disk lifetimes.

Assuming a disk is turbulent (and as explained in section 1.4 we need turbulence to explain the dispersion timescales we observe) this will lead to a diffusion of the dust working against the settling on a timescale

$$t_{\text{diff}} = \frac{z^2}{\nu} \quad (2)$$

where ν is an effective diffusion coefficient used to model the turbulence as a "viscosity" (see also section 1.4). If we use the alpha-viscosity model, it becomes apparent that only the settling timescale scales with particle radius (and thus mass!). This means that while small particles are diffused through much of the gas disk, bigger particles will still be able to settle comfortably. This diffusion itself will also help particles settle faster, because it produces a reservoir of mass that can coagulate onto the bigger, settling particles and will thus speed up their settling by increasing their mass.

So while vertical settling works in favour of growth rate by increasing dust density towards the mid-plane, gravity will also cause radial drift. As the dust is not supported by a pressure, the drag a particle experiences from the gas will gradually decrease its orbit until it gets lost in the star. Small particles will be well coupled to the gas and such a drift will be very low. However, as particles grow this coupling weakens and inwards motion will begin to be much more significant, up until the "particle" in question is big enough that gas drag becomes negligible (at that point type 1 migration will start to become important, see section 1.5).

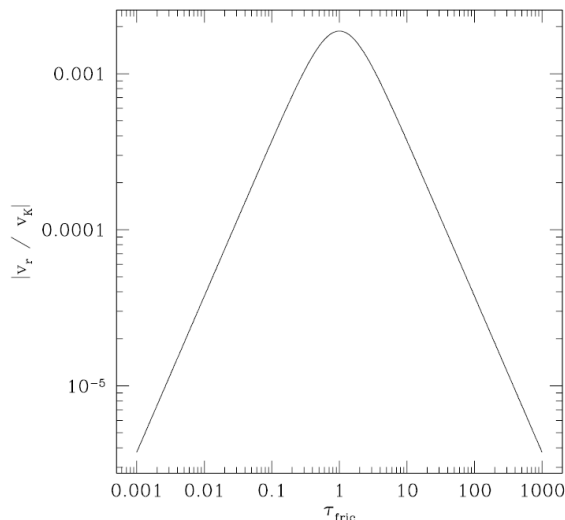


Figure 2: This plot shows the radial velocity of dust particles of varying sizes (parametrised in the friction timescale) in a protoplanetary disk with an scale height $h/r = 0.05$. At around 1 AU the peak velocity (which will always be where $\tau_{\text{fric}} = 1$) is attained by cm to m sized particles and it means that these particles will spiral inwards onto the star in as few as 100 yrs. This clearly demonstrates the radial drift problem. (Graphic is taken from Armitage [Armitage 2017])

[Armitage 2017] did the calculations (see fig. 2), which shows that particles drift the fastest in the 10 cm to a few m range and do get lost due to this drift very fast, in the order of 100 yrs. This is a huge problem, because that means that \approx m sized is a barrier that cannot be overcome and obviously planets are much larger than that. So there has to be some mechanisms to allow for planetesimals to form, be that either fast enough accretion past this barrier so that gas drag

becomes less relevant or some sort of pressure bump that is steep enough to trap even bigger objects in it.

[Weidenschilling 1980] and [Windmark et al. 2012] also predicted another problem with growth based on pairwise collisions: in the inner system of a disk, inspiraling particles will reach very high velocities (in itself a problem because they get lost fast) and as a result, collisions between particles can easily reach velocities of several meters per second, which for sizes larger than \approx mm will lead to anywhere between bouncing and fragmentation, which means that they can not really grow past that size anymore. fig. 3 shows that, at 3 AU in a minimum mass Solar nebula (MMSN) model, particles will have a very hard time growing past at most mm size.

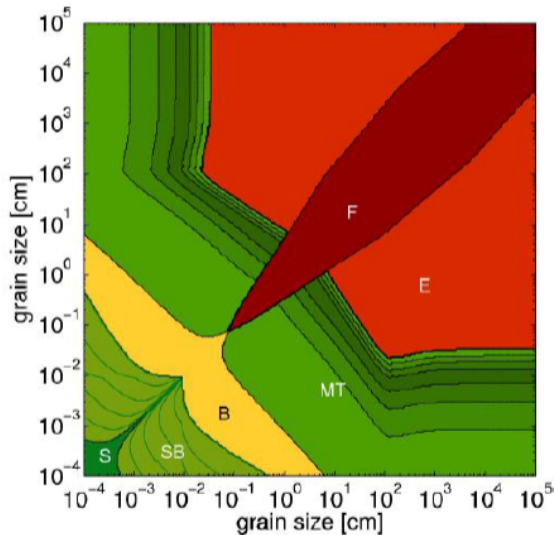


Figure 3: This graphic shows the outcome of collisions between two particles of varying sizes (as seen on the 2 axes). The green regions denote collisions that end in growth (where S means sticking, SB means stick and bounce and MT means mass transfer), the red regions denote loss (where E means erosion and F means fragmentation) and the yellow region denotes neither of the two (so particles bounce off of each other, hence B for bounce). This graphic shows that growth beyond \approx cm just by collision is very hard, which is called the fragmentation barrier. The values were computed in an MMSN at 3 AU. (Graphic is taken from [Windmark et al. 2012])

This problem is less important in the outer disk due to lower relative velocities as well as the presence of ice, which has a sticking effect, however [Birnstiel, Fang & Johansen 2016] showed that even then growth past cm size remains hard. A possible way to solve this would be that if collisions create porous instead of compact particles. [Okuzumi et al. 2012] argued that such particle could absorb the collisional energy much better, making them more resistant to breaking and in addition, their low density would also mean they wouldn't migrate as fast. As they grow bigger, gravity would eventually lead to them becoming more compact and thus build more classical planetesimals. However, this has also the problem that it can only really work in the outer parts, where ice allows such porous structures to form and meteorite data shows that asteroids are mainly made of of chondrules, that is particles the size between microns and mm.

1.3.2 Terrestrial planets

The Goldreich-Ward mechanism As opposed to growth just by pairwise collisions, an alternate hypothesis is that vertical settling creates a dust sub-disk, which could gravitationally fragment if it becomes dense enough, which is called the Goldreich-Ward mechanism ([Goldreich & Ward 1973]). This is an attractive model because it could allow for planetesimals (bodies in the \approx km range) to form fast enough to bypass the radial drift vulnerability.

Consider a very flat, uniformly rotating fluid sheet with a constant surface density Σ_0 and an

angular velocity $\vec{\Omega} = \Omega \hat{z}$. In a co-rotating frame we can write the fluid equations as

$$\frac{\partial \Sigma}{\partial t} + \nabla(\Sigma \vec{v}) = 0 \quad (3)$$

$$\frac{\partial \vec{v}}{\partial t} + (\vec{v} \nabla) \vec{v} = -\frac{\nabla p}{\Sigma} - \nabla \Phi - 2\vec{\Omega} \times \vec{v} + \Omega^2(\vec{x} + \vec{y}) \quad (4)$$

$$\nabla^2 \Phi = 4\pi G \Sigma \delta(z) \quad (5)$$

where \vec{v} is the velocity in the rotating frame, Σ is the surface density and the pressure $p = p(\Sigma)$ depends on surface density. On these one can apply perturbation theory and retain only the linear terms, which gives the equations (while defining $c_s^2 = \frac{dp}{d\Sigma}$ at $\Sigma = \Sigma_0$)

$$\frac{\partial \Sigma_1}{\partial t} + \Sigma_0 \nabla v_1 = 0 \quad (6)$$

$$\frac{\partial \vec{v}}{\partial t} = -\frac{c_s^2}{\Sigma_0} \nabla \Sigma_1 - \nabla \Phi_1 - 2\vec{\Omega} \times \vec{v}_1 \quad (7)$$

$$\nabla^2 \Phi_1 = 4\pi G \Sigma_1 \delta(z) \quad (8)$$

where the subscript 0 stands for the unperturbed values and 1 are the 1st order perturbation terms. As we disregard higher order terms than linear, this can be decomposed into Fourier modes and we can write

$$\Sigma_1(x, y, t) = \Sigma_a e^{i(kx - \omega t)} \quad (9)$$

$$\vec{v}_1 = (v_{a,x} \hat{x} + v_{a,y} \hat{y}) e^{i(kx - \omega t)} \quad (10)$$

$$\Phi_1 = \Phi_a e^{i(kx - \omega t)} \quad (11)$$

where \vec{k} is a wavevector parallel to \hat{x} , the subscript a applies to normalization values and the perturbation in Φ only apply to the mid-plane. One can recognize that Φ and Σ are connected to simplify the system and upon entering the above solutions into the fluid equations, one ends up with a series of purely algebraic equations. These can be used to get the dispersion relation, which is a formula for the growth rate ω

$$\omega^2 = c_s^2 k^2 - 2\pi G \Sigma_0 |k| + 4\Omega^2 \quad (12)$$

As we are interested to find out the criteria for when the disk fragments, we are interested in the unstable modes $\omega^2 < 0$, as then ω is imaginary and the perturbations grow exponentially and the most unstable mode can be found to be $k_{\text{crit}} = \frac{\pi G \Sigma_0}{c_s^2}$. This result is very specific to the thin disk assumed here and one can extend this to disks with other properties (such as e.g. differential rotation), but in general one can define a parameter to judge stability, the so called Toomre Q :

$$Q = \frac{c_s^2 \Omega}{\pi G \Sigma} \quad (13)$$

The precise critical Q values when instability occurs is dependent on the exact situation, but in general $Q_{\text{crit}} \simeq 1$ is a good general value. This calculation is for a thin fluid disk, but a dust disk can be approximated by a collisionless disk and the results mostly carry over if one replaces c_s with σ , the 1D velocity dispersion. Using this, one can estimate the time it would take for the dust disk to fragment into planetesimals and [Goldreich & Ward 1973] estimated that it could be as short as 10^3 years.

However, if one works out how thin a dust disk has to be for this process to set in, it becomes apparent that it is extremely unlikely for this to happen. Even in a totally non-turbulent disk,

the process of settling the dust to the mid-plane would in itself induce enough turbulence to work against fragmentation. So while the rapidity of this process is very alluring as an origin to \approx km sized objects, it has very little chance of working the way it does.

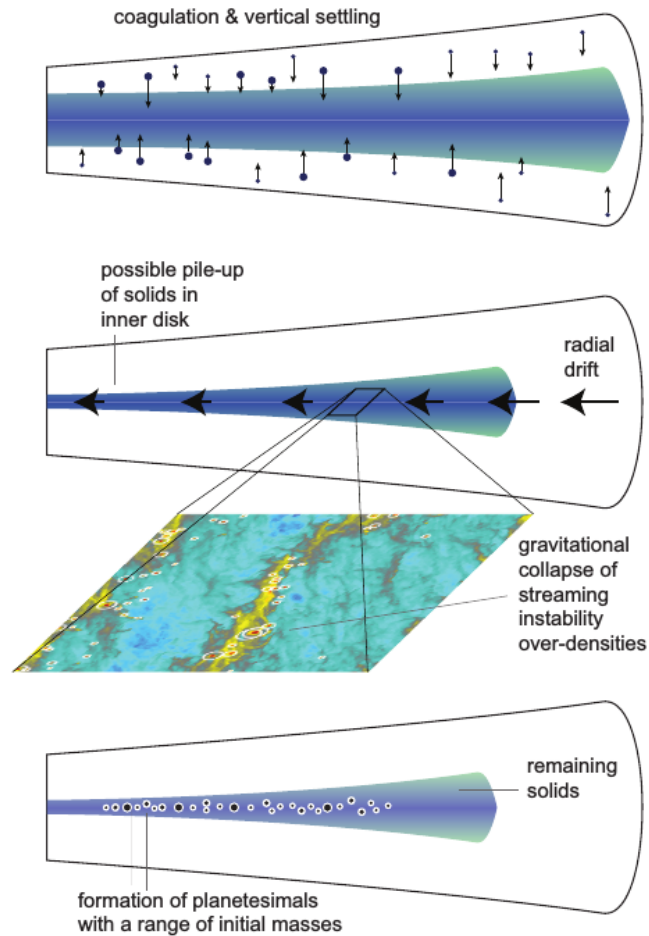


Figure 4: This graphic shows schematically how the streaming instability works. At first the dust will settle towards the mid-plane due to gravity and simultaneously drift inwards. Any of the processes called "streaming instabilities" lead to under- and overdense regions in the plane and if the overdense regions have a high enough dust-to-gas ratio, they then gravitationally collapse, forming planetesimals of a varying mass. The Goldreich-Ward mechanism works very similar, although the collapse happens as a result of a very dense dust subdisk. (Graphic is taken from [Armitage 2017])

Streaming Instabilities While settling alone may not be able to make a dust disk fragment, there are other processes that would enhance the dust-to-gas ratio around the mid-plane enough for fragmentation to occur, which are usually grouped under "streaming instabilities". The original theory by [Youdin & Goodman 2005] looked at a vertically unstratified system of 2 gases, one compressible and the other incompressible (the particle "fluid"), that interact via two-way aerodynamic forces. This turns out to be linearly unstable for a wide range of parameters and can create dense clumps of particles, which can then collapse gravitationally to form planetesimals ([Johansen et al. 2007]). [Carrera et al. 2017] and [Yang, Johansen & Carrera 2016] showed that even if non-linear evolution is considered it would lead to strong clumping of particles in certain areas and simulations by [Johansen et al. 2015] and [Simon et al 2016] showed that this can produce a wide variety of planetesimals, where most of the resulting mass is carried in bodies the size of about 100 km, which is a prominent size in for both asteroids and Kuiper-belt objects, and on very fast time scales (see also fig. 5).

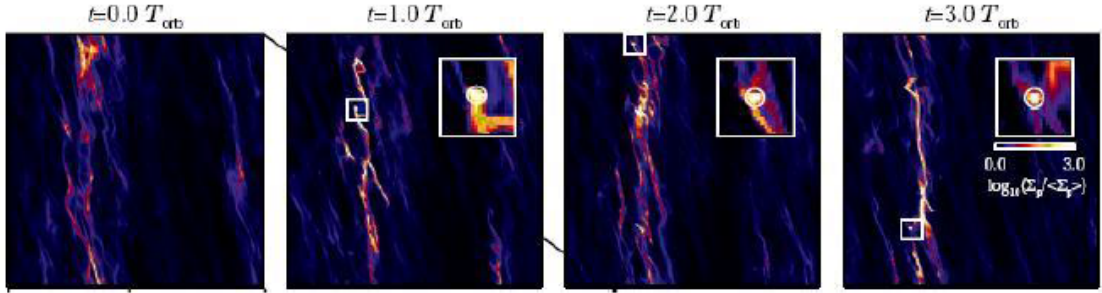


Figure 5: This figure shows the progression of clumping due to streaming instability. The x and y axes show radial and azimuthal coordinates and the colors show the density of solids, where darker colors are less dense and brighter colors are denser and the time progression is from left to right with times stated on top of the panels. The box follows the most massive self-gravitation clump of solids and eventually it reaches a mass higher than that of Ceres. (Graphic is taken from [Johansen et al. 2007])

Although this process happens most optimally for concentrations of at least dm size particles, [Yang, Johansen & Carrera 2016] have shown that chondrules, which are ubiquitous in a CPD, can trigger a streaming instability, but only if the disk has a dust-to-gas ratio of around 4%, although simulations with a higher resolution might lower this threshold.

Other processes which are generally considered to be streaming instabilities are local pressure maxima in zonal flows (e.g. [Simon & Armitage 2014]) or vortices ([Bargel & Sommeria 1995]) or the enhancement of dust-to-gas ratio via loss of gas through dispersion and subsequent formation of an inner hole in the disk ([Throop & Bally 2005], [Alexander & Armitage 2007]).

A current model also suggests that there are regions in a CPD (around the snowline ([Ida & Guillot 2016],[Schoonenberg & Ormel 2017]) and around 1 AU ([Drazkowska, Alibert & Moore 2016])) where radial drift is slowest and leads to a pile up in particles, which leads to a local enhancement in dust-to-gas ratio and could lead to streaming instabilities, while in the rest of the disk the conditions are only met once gas dispersion has enhanced the dust-to-gas ratio globally (assuming particles remain abundant as well). This would also fit observational evidence from the Solar System, where we find both very old meteorites (formed within the first few 10^5 yrs, presumably in such a pile-up location) and somewhat younger meteorites (formed \approx Myrs later, which would then have been formed in the disk at large).

Growth of planetesimals Planetesimals (which are usually defined as being large enough objects that gas drag is not a significant influence on migration) then continue to grow via two processes: direct planetesimal-planetesimal collisions and pebble accretion.

For bodies this size, gravity significantly enhances the collisional cross-section, which can be parametrised by a so-called focusing factor

$$F_g = 1 + \frac{v_{\text{esc}}^2}{v_{\text{rel}}^2} \quad (14)$$

Assuming density is independent of mass, one can then approximate the growth rate of a body as

$$\frac{dM}{dt} \simeq M^{2/3} F_g \quad (15)$$

So if we assume two bodies, with escape velocities v_{esc} much larger than their relative velocities v_{rel} with respect to the population of planetesimals, this means that $F_g \simeq 1$ and thus

$$\frac{dM}{dt} \simeq \frac{M^{4/3}}{v_{\text{rel}}^2} \quad (16)$$

This will then lead to the mass ratio between two bodies to grow with time, that is small differences among the masses of planetesimals will increase exponentially, which is called *runaway growth* ([Greenberg et al. 1978],[Wetherill & Stewart 1989]). This holds so long as $v_{\text{esc}} \gg v_{\text{rel}}$, but the velocity dispersion of planetesimals is largely influenced by the most massive bodies, as near-misses tend to set the relative velocity of the smaller body to be the escape velocity of the larger one (upon the next return). Thus runaway growth only happens for a certain amount of time, until the mass ratios reach roughly unity. There are processes that would allow for such conditions to hold for a more extended amount of time; for example gas drag tends to circularize orbits, which helps reduce relative velocities. Moreover, this is much more efficient if the bulk of solids is in small planetesimals and as seen above, streaming instability would concentrate the mass in bigger ones, leading to a very short runaway growth period.

Once relative velocities and escape velocities become of the same order, the focusing factor becomes roughly unity and the planetesimals enter a phase of *oligarchic growth* ([Kokubo & Ida 1998],[Kokubo & Ida 2000]). Now, the change in relative masses becomes negative and is of a form where it reaches zero once mass ratios are around unity. This holds for large masses, as large relative velocities prevents the small ones to accrete on each other, so they only contribute to the growth of the larger ones, leading to the concentration of dust mass onto a few satellites (called the *oligarchs*), which are embedded into a population of smaller planetesimals.

For Terrestrial planets, numerical simulations have shown that it is very likely that the inner system was populated by a number of roughly Mars sized protoplanets, which is supported by some observations, e.g

1. Earth's moon was very likely created due to a Mars-sized body impacting on the early Earth (see [Canup 2014] for a review on several models)
2. Mercury has a higher iron/silicate fraction compared to the other inner planets, suggesting some of its mass was stripped by giant impact(s). If one assumes a regular fraction, it would also be roughly Mars sized.

If one assumes now that such a population of Mars sized bodies exists after the gas has dispersed, direct gravitational interaction leads to unstable orbits for all of them and they enter a period of chaotic orbits, leading to a high possibility of giant impacts and the eventual formation of Earth (on time-scales consistent with geological records) and Venus. For Mars to remain its size, the region around its current orbit had to have been depleted of solids ([Hansen 2009], which could be explained by the migration pattern of Jupiter ([Walsh et al. 2011]) or the possibility of streaming instability only operating within ≈ 1 AU ([Drazkowska, Alibert & Moore 2016]).

This alone has a hard time explaining why in the Solar System the outer planets are much more massive than the inner ones (where the difference between the proto-planets would have to have been 2-3 orders of magnitude, so that the outer ones could be able to accrete a significant amount of gas and formed the gas giants). Dynamical times alone are much higher due to the larger orbits and on top of that, in the outer regions, protoplanets of around 1 Earth mass tend to scatter planetesimals away rather than accrete them.

To remedy this, the pebble accretion model has been suggested ([Ormel & Klahr 2010], [Lambrechts & Johansen 2012],[Lambrechts & Johansen 2014]). It says that after formation, a planetesimal remains embedded in a disk that contains *pebbles* (self-gravitating clumps of small particles) and that it can grow significantly by accreting such pebbles. In planetesimal-pebble encounters, the focusing factor can be much larger, because any deflection increases the gas drag a pebble experiences, which bends the trajectory even further. On top of that, pebbles drift inwards faster than planetesimals do, so it is much more unlikely for a planetesimal to clear its environment of pebbles, as there is a continuous replenishment from the outer regions.

[Lambrechts & Johansen 2012] and [Lambrechts & Johansen 2014] have shown that pebble accretion can indeed build up protoplanets in the outer regions to become big enough to accrete a gas envelope. Past the snowline, this process is also much more effective as there is ice there which increases the general size of the pebbles.

1.3.3 Giant planets

There are two leading models on how giant planets (such as Jupiter, Saturn and possibly Neptune and Uranus) form:

Core accretion model The classical core accretion model works as an extension of terrestrial planet formation ([Bodenheimer & Pollack 1986], [Mizuno 1980], [Pollack et al 1996]): a core consisting of rock and/or ice forms through processes outlined above. It will initially not be able to hold a significant gas envelope, but if it can continuously grow past a couple of Earth masses, eventually a gas envelope will form. This envelope will be in a hydrostatic equilibrium while the core continues to accrete planetesimals and pebbles (if this happens outside of the snowline, the ice will help this process as it is generally stickier than just the rocky material) until a certain critical mass is reached. At this point, the envelope loses the equilibrium and starts to Kelvin-Helmholtz contract, which will jump start a runaway accretion phase. This phase will end if either the planet can open a gap in the disk (see section 1.5), which will slow down growth considerably, or until the disk completely disperses (see section 1.4).

This model has some open questions that one has to be aware of:

1. Opacity: [Hubickyj, Bodenheimer & Lissauer 2005] and [Movshovitz et al 2010] have done numerous models with varying values and ways to compute gas opacity and found that this can influence the growth rate significantly.
2. Planetesimal versus pebble accretion: Often in planetary creation models the cores which eventually become giant planets grow mainly through accreting planetesimals, but it has been shown (e.g. [Lambrechts & Johansen 2012], [Ormel & Klahr 2010]) that pebble accretion plays at least an equal if not bigger role to core growth. It has also been shown that the size of planetesimals determines how important they are to core growth ([Schäfer, Yang & Johansen 2017], [Simon et al 2016]), where smaller ones are more and bigger ones are less important.
3. Migration: section 1.5 shows the theory behind migration of bodies in a disk. This has huge implications for core-accretion models, because it means that the core, which eventually grows into the planet, is very susceptible to inward migration. That means the whole process has to happen fast enough so that the core doesn't migrate into the star and even fast enough that the core is far enough away to be able to accrete all the gas it needs (as the closer it is to the star the smaller its accretion radius becomes).

Gravitational instability As already discussed in section 1.2, a gas cloud or a portion of a gas cloud can be massive and/or cold enough to be unstable and collapse in on itself ([Cameron 1978], [Kuiper 1951]). One criterion, which is mostly applied to molecular clouds/star formation, is the Jeans criterion, which puts gas pressure against gravitation: it essentially says that a cloud of radius R collapses if the time it takes for a sound wave to cross it $t_{\text{sound}} = \frac{R}{c_s}$ (c_s being the speed of sound) is bigger than the free-fall time (the time it takes for a system to collapse under gravity and no other forces) $t_{\text{ff}} = \frac{1}{(G\rho)^{1/2}}$ and thus one can say that a cloud collapses if its radius is bigger than the Jeans length:

$$\lambda_J = \frac{c_s}{(G\rho)^{1/2}} \quad (17)$$

This is for stationary clouds and for a gas giant, which would be created in a disk, the Toomre Q parameter is a much better parameter to estimate this. Usually the criterion is

$$Q = \frac{c_s \Omega}{\pi G \Sigma} < 1 \quad (18)$$

where 1 is the critical Toomre Q for small, axisymmetric disturbances specifically. This can be, as a general threshold, applied to many disks. However, it has been shown that for $Q < 1.7$ ([Durisen et al. 2006]) spiral arms can form, which are high density waves (see also fig. 6), that can fragment into clumps if they either cool very fast or experience a high infall of gas (usually around $Q < 1.4$ ([Nelson et al. 1998])). For a planet to be formed like this, a clump has to collapse fast enough to not be torn apart by disk shear and eventually can form a gas giant on a timescale of 10^4 to 10^5 years, which would be fast enough for it to not migrate into the star. The major problem this model has is that it needs regions of fast cooling, even in massive disks, for such an instability to form. As such, it is very hard to form them anywhere but in the very outer regions past ≈ 30 AU, although it is feasible that instabilities are induced by external processes such as perturbations in the disk due to close encounters with heavy objects.

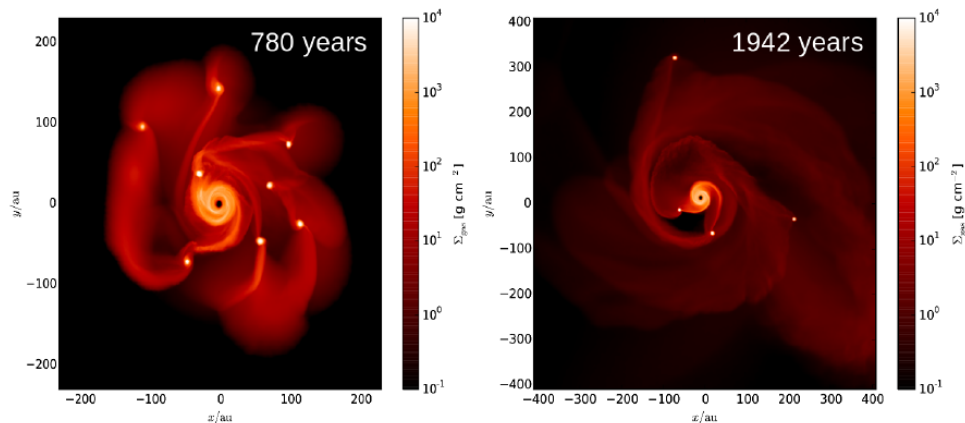


Figure 6: This graphic shows the result of simulations meant to create gas giants via gravitational instability. There are spiral arms (which are overdense regions compared to the rest of the CPD) in which clumps are formed that constitute the early stages of giant planet formation. Although as many as 8 formed initially in this specific simulation, chaotic interaction reduced that number to four in a short time. (Simulations were done by L. Mayer and T. Quinn, graphic from [Szulágyi et al. 2016a])

1.4 Disk dispersion

One of the driving processes of planet and satellite formation is the dispersal of CSD/CPD. Not only does it determine how long and how much the bodies accrete (the faster the disk disperses, the less mass can be accreted) but it also influences the migration pattern (as migration is directly related to the gas density, see section 1.5)

1.4.1 Dispersal mechanisms and models

There are a number of mechanisms that are commonly seen as the main drivers of disk dispersion:

Accretion Accretion of the gas (and dust) onto the central object (be that a star or a planetary body) driven by outward momentum transport: This transport is most commonly thought of as being the result of turbulence within the disk which act as an "inner friction" or a "viscosity" and thus the modern way to model it is the Shakura-Sunyaev alpha viscosity ([Shakura & Sunyaev 1973]), which gives for the viscous timescale:

$$t_\nu = \frac{1}{\alpha\Omega} \left(\frac{H}{R} \right)^{-2} \quad (19)$$

where the α is a dimensionless parameter that represents the strength of the turbulence and is usually taken between $[10^{-2}, 10^{-4}]$. With this, viscous timescales at the edge of a disk are around ≈ 1 Myr and as such, given observational constraints, can by itself not account for the dispersion of the whole disk, seeing as that would be at best a couple of rotations.

Photoevaporative wind CSDs will usually be flared and thin enough near the star that the star can not only heat the disk by radial penetration but also by hitting the surface of the disk. This will lead to gas being heated enough that it can escape the star's gravity, which is generally called "photoevaporation". The exact mass loss due to this mechanism will depend on the disk properties in question and the central star, because different wavelengths will penetrate the disk in different ways. Generally there are three regimes that are considered: EUV heating where the photons are energetic enough to ionize hydrogen atoms, X-Ray heating where photons primarily ionize the K-shell of heavy elements like O and also C and Fe and FUV heating where the photons are mostly absorbed by dust and re-emitted as IR radiation.

Magnetohydrodynamic (MHD) wind If the disk is sufficiently ionic, the magnetic field of the central object strong enough and the magnetic flux through the disk large enough ([Salmeron et al. 2011]), that might lead to removal of material and angular momentum through jets launched outwards. [Balbus & Hawley 1998] and [Shu et al. 2007] have shown that in principle these winds can coexist with turbulent transport and [Suzuki et al. 2010] have shown that mass loss due to MHD winds can easily be big enough to drive disk dispersion.

External influences Some star formation clusters are dense enough that neighbouring stars can have a major influence on a disk development. On one hand, there is the radiation by surrounding stars which will have a photoevaporative effect on top of the central star and on the other hand, gravitational interactions can lead to tidal stripping of some of the material in the CSD, as well as induce turbulence into the disk which can drive accretion.

Planet/satellite formation In principal, the formation of bodies in the disk will also in a way help the dispersion, as it removes material from the disk. However, planetary systems rarely have more mass than maybe a few % of the star and formation processes are usually too long for them to have a major influence (see also 1.3)

Out of these, accretion due "viscosity" and photoevaporation are considered the driving forces of disk evaporation and are included in most models of CSD and even CPD formation. [Alexander et al. 2014] put together a schematic overview of the stages of disk dispersal: In the early stages "dispersion" is mainly driven by accretion onto the disk due to gravitational instabilities but there are also jets and outflows driven by magnetic effects close to the star. The middle stages are still dominated by accretion onto the star, but low-velocity winds carry a not insignificant amount of mass away as well. These winds are mostly neutral and probably driven by some combination of X-rays, FUV photons and magnetic field. In the final stages mass loss by wind driven by X-ray and EUV photons starts to dominate. There will then be two regions in the disk: an inner one where the star's gravity dominates over the winds and mass gets accreted and an outer disk where the winds are stronger than the gravity which leads to a photoevaporative hole being opened (the position of which depends on the disk parameters and the exact combination of wind origins). Then the inner part gets swept up by the star's gravity and the outer parts get swept up from the inside out by photoevaporation, which now due to the geometry is much more effective (see fig. 7).

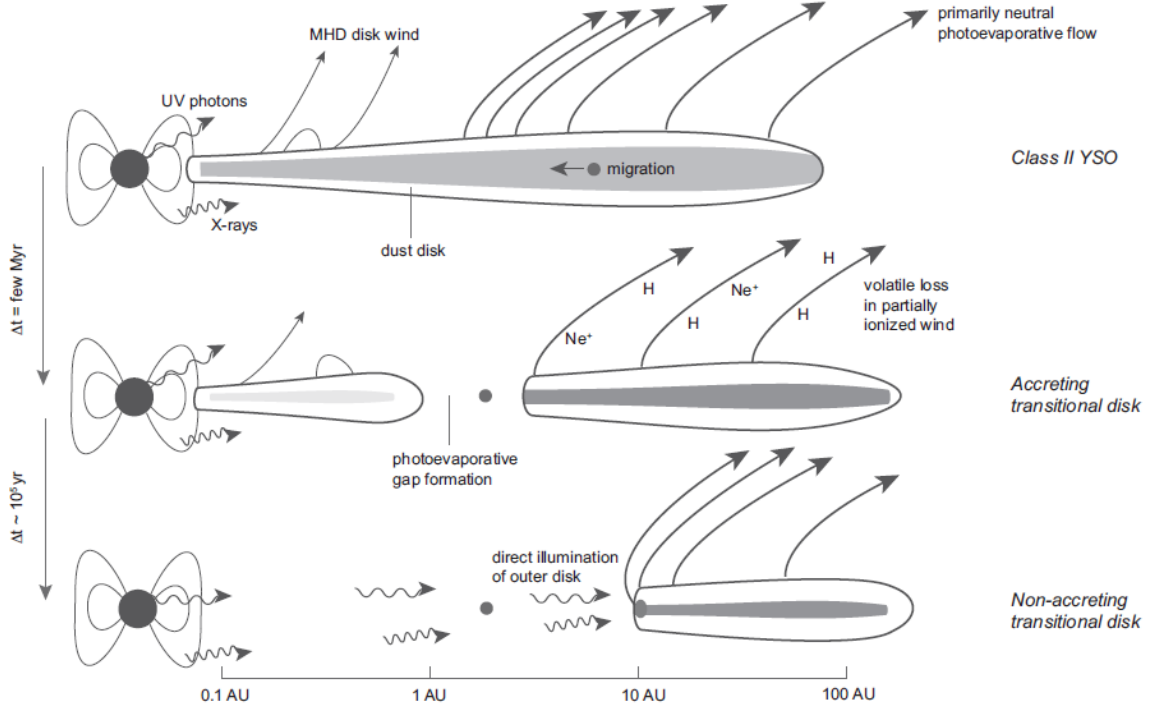


Figure 7: Schematic overview of how disk dispersion happens: early stages are dominated by accretion onto the planet and only a low mass loss due to wind. As time goes on the mass loss via wind will start to dominate and a photoevaporative hole will form. To the inside of this hole gravity dominates and accretes mass inwards, while to the outside the winds are stronger than gravity and blow the mass away from the star. This will then lead to very rapid sweeping of the disk both by gravity inwards and wind outwards. (Graphic taken from [Alexander et al. 2014])

1.5 Migration

Type 1 Migration The migration of bodies in a disk is the result of the gravitational interaction with the gas particles. On a basic level, one can start with one gas particle and a satellite of mass M_s . In the reference frame of the satellite, a particle moving past with an impact parameter b and a velocity Δv , one can sum up the force over the whole unperturbed trajectory and gets a change in the perpendicular velocity like

$$|\Delta v_{\perp}| = \frac{2GM_s}{b\Delta v} \quad (20)$$

This is a perpendicular change in velocity, so this does not change the angular momentum. However, as the kinetic energy is conserved, this means the parallel velocity necessarily has to change and (for small deflections) one can get:

$$|\Delta v_{\parallel}| = \frac{1}{2\Delta v} \left(\frac{2GM_s}{b\Delta v} \right)^2 \quad (21)$$

In the end, one can get an implied angular momentum change per unit mass of gas of

$$\Delta j = \frac{2G^2 M_s^2 a}{b^2 \Delta v^3} \quad (22)$$

for a satellite with a semi-major axis a . To this one has to add the appropriate sign as well: gas outside of the satellite's orbit moves slower and thus interaction with the satellite increases its parallel velocity, pushing it outwards. Conversely, gas inside gets slowed down and pushed

inwards. As the gravitational interaction has to be equal and opposite on the satellite, this means gas outside pushes the satellite inwards and gas inside pushes the satellite outwards, while being pushed inwards. Usually, satellites are embedded in a disk, so there is gas inside and outside of its orbit, which means the direction of the resulting migration depends on the distribution of gas (although for most cases, type 1 migration will be radially inwards). The total torque can then be calculated by integration over the whole disk mass, where one can estimate the mass of an annulus $dm = 2\pi a \Sigma db$ and the difference in orbital period of annulus and satellite $|\Omega_{\text{annulus}} - \Omega_s| \approx \frac{3\Omega_s}{2a} b$ (if $b \ll a$), which then gives

$$\frac{dJ}{dt} = - \int_{b_{\min}}^{\infty} \frac{8G^2 M_s^2 a \Sigma}{9\Omega_s^2} \frac{db}{b^4} = - \frac{8}{27} \frac{G^2 M_s^2 a \Sigma}{\Omega_s^2 b_{\min}^3} \quad (23)$$

where the lower limit b_{\min} was chosen to get around a divergent integral. This is still an approximation and can be improved, for example by actually taking into account the effects of the rotation of the planet frame around the star, which would add a correction factor.

A much more powerful, if also more complicated to calculate, way to get the migration torque would be by decomposing it into partial torques at resonant locations ([Goldreich & Ward 1979], [Tanaka et al. 2002]). So if we have a satellite orbiting with an angular frequency Ω_s , one can define

1. Co-rotation resonance at a radius in the disk with $\Omega = \Omega_s$
2. Lindblad resonances at radii where $i(\Omega - \Omega_s) = \pm \kappa_0$, where $\kappa_0 = \left(\frac{d^2\Omega}{dr^2} + 3\Omega^2\right)$ is the epicyclic frequency, Ω is the star's gravitational potential and i is an integer.

In the same way as the simpler picture, all the resonances inside the satellite's orbit will push the satellite outward (and cause the gas to fall inwards), while all the resonances outside will push the satellite inwards, so in the end the torque would be calculated like

$$T_s = \sum_{inner} T_{LR} + \sum_{outer} T_{LR} + T_{CR} \quad (24)$$

This formula is deceptively simple though; actually calculating Lindblad resonances is not an easy feat, not to mention the co-rotation resonance (see e.g. [Baruteau et al. 2014] for a review on different approaches and results). A typical result that is used in many works is provided by [Tanaka et al. 2002], who calculate the torque as

$$T = -b_I \left(\frac{M_s}{M_{\text{star}}} \frac{r_s \Omega_s}{c_s} \right) \Sigma_s r_s^3 \Omega_s^2 \quad (25)$$

where the subscript s means at the position of the satellite and the b_I is a correction factor one can apply.

Type 2 Migration Type 1 migration is only viable so long as the satellite in question is encased in gas. As it grows more massive though, the satellite-gas interaction can be strong enough that the satellite pushes all the gas close to it away, forming a so called gap. Generally, there are two conditions that have to be fulfilled for a gap to open:

1. The satellite has to be massive enough so its influence extends up to the "top" of the disk. This is measured by the Hill-sphere and the condition then is $r_H = \left(\frac{M_s}{2M_{\text{planet}}}\right)^{1/3} > h$, where h is the scale height of the disk.
2. The torque the satellite extends on the gas has to be strong enough to overcome the viscous spreading in order to keep the gap empty (e.g. [Papaloizou & Lin, 1984]). So it comes down to comparing the time it takes for the gas to filled a gap of width Δr $t_{\text{close}} \simeq \frac{(\Delta r)^2}{\nu}$ and the time it takes for the torque to open the gap at an i -th order Lindblad resonance $t_{\text{open}} \simeq \frac{1}{i^2 q^2 \Omega_s} \left(\frac{\Delta r}{r_s}\right)$, where q is the ratio of satellite to planet mass.

These are very general conditions and can be improved upon (see section 2.3.2) but give a general understanding of why gap opening happens. Once a gap opens, the reason and rate of migration changes. Now, the orbital evolution is coupled to the viscous evolution of the disk (as the gas-satellite interaction keeps the gas at the edge of the gap) and the satellite simply migrates on the same timescale as the gas, which can be estimated as $v_{\text{radial}} = -\frac{3}{2}\frac{\nu}{r}$.

2 Model

The Model used here is a simple 1D model, that is orbits of satellites are assumed to be circular and co-planar and changes in the orbit are only given in changes to the radius. The model works by putting embryos in a given disk and letting them migrate, accrete matter and even collide or enter into resonance configuration given the right circumstances. A population synthesis model is used to get a statistic on different outcomes where the timescales on which the disk disperses and new material enters the disk, the dust-to-gas ratio, the initial positions of points where the embryos are seeded as well as the number of such positions are varied over many simulations.

2.1 Disk structure and evolution

The two different disks used here are taken from [Szulágyi et al. 2016a] where the planets and disks were modeled in as much as possible the same environment to directly compare them. This is then used here to directly compare the satellite creation in those disks. The disks are assumed to be axisymmetric and co-planar and the mid-plane values for surface density and temperature are used, which is also where the satellites are assumed to be.

2.1.1 Core Accretion Disk

Hydrodynamic Simulation For the core accretion case, the simulations were hydrodynamic, grid-based, radiative and 3D, and were performed with the *Jupiter* code ([de Val-Borro et al 2006], [Szulágyi et al. 2014], [Szulágyi et al. 2016b], [Benítez-Llambay et al. 2015] and [Szulágyi et al. 2015]) developed by F. Masset and J. Szulágyi. It is based on a higher order Godunov scheme and uses nested meshes, so that it can both treat the whole disk while also better resolving the vicinity of the planet. The disk's heating is determined by both viscosity and adiabatic compression while cooling is determined by adiabatic expansion and radiation, which is usually called a two-temperature approach (e.g. [Commerçon et al 2011]). Despite only being a gas simulation, using the gas and dust opacities of [Bell & Lin 1994] still allowed for the dust component to be taken into account. A dust-to-gas ratio of 0.001 was assumed, to take into account that by the time of planet formation this simulation is interested in, most dust will have formed into larger bodies and thus lowering the opacity (eg [Ormel et al 2009],[Ormel et al 2011]). Other parameters were: the molecular weight of 2.3, the equation of state for the pressure $P = (\gamma - 1)e$ (which is that of an ideal gas, with e the internal energy and the adiabatic index $\gamma = 1.43$), a constant kinematic viscosity $10^{-5}a_p^2\Omega_p$ (a is the semi-major axis and Ω the orbital frequency of the planet that will be introduced) and no self-gravity. The CSD was centered on a one solar mass star with an initial flat surface density. To achieve a thermal equilibrium first, the simulation ran for 150 orbits without any planet, and then a 10 Jupiter-mass planet was gradually built up during 50 orbits (which was a fixed mass thereafter) and results were taken after a steady state was achieved again. For a more detailed description of this scheme, see [Szulágyi et al. 2016a].

Structure The following fits were used to describe the structure of the CA CPD:

$$\begin{aligned} \Sigma_{\text{gas},0}(r) = & 1.4569 \cdot 10^{-6} \cdot r^{-0.0847} \cdot \frac{1}{1 + e^{0.0291 \cdot (\frac{r}{R_{\text{Jup}}} - 201.78)}} \\ & + 1.1654 \cdot 10^{-3} \cdot r^{-1.3811} \cdot \frac{1}{1 + e^{0.0378 \cdot (\frac{r}{R_{\text{Jup}}} - 238.14)}} \left[\frac{M_{\text{Jup}}}{R_{\text{Jup}}^2} \right] \end{aligned} \quad (26)$$

$$\begin{aligned}
T_0(r) = & 1.6114 \cdot 10^4 \cdot e^{-3.4579 \frac{r}{1 \text{ AU}}} \cdot \frac{1}{1 + e^{6.2612 \cdot (\frac{r}{1 \text{ AU}} - 1.2762)}} \\
& + 2.1054 \cdot 10^3 \cdot e^{-0.1381 \frac{r}{1 \text{ AU}}} \cdot \frac{1}{1 + e^{-8.4797 \cdot (\frac{r}{1 \text{ AU}} - 0.7164)}} \\
& + 1.7789 \cdot 10^3 \cdot r^{-0.7016} \cdot \frac{1}{1 + e^{-7.0884 \cdot (\frac{r}{1 \text{ AU}} - 1.2447)}} \text{ [K]}
\end{aligned} \tag{27}$$

2.1.2 Gravitational Instability

Hydrodynamic Simulation For the gravitational instability case, a 3D global disk SPH simulation with as many as 42 million particles was used, which can achieve a high resolution of 0.01 au in a 200 au disk. It used the ChaNGa Tree+SPH code (which employs a CHARM++ parallel programming environment) ([Jetley et al. 2008], [Menon et al. 2015]). ChaNGa uses a Monaghan viscosity, with parameters $\alpha = 1$ and $\beta = 2$ and limits the viscosity in purely rotational flows ([Balsara 1995]). Local gas properties determine the radiative cooling with a energy loss per time per volume like

$$\Lambda = (36\pi)^{1/3} \frac{\sigma}{s} (T^4 - T_{\min}^4) \frac{\tau}{\tau^2 + 1} \tag{28}$$

with τ the optical depth (taking as constant across a resolution element), T_{\min} the minimal gas temperature and σ the Stefan-Boltzmann constant. This is an equation to approximate radiative cooling without actually solving radiative transfer equations, which lessens computation time. This however means that, while compressional heating through PdV work and shock heating are taken into account, any heating that contracting clumps would add (through luminosity) is not included. It was made sure though that this approximation is valid in this case. Optical depths were computed by using tabulated Rosseland mean and Planck opacities ([D’Allesio et al. 1997], [D’Allesio et al. 2001]) at a dust-to-gas ratio of 0.01. To further capture the thermodynamics around spiral shocks, a variable adiabatic index was used to account for the ortho/para ratio of molecular hydrogen. The CSD was centered around a 1.35 Solar mass star and it’s temperature profile was set up in hydrostatic equilibrium. The surface density profile was chosen as a power law with exponent of -1 in the region around 30-100 AU.

Structure The following fits were used to describe the structure of the GI CPD:

$$\Sigma_{\text{gas},0}(r) = 2.56 \cdot 10^{-6} \cdot e^{-2.57 \cdot \frac{r}{1 \text{ AU}}} + \frac{1}{1 + e^{-3.22 \cdot (\frac{r}{1 \text{ AU}} - 1.49)}} \cdot 3.02 \cdot 10^{-7} \cdot e^{-0.99 \cdot \frac{r}{1 \text{ AU}}} \left[\frac{M_{\text{Jup}}}{R_{\text{Jup}}^2} \right] \tag{29}$$

$$T_0(r) = 381.14 \cdot e^{-0.87 \frac{r_{\text{sc}}}{1 \text{ AU}}} + (1 - e^{-0.87 \cdot \frac{r_{\text{sc}}}{1 \text{ AU}}}) \cdot 11 \text{ [K]} \tag{30}$$

2.1.3 Evolution

As discussed in section 1.4 the dispersion of a disk is a complicated set of mechanisms, which are too involved for 1D model such as here. However, if one takes all these into account and models the dispersion, the evolution of the gas disk can be in first order approximated as an exponential decay on a certain timescale and as such it is modeled as:

$$\Sigma_{\text{gas}}(r, t) = \Sigma_{\text{gas},0}(r) e^{\frac{-t}{t_{\text{disp}}}} \tag{31}$$

For the temperature the situation is similar in its complexity and it can be similarly approximated by an exponential decay such as:

$$T(r, t) = T_{\min} + (T_0(r) - T_{\min})e^{\frac{-t}{t_{\text{disp}}}} \quad (32)$$

2.2 Satellite formation and evolution

A model like [Miguel & Ida 2015] is used, where embryos are seeded in the disk at the beginning of the Simulation. Here, the first generation of satellites are seeded into the disk between $[0, 0.5] t_{\text{disp}}$ yrs (so as to not lose too much to early collisions) and at log-normally distributed points between $[\log_{10}(0.01 \cdot R_{\text{disc}}), \log_{10}(0.8 \cdot R_{\text{disc}})]$ with a mass of $10^{-8} m_{\text{Jupiter}}$. 80 % of disk radius is farther out for satellite creation than usually assumed, but seeing as both CPDs are also more massive than in most other works (and thus the outer regions have much more mass) it should be possible to form satellites at those positions. A lognormal distribution is chosen because the possible radii span multiple orders of magnitude. Sequential generation is also possible and done by assigning a countdown to every seeding position every time an embryo is created. This countdown will be the accretion timescale (see 2.5) of an embryo, that is the time an embryo needs to accrete its own mass (at the time of creation of the previous one). This timescale is chosen because this ties the countdown to local conditions and because it seems a reasonable timescale to create embryos on. Further, the region where an embryo is created has to contain at least the mass of an embryo in it before creation happens.

2.3 Migration

Circular orbits are assumed so any migration will manifest in a change in orbital radius. There are two ways migration is usually modeled:

1. Type 1 migration, which is caused by satellite-disk interaction. It is most of the time an inward force and for these disks especially is always inward.
2. Type 2 migration, which happens if a satellite manages to open a gap in the disk. At that point it will migrate like the gas that falls into the planet.

2.3.1 Type 1 Migration

In this model the prescription given by [Tanaka et al. 2002] is used:

$$v = \frac{da}{dt} = b_{\text{I}} \frac{M_{\text{sat}} \Sigma_{\text{gas}} a^3}{M_{\text{planet}}^2} \left(\frac{a}{h}\right)^2 \Omega_{\text{K}} \quad (33)$$

Where M_{sat} is the satellite's mass, M_{planet} is the mass of the central planet, Σ_{gas} is the gas density at position of the satellite a , $h = \frac{c_s}{\Omega_{\text{K}}}$ is the scale height of the disk, Ω_{K} is the Keplerian orbital period. b_{I} is a correction factor, taken from ([Paardekooper et al. 2010], [Paardekooper et al. 2011]) to account for additional effects.

The satellite will influence the gas and dust density around it via this interaction and at least partially open a gap, i.e. lower the densities directly around. To account for this, an analytical model by [Crida et al. 2006] is used, where the velocity is then multiplied by a number between 0 and 1 which represent how deep this partial gap is (where 1 stands for no gap and 0 would stand for full gap, although at that point type 2 migration would already be happening).

2.3.2 Type 2 Migration

The most common criteria to determine whether a body opens a gap in a disk is usually taken as ([Crida et al. 2006]):

$$P = \frac{3}{4} \cdot \frac{h}{R_{\text{H}}} + \frac{50}{q \cdot Re} = \frac{3}{4} \frac{c_s}{\Omega_{\text{K}} a} \left(\frac{q}{3}\right)^{-1/3} + 50\alpha q \left(\frac{c_s}{\Omega_{\text{K}} a}\right)^2 > 1 \quad (34)$$

where $R_H = a \left(\frac{q}{3}\right)^{\frac{1}{3}}$ is the Hill radius (with $q = \frac{M_{\text{sat}}}{M_{\text{planet}}}$), Re is the Reynolds number and c_s is the local speed of sound. However, [Mueller et al. 2018] found that this criteria tends to overestimate the creation of gaps and in their work suggested two additional criteria, where either one can be added to the above. As they both have about the same effect for these disks, the one that compares the viscous timescale ($\tau_{\text{visc}} = a^2/\nu$) with the crossing timescale, that is the timescale it would take the satellite to migrate the width of the gap, $\tau_{\text{cross}} = R_{\text{HS}} \left(\frac{da}{dt}\right)^{-1}$ where $R_{\text{HS}} = 2.5 \cdot R_H$ ([Malik et al. 2015]) is chosen. So the criteria used is then:

$$P < 1 \text{ and } \tau_{\text{visc}} < \tau_{\text{cross}} \quad (35)$$

If a gap is opened, the migration is then determined by gas drift, as the process of keeping the gap evacuated of gas leads to the gas essentially "pushing" the gap inwards at its speed. This means the velocity is then given by

$$v_r = -b_{\text{II}} \frac{\alpha c_s h}{a} \quad (36)$$

where the factor $b_{\text{II}} = \frac{1}{1 + \frac{M_{\text{sat}}}{4\pi \cdot a \cdot \Sigma_{\text{gas}}}}$ reflects the fact that migration is slower the bigger the ratio between satellite mass and the mass of the gap is ([Syer & Clarke 1995]).

2.3.3 Resonant Capturing

As can be seen in Jupiter's case, the satellites can end up in resonance with each other, meaning the ratio between their orbital periods are integers. This will happen as a result of the interplay between satellite-disk and satellite-satellite if the interaction works out in a way where they will migrate together in a resonant chain. This can be modeled in a way where, as the orbital separation between two satellites shrinks, they exert a force on each other, working against them coming any closer. [Ida & Lin 2010] give a model for this which puts the change in separation $b_{ij} = |a_i - a_j|$ like this:

$$\frac{db_i}{dt} \simeq 7 \left(\frac{|a_i - a_j|}{R_H}\right)^{-4} \left(\frac{R_H}{a_i}\right)^2 v_{\text{K},i} \quad (37)$$

where $R_H = \left(\frac{m_i + m_j}{3M_{\text{planet}}}\right)^{1/3}$ in this case is the Hill radius of an object with both the satellite masses. With this, resonant configurations can occur if the above change in orbital separation is offset by their orbital closure given by different type 1 migration velocities.

2.4 Collision

As this is a 1D it is not really possible to treat collisions correctly. Nevertheless there are ways to at least improve the situation at least slightly. Here, an angle between $[0, 2\pi]$ is chosen and applied to the embryo at the time of creation. This angle will be updated every timestep with the Keplerian orbital velocity (the resolution in this is such that it doesn't really matter whether one takes the velocity at the old or new orbital radius or takes some point in between). Then for the collision criteria the 2D distance between two satellites is taken and a collision is said to happen if the two bodies are closer then the Hill radius of their combined masses ($R_H = \left(\frac{m_i + m_j}{3M_{\text{planet}}}\right)^{1/3}$).

2.5 Accretion

As the embryos migrate they accrete mass from the disk and the [Greenberg et al. 1991] solid-accretion model is used, which gives the following analytical function for the accretion:

$$\frac{dM_{\text{sat}}}{dt} = 2\sqrt{\frac{R_{\text{sat}}}{a}} \Sigma_{\text{dust}} a^2 \sqrt{\frac{M_{\text{sat}}}{M_{\text{planet}}}} \Omega_{\text{K}} \quad (38)$$

where R_{sat} is the embryo's radius and here the Σ_{dust} is the average dust over the whole feeding zone. The feeding zone is the region from which a body can accrete mass and [Greenberg et al. 1991] gives a value of $R_{\text{feeding}} = 2.3 \cdot R_{\text{H}}$ for the radius of this zone. The partial gap model is also used here, because the gas and dust are well coupled.

2.6 Dust depletion and refilling

This accreted mass has to be depleted from the disk and this is done in the following way:

$$\Delta M_i = \frac{M_i \cdot M_{\text{accretion}}}{M_{\text{feedingzone}}} \quad (39)$$

so the mass of the i -th cell M_i is depleted proportionally to its mass compared to the total accretion.

The simulations show that both the CPDs are continuously fed by an influx from the CSD. This means it also carries dust with it, at least the part that is well coupled. So we assume the gas influx has the same dust-to-gas ratio as the CPD and the infall from the simulations is taken, which gives over the whole disk

1. for the GI disk: $\dot{M}_{\text{in},0} = 7.44 \cdot 10^{-5} \frac{M_{\text{Jupiter}}}{\text{year}}$ at $t=0$
2. for the CA disk: $\dot{M}_{\text{in},0} = 2.0 \cdot 10^{-8} \frac{M_{\text{Jupiter}}}{\text{year}}$ at $t=0$

These will decay the same as the CSD, and consequently as the CPD, so $\dot{M}_{\text{in}} = \dot{M}_{\text{in},0} e^{-\frac{t}{t_{\text{disp}}}}$. These values represent the total influx into the CPD, so a model is needed to describe how exactly this is distributed over the disk. For this a model like [Cilibrasi et al. 2018] is adapted: The disk at the start is assumed to be in equilibrium and the influx is a result of accretion disturbing it. So the assumption is that every cell wants to regain its equilibrium state on a timescale $t_{\text{refilling}}$ and the refilling formula looks like this:

$$\Delta \Sigma_{\text{dust}} = \frac{\Sigma_{\text{dust},0} - \Sigma_{\text{dust}}}{t_{\text{refilling}}} dt \quad (40)$$

As there are instances where the influx might not fully refill the depleted cells, so the refilling is always lesser or equal to the total influx.

2.7 Initial parameters

There are some parameters that are a priori unknown, so using a population synthesis method by running many simulations with varying initial parameters is the best option. The parameters that are varied are:

1. Based on observational constraints of circumstellar discs ([Ansdell et al. 2016]), the dust-to-gas ratio of the disc is varied in the range $[10^{-3}, 10^{-1}]$.
2. The dispersion time-scale of the disc is in the range $[10^{4.698970}, 10^{5.60205}]$ years. [Picogna et al. 2019] was used to estimate disk dispersion for both disks and then the overlap was taken as a range, as that allows for a direct comparison while still being reasonable timescales for both CPDs. As both are still T-Tauri stars, the model of [Picogna et al. 2019] was also used for the bigger, 1.35 Solar mass star.

3. The refilling time-scale is the least known process, so the range is $[10^{2.698970}, 10^{5.60205}]$ years, always bigger than the smallest timestep and never higher than the longest dispersion timescale.
4. The initial embryo positions are varied between 1% and 80% of disk radius.
5. The amount of initial embryos (which are then the amount of seeding positions) are chosen between 5 and 20. Increasing this number has no significant effect on the results.

The dispersion timescales are distributed exponentially like [Fedele et al. 2010], while the initial embryo positions, the refilling timescales and the dust-to-gas ratio us a log-uniform distribution, to account for the numerous orders of magnitude involved. To investigate the influence of the specific initial conditions, simulations were also done where a specific parameter was set to be fixed while all others are varied. The set parameters in that case are

1. $t_{\text{refilling}} \in [10^{2.698970}, 10^{4.15}, 10^{5.60205}]$
2. $t_{\text{dispersion}} \in [10^{4.698970}, 10^{5.15}, 10^{5.60205}]$
3. dust-to-gas ratio $\in [0.1\%, 1\%, 10\%]$

2.8 t-SNE algorithm

As a way to compare the resulting satellite systems, the machine learning approach by [Alibert 2019] is applied to the resulting systems, based on a "distance" between the satellite systems. It works as follows: first, a 2D function (which depends on a Mass M and a semi-major axis a) is defined as:

$$\phi_i(M, A) = \sum_{\text{satellites}} f_s(M, a) \quad (41)$$

where

$$f_s(M, a) = \exp\left(-\frac{1}{2}\left(\frac{\log_{10}M - \log_{10}M_s}{\sigma_M}\right)^2 - \frac{1}{2}\left(\frac{\log_{10}a - \log_{10}a_s}{\sigma_a}\right)^2\right) \cdot F(M_s) \quad (42)$$

So f_s is essentially a gaussian 2D profile for each satellite s with a width of σ_M and σ_a , which are both chosen to be 0.1 (although this is a tuneable parameter) and the ϕ_i is then the sum of all these gaussian profiles, essentially giving a density map of a given satellite system i based on the masses and semi-major axes of the satellites s . The $F(M_s = \log_{10}M_s + 9)$ is a weight function, which means heavier satellites are more important than lighter ones. Based upon this, a norm

$$\|\phi_i\| = \int \int |\phi_i(M, a)|^2 d\log_{10}M d\log_{10}a \quad (43)$$

can be defined, where the integration boundaries are the chosen such that it encompasses at least all possible options (in this case the whole disk for the semi-major axis and for the masses from 10^{-9} to 10^{-1} planet masses. This can then be used to define a mathematical distance between a system i and a system j

$$d_{ij} = \|\phi_i - \phi_j\| \quad (44)$$

[Alibert 2019] proved that this indeed fulfills all the requirements for a distance in an L^2 space. Then to visualize this data in a 2D fashion, a T-distributed Stochastic Neighbor Embedding (t-SNE) algorithm is applied. It is designed to take high dimensional data (in this case, the data has a dimension of $2 \cdot (\#\text{satellites})$, where 2 is for the mass and the semi-major axis) and reduce it to lower-dimensions (typically to 2D). It does this non-linearly by minimizing a cost function

(see [Van der Maaten & Hinton 2008],[Van der Maaten2014] for a detailed description) and assigning coordinates in an arbitrary-unit space. The algorithm is meant to link similar objects (in this case satellite systems) to close points and dissimilar ones to distant points, allowing for a low-dimensional picture of high-dimensional data. The t-SNE algorithm is part of the python package Scikit-Learn [Pedregosa et al. 2011], which was used here to produce the plots.

3 Results

3.1 Mass Distribution

3.1.1 All parameters random

Table 5: Mean and standard deviations of the mass distributions

Disk type	Mean [M_{planet}]	Standard deviation [M_{planet}]
GI	$1.137 \cdot 10^{-5}$	$1.123 \cdot 10^{-4}$
CA	$8.746 \cdot 10^{-6}$	$4.407 \cdot 10^{-5}$

The mass distributions can be seen in fig. 8. One can see that in the CA case less satellites reach these masses than in the GI case (see also section 3.2). In fact, in the CA case the vast majority barely accrete mass at all, leading to a vast population of close to formation mass embryos, which is the result of both competition and low mass infall: as migration is low (see section 3.3) many of the first generation satellites remain close to the regions they were formed and accrete a lot of mass from the disk. So second generation satellites and later are formed around already heavy satellites with large feeding radii, so they can accrete maybe their own mass (because the model requires their feeding radii to contain an embryo mass) before the feeding radii start to compete. At this point, much of it will go to the heavier ones because the larger radii mean proportionally more infall. This can also be seen in the mean masses of all the surviving satellites and satellitesimals as shown in table 5. The CA mean is lower, because there are much more low mass embryos that pull it in that direction while the GI case has a higher maximum mass attainable. However, if one restricts the mean calculation on satellites with mass $> 10^{-6}$, the mean values are ([GI disk, CA disk])[$3.267 \cdot 10^{-5}$, $4.155 \cdot 10^{-5}$] and the standard deviations are [$2.079 \cdot 10^{-4}$, $8.891 \cdot 10^{-5}$]. There one can see that the CA population tends to have comparatively a bigger population of higher mass satellites (which can be seen clearly around 10^{-4} to 10^{-3} planet masses where there are more cases by almost a factor of 2 when compared to the GI case. The difference in maximum mass can also be seen in the standard deviations, which are lower in the CA case where the maximum mass is lower by about an order of magnitude.

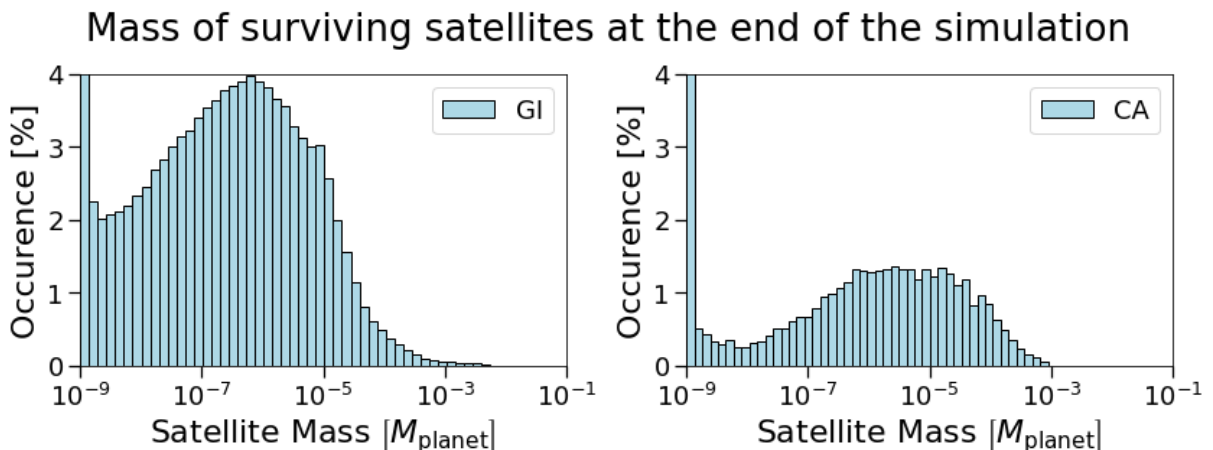


Figure 8: This plot shows the distribution of satellite masses in planet masses. In the GI case the majority of satellites are between 10^{-6} and $\simeq 3 \cdot 10^{-5}$ with an almost exponential decay towards the maximum of almost 10^{-2} . In the CA there are less of them as a whole. The majority are between 10^{-6} and 10^{-4} but with a very flat distribution which slowly decays.

The plot of lost mass versus retained mass fig. 9 follows the trend of the mass plot. In the GI disk the spread of lost masses is about 2 orders of magnitude (table 6). This is a consequence of the fact that lost mass is mainly from the first generation of satellites, who have the most massive disk to draw mass from and the spread of roughly two orders of magnitude coincides with the spread in dust-to-gas ratios. These satellites can also by and large all migrate significantly

Table 6: Mean and standard deviations of the lost and retained masses

Disk type	Mean [M_{planet}]	Standard deviation [M_{planet}]
GI, lost mass	$2.979 \cdot 10^{-2}$	$4.060 \cdot 10^{-2}$
CA, lost mass	$8.130 \cdot 10^{-4}$	$1.488 \cdot 10^{-3}$
GI, retained mass	$3.079 \cdot 10^{-3}$	$8.377 \cdot 10^{-4}$
CA, retained mass	$6.794 \cdot 10^{-5}$	$1.440 \cdot 10^{-4}$

because that early in the disk’s life, they can accrete mass fast enough to get past the ”migration barrier” (see section 3.3 for more details on this), which should also contribute to a tight spread as they can get lost easily regardless of where they formed. The retained mass spreads much wider and is lower. This is because these masses are made up of mostly second generation and later, which means their masses are much more dependent on where and when they formed. It also shows that the vast majority systems have at least one embryo that managed to grow by 2 orders of magnitude or more, as there are very few systems with a retained mass of below 10^{-7} planet masses. Furthermore, there is a slight correlation between lost and retained mass, where more lost also means more retained. This makes sense given that in this case embryos can be created and accrete mass over essentially the whole disk lifetime.

In the CA disk the average lost mass is almost 2 orders of magnitude lower, although this is driven down by the many systems where only very few satellites are lost (if one ignores systems with lost mass $< 10^{-6}$ the difference reduces by about an order of magnitude). In the CA disk it is harder for satellites to get lost because they start on average farther out and need special conditions to make it pas the migration barrier. However one can also see that if a satellite is lost it is either below about 10^{-8} planet masses or above around 10^{-5} . This is essentially the difference between whether one of the first generation satellites that is formed far out can accrete mass fast enough to migrate into the planet or not. In the case where only low mass satellites get lost, the conditions of their formation where favourable enough that they could migrate inwards but mostly in a too hot a disk to accrete much mass. From the retained mass one can see that there are many systems that are made up of only embryos or embryos that barely accreted, which again reflects the systems where first generation satellites get lost but the disk can’t sustain significant accretion for second generation and later, and there is almost no correlation between lost and retained mass. There are also a fair amount of systems where almost no mass is lost but a lot of mass is retained, which means that there are first generation satellites still around in these systems.

In comparison, masses are a bit higher in the GI case (again owing to the fact that the CA disk is hot enough to evaporate dust in a significant part at the start) and the spread in retained mass is bigger in the CA case, as there are systems where all embryos accrete only low amounts of mass.

Table 7: Mean and standard deviations of the integrated mass distributions

Disk type	Mean [M_{planet}]	Standard deviation [M_{planet}]
GI	$3.050 \cdot 10^{-4}$	$8.343 \cdot 10^{-4}$
CA	$6.794 \cdot 10^{-5}$	$1.439 \cdot 10^{-4}$

The integrated masses fig. 10 further illustrate the distribution of system masses. In the GI case it is almost a bell curve and most of the systems are close to the mass that we observe in the Solar System’s gas giants (around 10^{-4} planet masses, see table 7). This again shows that it is almost a given for any system in a GI disk to have at least one satellite that can accrete at least 100 times its formation weight. In the CA disk there is still a peak roughly around 10^{-4} planet masses but now the spread is much larger (and thus the mean is lower than in the GI case), all the way to the embryo mass, and there is even a smaller peak around 10^{-8} . This is a big difference between the two cases: the GI disk creates satellites such that at least one of them

Lost versus retained mass

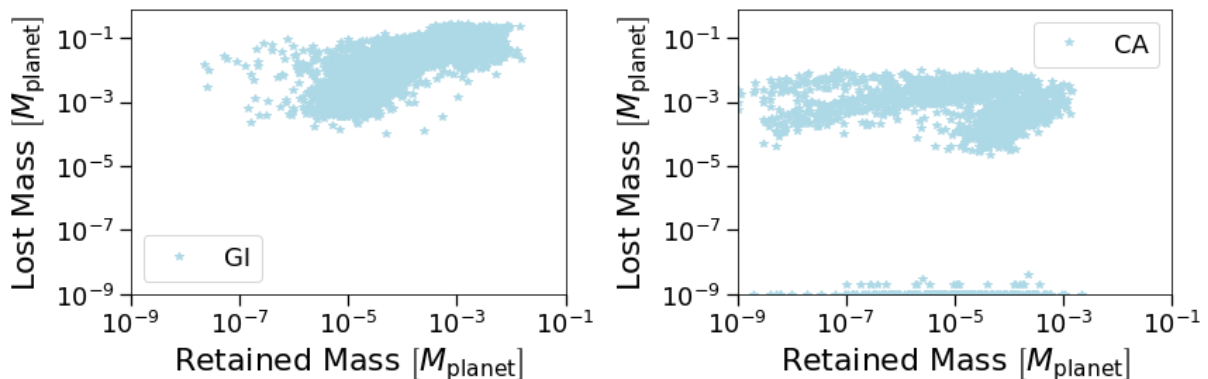


Figure 9: This plot shows the distribution of lost mass versus retained mass of the satellite systems. In the CA case the spread in lost mass is very narrow, between about 10^{-1} and 10^{-3} . The retained mass is wider spread between about 10^{-6} and 10^{-2} and there is a correlation between the two where the higher the lost mass the higher the retained mass. In the GI case the lost mass is spread about as narrow, but the values are smaller by about an order of magnitude. The retained mass is much more spread, from the minimum mass (the formation mass of embryos) to the maximum of about 10^{-2} , with little correlation. Further, The CA case has a number of systems that loose barely any mass (at most a few embryo masses) but retain masses on the whole spectrum.

is almost always bigger than roughly 10^{-7} planet masses but the CA changes creation in such a way that a much more diverse outcome is possible, where entire systems consist of nothing more than slightly larger than embryo sized satellites.

3.1.2 One parameter set

The influence on different set parameters on the mass distribution has the following behaviour:

1. Set dust-to-gas ratio (fig. 11): In the GI disk the influence of the dust is fairly straight forward: the higher the ratio is, the higher the average mass is. The percentages don't change much because as the satellites become higher mass, their migration will speed up and more will be lost, which can also be seen in the lost mass plots (see fig. 14). The CA case is more interesting. The maximum masses also scale with the ratio, but the distribution is much more concentrated: there are a lot that don't really accrete and stay around 10^{-9} planet masses and there is an obvious dip between them and around 10^{-8} , meaning that if they accrete, they can accrete at least almost an order of magnitude. In intermediate ratios, the whole distribution moves towards higher masses and more of the satellites that in low dust-to-gas ratios don't accrete start to accrete significantly. The dip however still remains, again pointing to the fact that if they can accrete two orders of magnitude they can also easily accrete more. That shows that the ones that do accrete significantly are the first generation ones and the ones that need higher dust-to-gas ratio are the second and later generation ones that need a higher dust available to be able to accrete, which is supported by the formation times (see fig. 37). If the dust-to-gas ratio is high enough, the distribution equalizes, because now the higher mass satellites manage to migrate fast enough to get lost and the later generations can accrete appreciably. Overall, the different dust-to-gas ratios give a somewhat similar distribution, if moved to higher mass, in the GI disk, whereas in the CA disk the distributions look very distinct in each different ratio, so the influence is felt stronger in that disk.
2. Set dispersion timescale (fig. 12): In the GI disk it is again as one would expect: at low timescales (which also means low disk lifetimes) the satellites are heavy overall. As the timescale becomes longer, the heaviest ones will migrate into the planet, shifting the

Integrated mass of all satellite systems

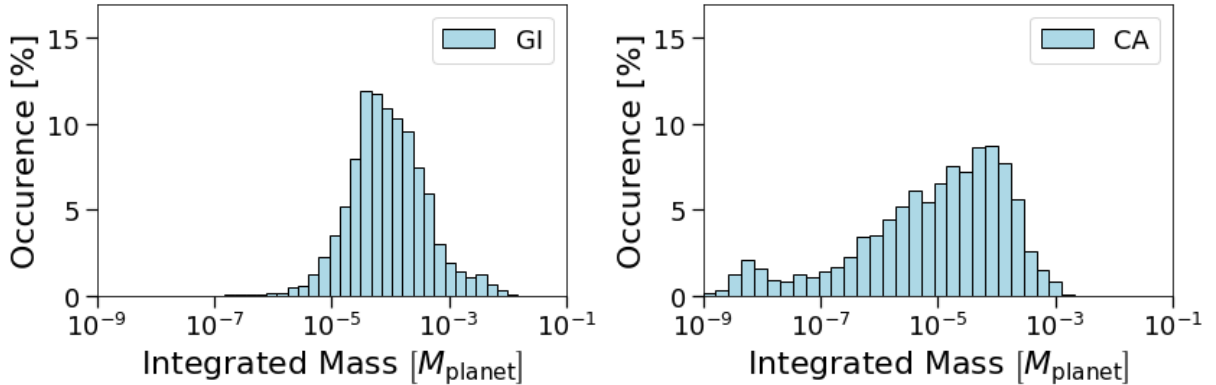


Figure 10: This plot shows the integrated mass of the satellite systems (equivalent to the retained mass in fig. 9). In the GI case the distribution is almost normal around roughly 10^{-4} planet masses (which is roughly the value all the satellite systems in the Solar System have) and most are within \pm one order of magnitude. In the CA case, while there is still a peak around 10^{-4} , the spread is much wider, ranging down to the minimum mass. Furthermore there is an small peak around 10^{-8} denoting very light satellite systems.

distribution to lower masses for intermediate timescales. For the longest living disks, the satellites that don't migrate have longer to accrete and thus are on average more massive again. In the CA disk the situation is much the same but instead now the distribution starts wide and narrows to the average. So in this disk it is harder to migrate into the planet but will happen more consistently past a certain mass, so the resulting distribution is narrower.

3. Set refilling timescale (fig. 13): In the GI disk the influence of the refilling timescale only shows for very low values (fast refilling), when there are more high mass satellites being created. For intermediate and high values the distributions are very similar, meaning in these cases dust-to-gas ratio and disk lifetimes have a higher influence. In the CA disk the refilling timescale has almost no influence on the distribution, which also has to do with the fact that a lot of infall will be distributed to the inner disk that is depleted due to the dust being vaporized.

The influence of different set parameters on the lost and retained mass shows the following behaviour:

1. Set dust-to-gas ratio (fig. 14): In the GI disk the lost mass increases as dust-to-gas ratio does, but the spread decreases, meaning that the heaviest satellites that are lost grow less in mass compared to the smaller ones because at some point they become so heavy that migration timescales are much faster than accretion timescales and the dust-to-gas ratio becomes less important. The retained mass on the other hand spreads wider as the ratio increases. This means that distribution of lighter satellites should be roughly the same, but that there are more heavy satellites that shift the maximum farther than their minimum, which is supported by the distribution of number of satellites (see fig. 21). In the CA disk the lost mass increases as well as the dust-to-gas ratio increases. For intermediate dust-to-gas ratios one sees the dip in masses even clearer and one also sees the divide between systems where the first generation satellites (the heaviest ones) migrate into the planet and the ones where they don't.
2. Set dispersion timescale (fig. 15): In the GI disk, the dispersion timescale has only a small influence on the lost mass: the spread is very similar, with the overall loss a bit higher. The retained mass however is strongly influenced, the spread becomes much smaller, as the longer dispersion timescale also means longer disk lifetime for the surviving ones to accrete

Mass of surviving satellites at the end of the simulation

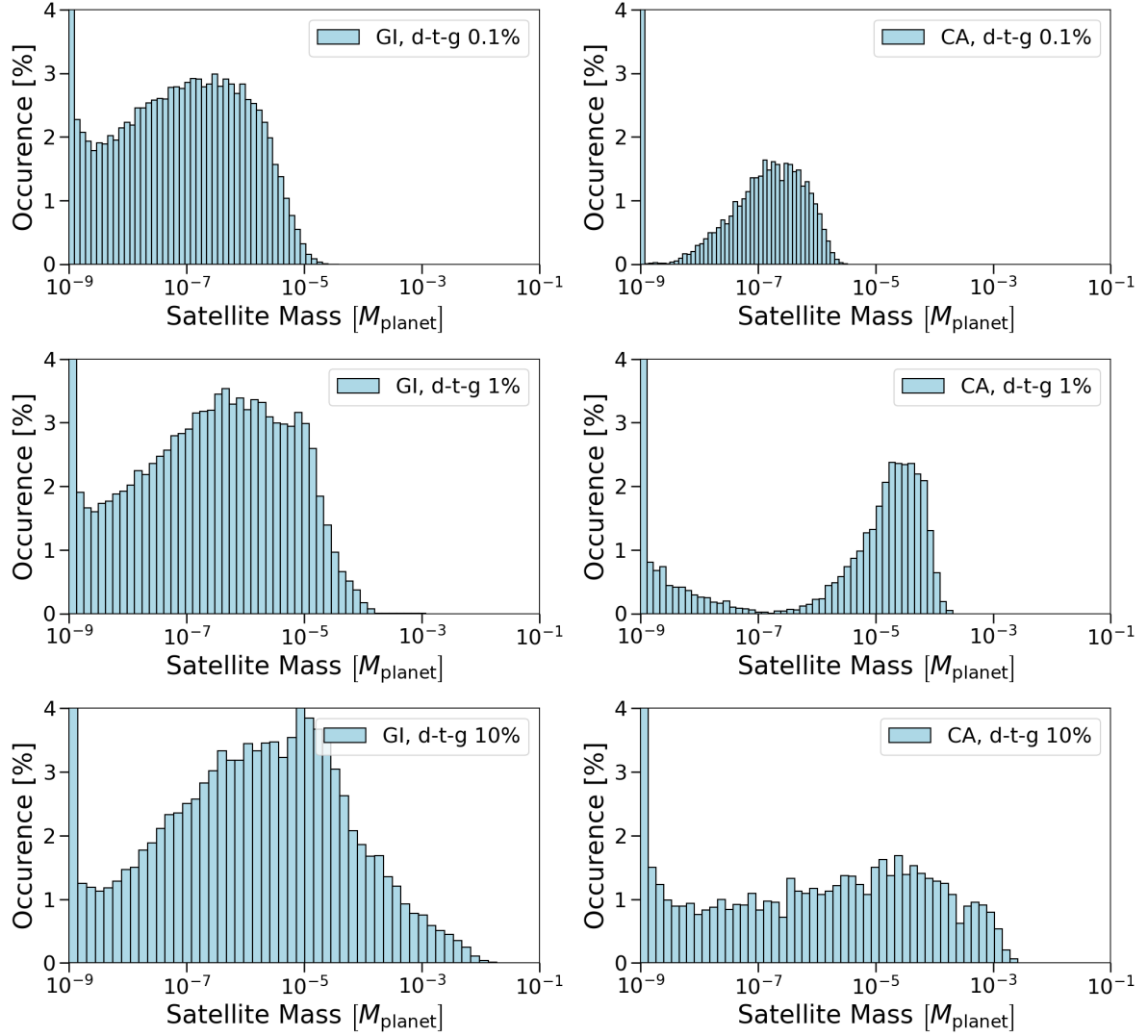


Figure 11: This plot shows the distribution of satellite masses in planet masses, split into the GI and CA case and for simulations where the dust-to-gas ratio was set at different numbers instead of varying them.

Mass of surviving satellites at the end of the simulation

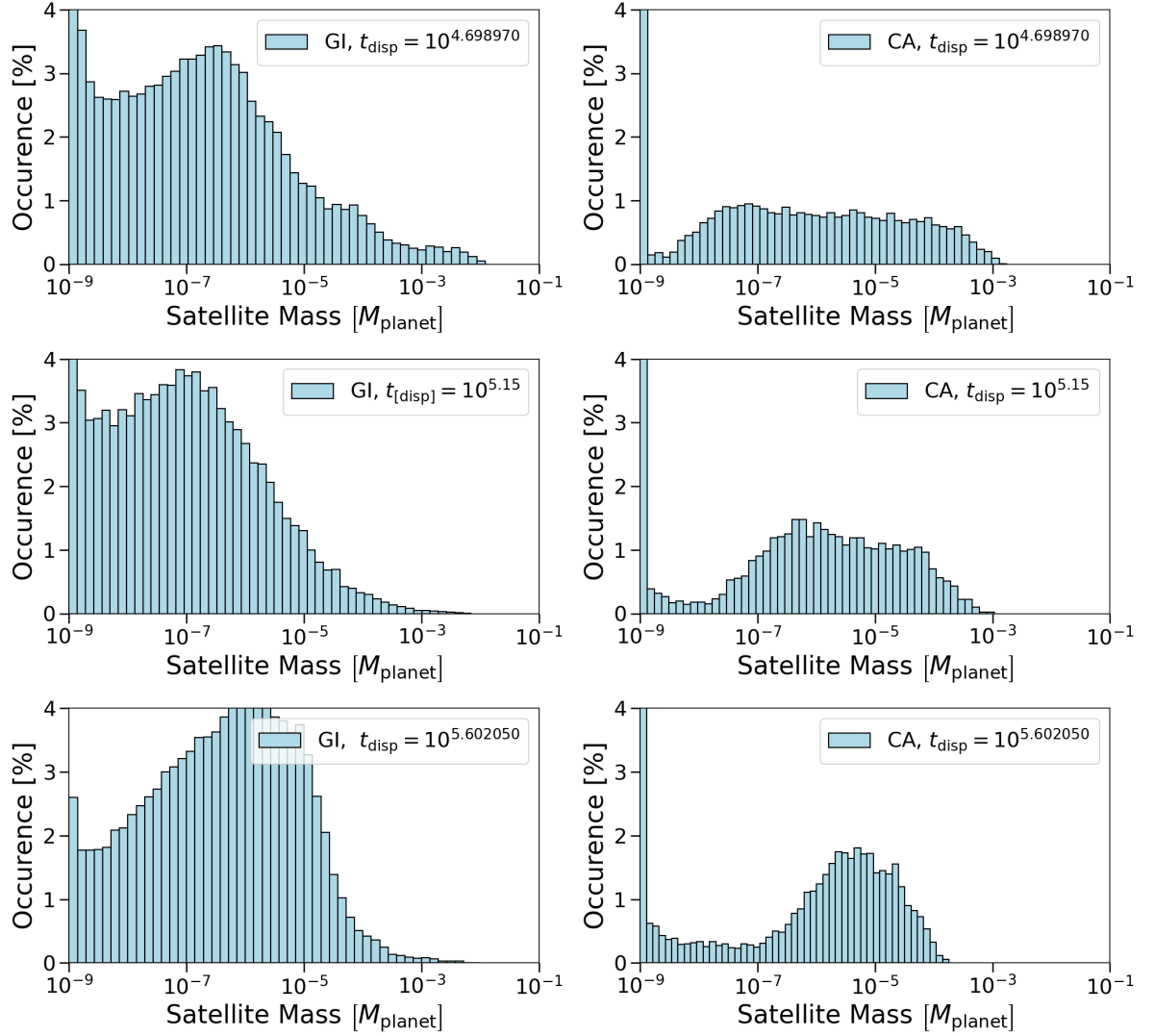


Figure 12: This plot shows the distribution of satellite masses in planet masses, split into the GI and CA case and for simulations where either the dispersion timescale was set at different numbers instead of varying them.

Mass of surviving satellites at the end of the simulation

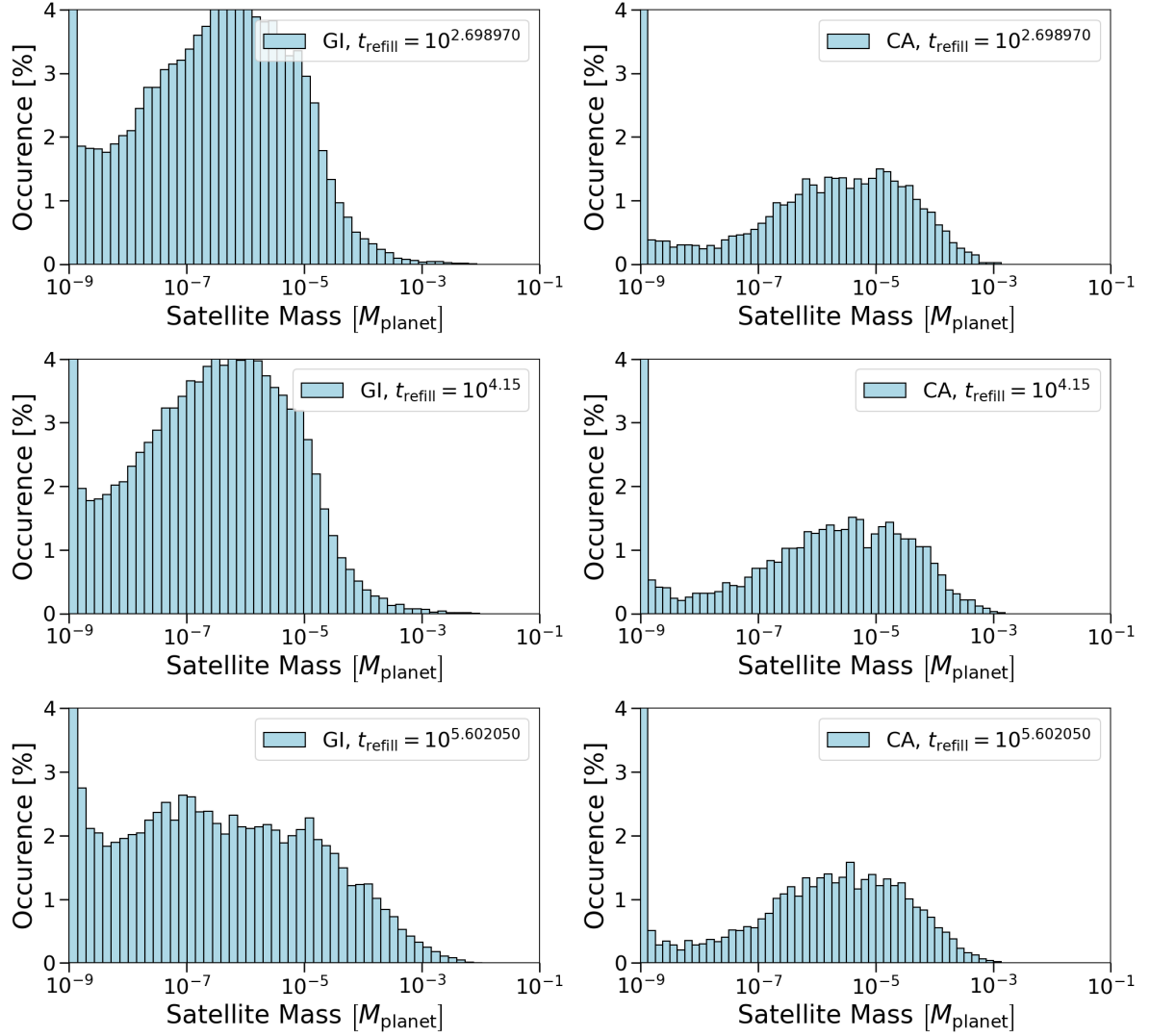


Figure 13: This plot shows the distribution of satellite masses in planet masses, split into the GI and CA case and for simulations where either the the refilling timescale was set at different numbers instead of varying them.

Lost versus retained mass

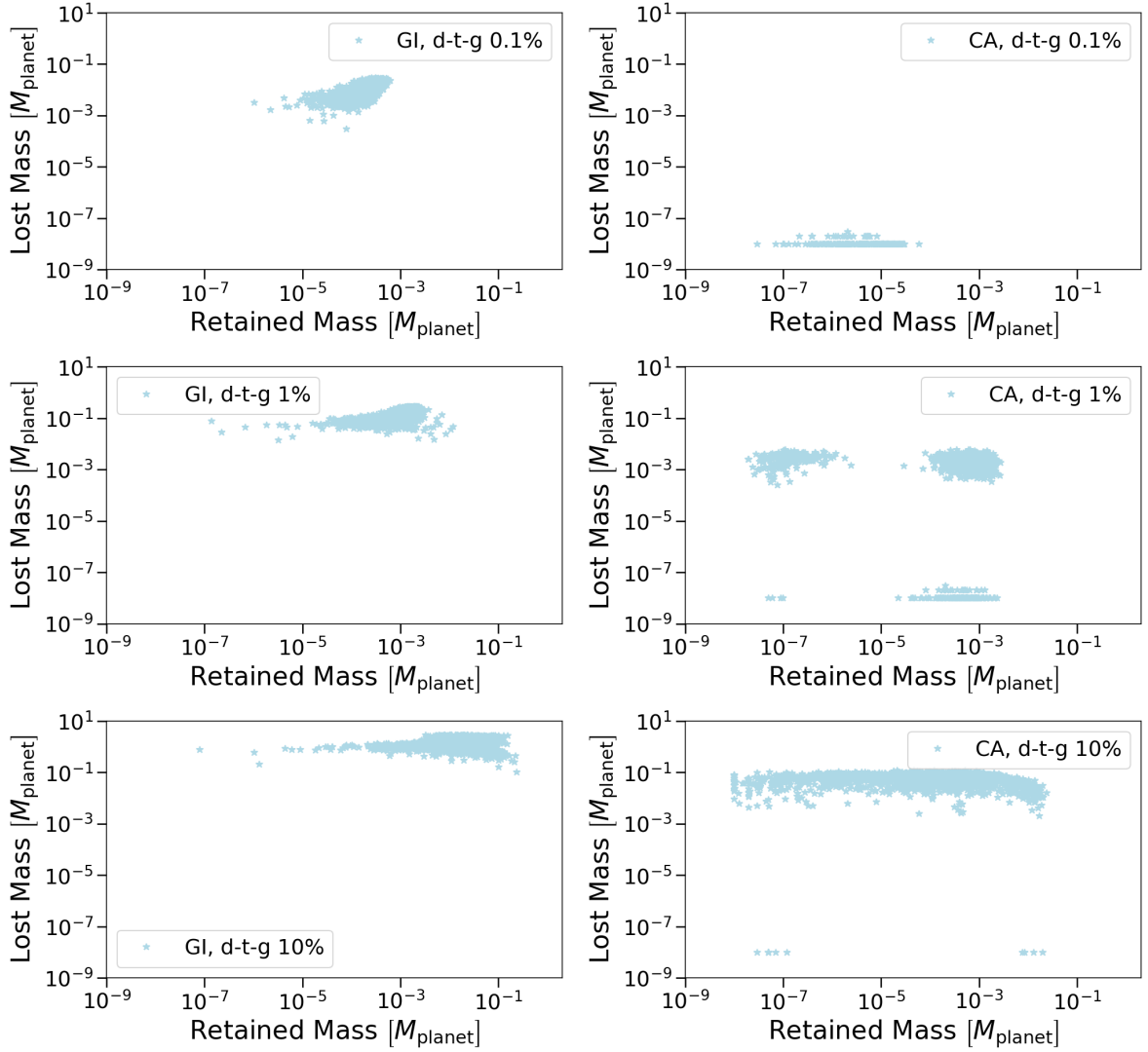


Figure 14: This plot shows the lost mass versus the retained mass of a given satellite system, split into the GI and CA case and for simulations where the dust-to-gas ratio was set at different numbers instead of varying them.

Lost versus retained mass

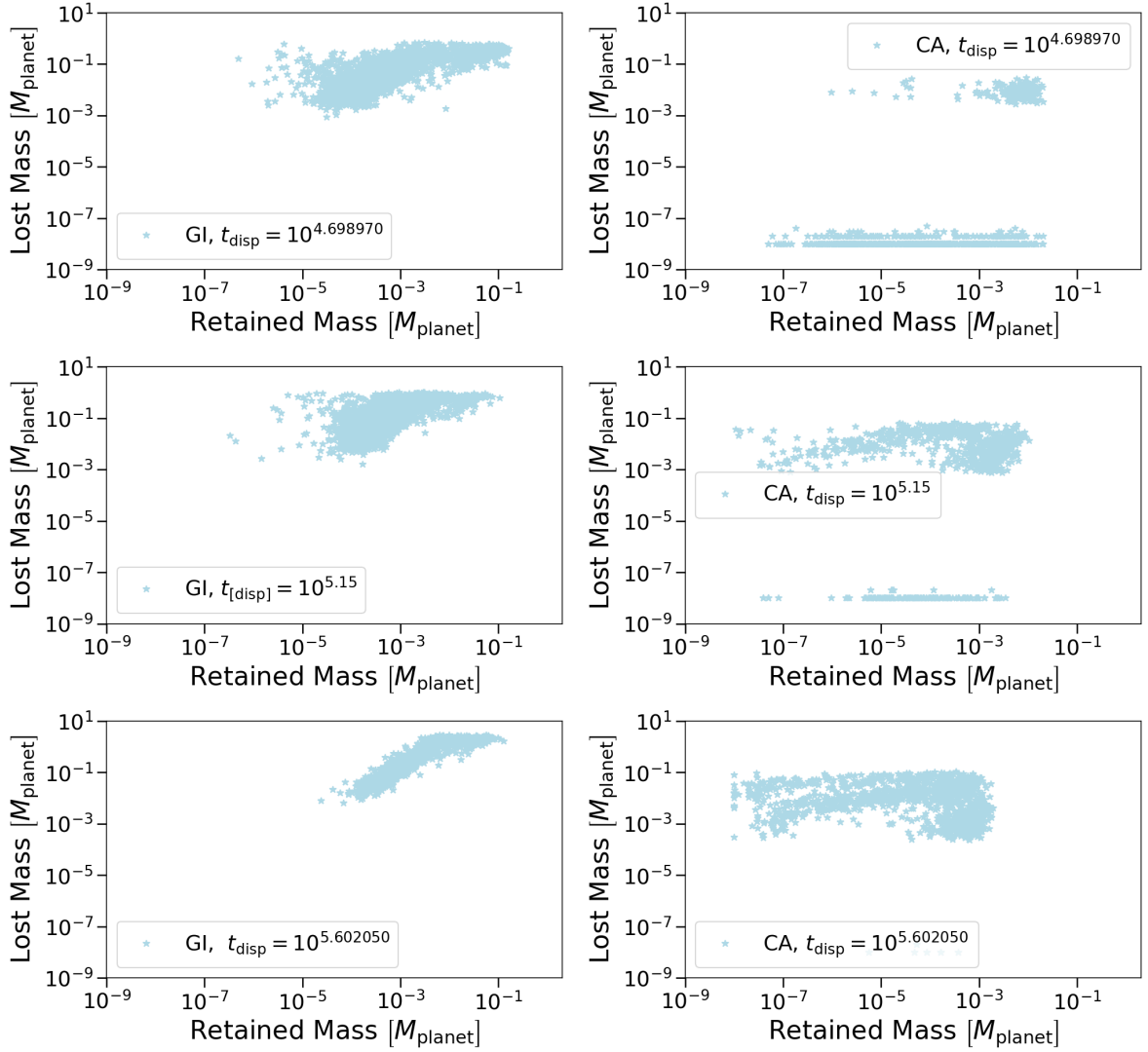


Figure 15: This plot shows the lost mass versus the retained mass of a given satellite system, split into the GI and CA case and for simulations where the dispersion timescale was set at different numbers instead of varying them.

Lost versus retained mass

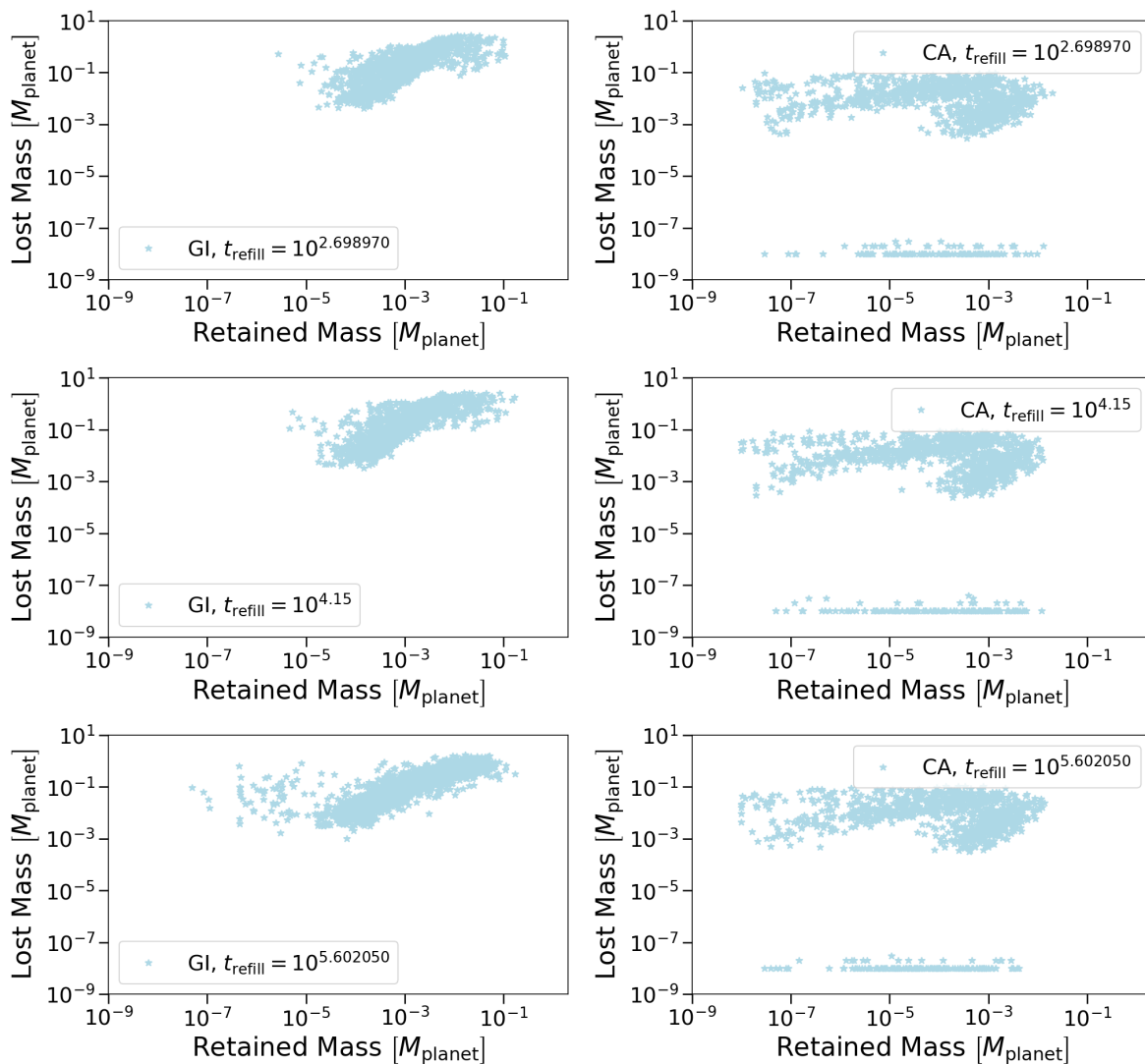


Figure 16: This plot shows the lost mass versus the retained mass of a given satellite system, split into the GI and CA case and for simulations where the refilling timescale was set at different numbers instead of varying them.

more mass. In the CA disk again the lost mass increases as dispersion timescales do, as now the longer disk lifetimes mean more first generation satellites get lost. Accordingly, the retained mass lowers.

3. Set refilling timescale (fig. 16): In both disks, the refilling timescale has only a slight influence, although for different reasons: In the GI disk the masses are higher on average for lower refilling timescales, so for there to be few changes there have to be less satellites on average over all which we see in fig. 23. In the CA disk masses and number of satellites remain the same so retained mass does as well. In both cases, the lost mass is made up of first generation satellites which take their mass mostly from the disk and not the infalling material, so refilling is not a driving influence on them.

Fig. 17, fig. 18 and fig. 19 show the integrated mass of the systems, which follow the conclusions drawn in the previous discussions.

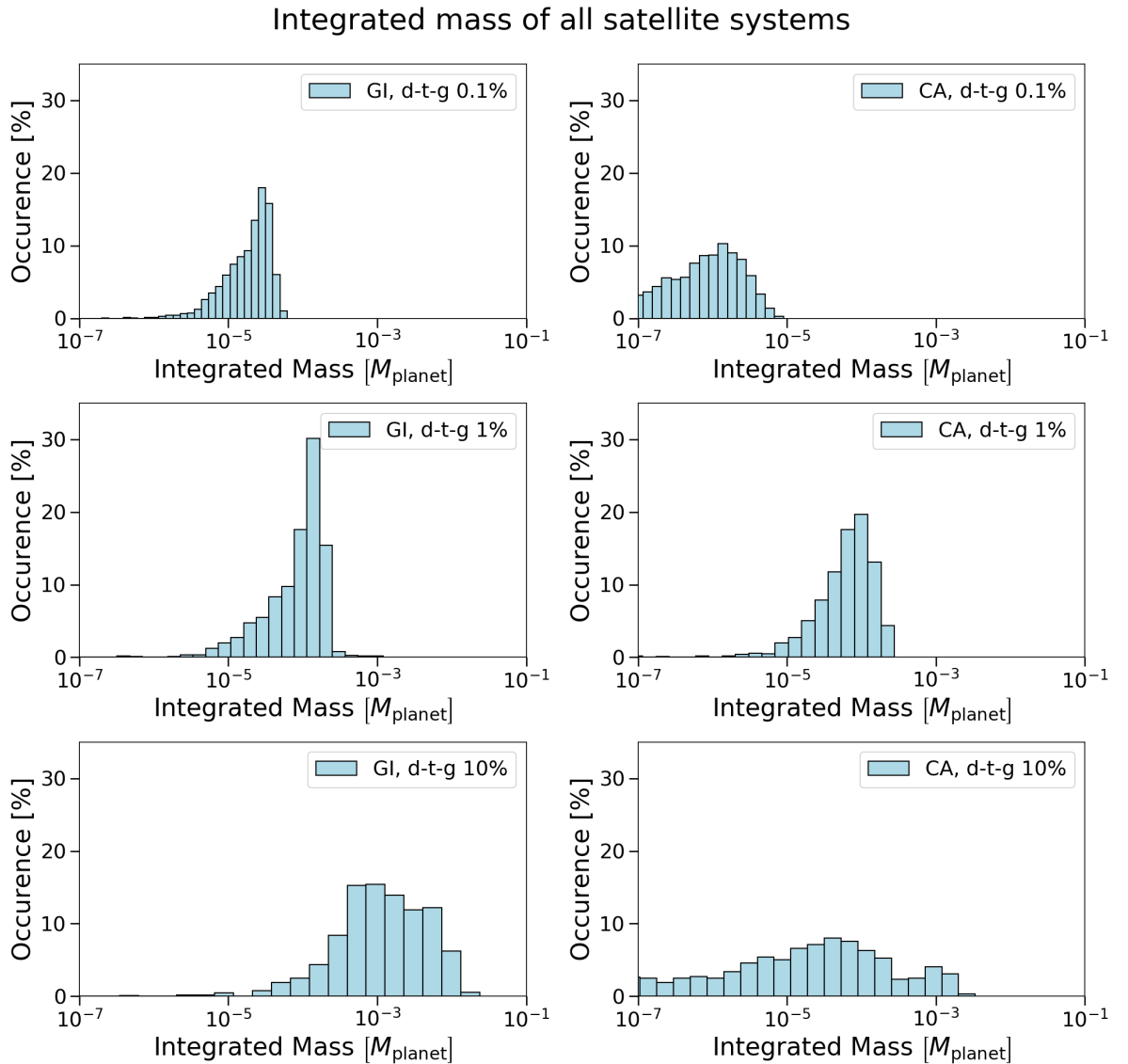


Figure 17: This plot shows the distribution of the integrated masses of satellite systems, split into the GI and CA case and for simulations where the dust-to-gas ratio was set at different numbers instead of varying them.

Integrated mass of all satellite systems

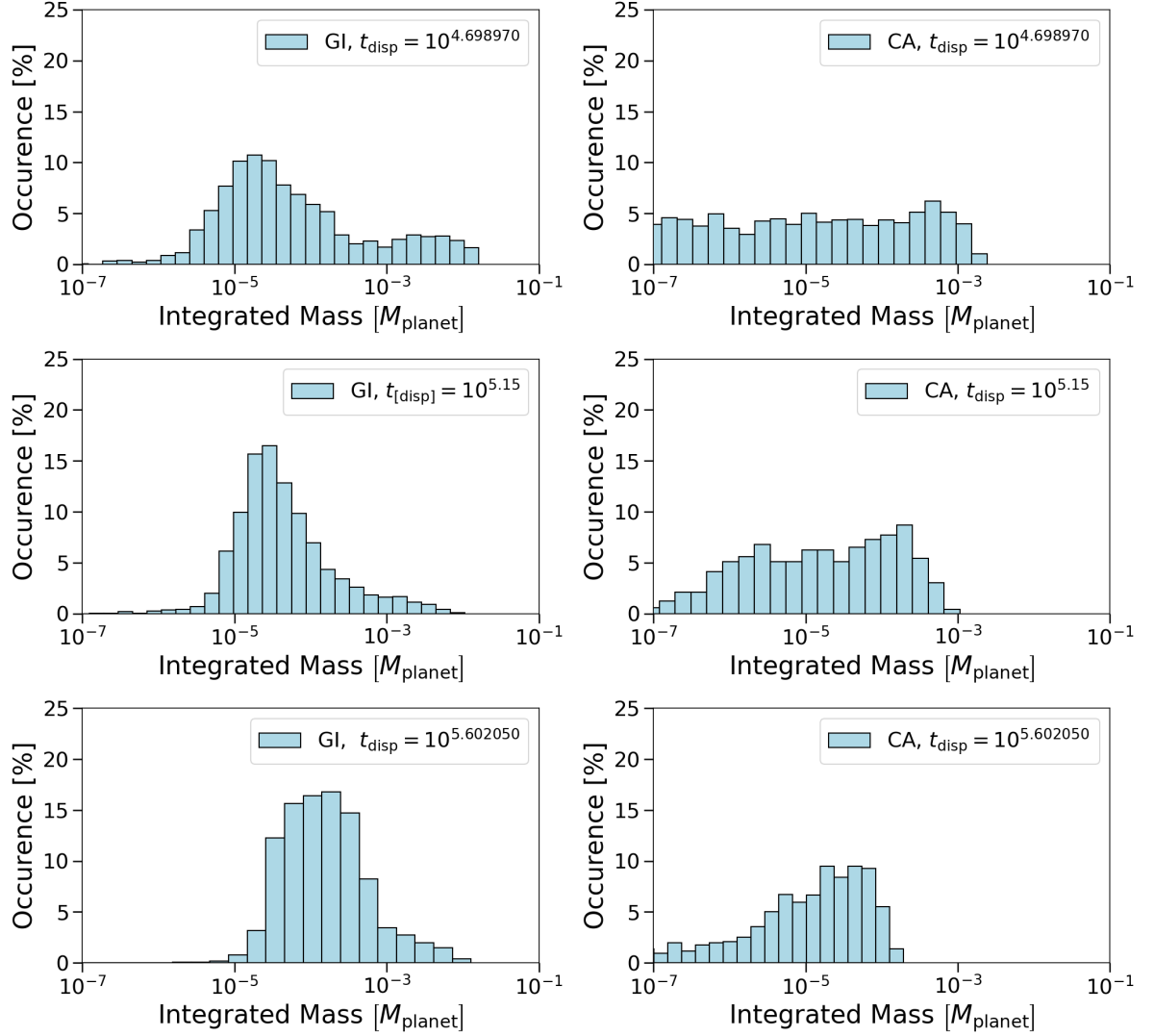


Figure 18: This plot shows the distribution of the integrated masses of satellite systems, split into the GI and CA case and for simulations where the dispersion timescale was set at different numbers instead of varying them.

Integrated mass of all satellite systems

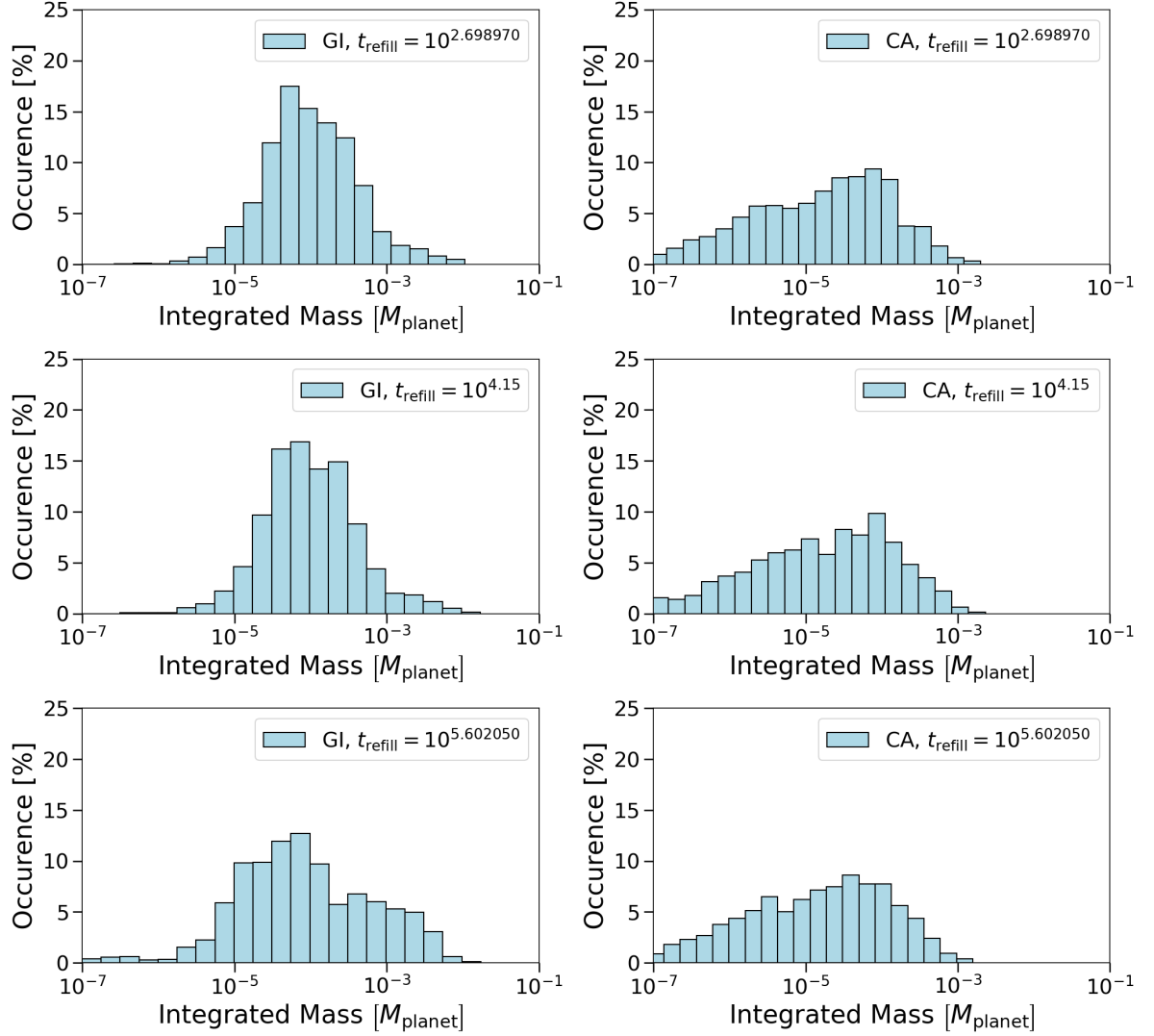


Figure 19: This plot shows the distribution of the integrated masses of satellite systems, split into the GI and CA case and for simulations where the refilling timescale was set at different numbers instead of varying them.

3.2 Number of satellites

3.2.1 All Parameters random

Figure 20 shows the distribution of the number of satellites that reach either at least 10^{-5} planet masses (roughly Europa’s mass) or at least 10^{-6} planet masses (roughly Europa mass relative to the host planet), from here on referred to as case 1 and case 2) and their means and standard deviations can be seen in table 8.

Table 8: Mean and standard deviations of the distributions

Disk type and case	Mean	Standard deviation
GI, case 1	2.943	2.925
GI, case 2	9.245	5.553
CA, case 1	0.847	1.128
CA, case 2	1.628	1.534

In the GI disk there can be a lot of heavy satellites (reaching Earth mass and higher), in a few cases more than 10, but in most cases there are only a handful that reach this mass and the higher the number the less likely it becomes. This may seem like a lot, but the disk is very big and in principle has the space for so many to form. In comparison, Jupiter has 4 massive satellites (although none that are this heavy relatively) and if we assume the CPD size scales with the Hill radius (which it roughly does) than, as this planet is 10 Jupiter masses, the CPD would be roughly 3 times bigger and thus 10 satellites does seem like a reasonable number.

Looking at effectively roughly Europa sized satellites, there are even more of them, up to more than 20 and the distribution is much flatter. There are few systems that don’t have at least one case 2 satellite (which agrees with the observations in fig. 9 about the retained masses) and there is one peak around 3 and another, less pronounced one around 12.

The two distributions look very differently, where it is a lot easier to create case 2 satellites and it gets a lot harder to create heavy satellites.

In the CA disk, things are very different. It is much harder to produce many satellites and generally it will be less than 10 and in only about half the systems such heavy satellites even form and the possibility of forming them declines rapidly the higher the number is (so for 4 or higher it is already less than 10% of the cases). This is a consequence of the hot disk which pushes formation positions farther out and thus there will be less dust available and thus less chances for satellitesimals to grow this big. This can also be seen when looking at case 2 satellites, as the distribution looks very similar. This means that those that do form have an easier time to become very heavy, but at the cost of others reaching roughly Europa mass.

3.2.2 One parameter set

The influence of different set parameters on the number of satellites shows the following behaviour:

1. Set dust-to-gas ratio (fig. 21): In the GI disk both case 1 and 2 behave similarly as dust-to-gas ratio increases: there are more of both of them. In the CA disk for both low and intermediate ratios, in both case 1 and 2 the maximum number of satellites increases with the ratio. However, for the high dust ratio the maximum lowers but overall there are higher occurrence rates, as with higher dust-to-gas ratio the high mass ones are lost easier so systems with more heavy satellites become less likely.
2. Set dispersion timescale (fig. 22): The GI disk again shows the same tendency for both case 1 and 2: the higher the dispersion timescale the more satellites can accrete the threshold masses. For the CA disk the dispersion time doesn’t have much influence on the numbers.
3. Set refilling timescale (fig. 23): In the GI disk for case 1, the refilling timescale has only a little influence, making it a bit harder for systems with more than 6 or 7 satellites to

Number of surviving satellites at the end of the simulation

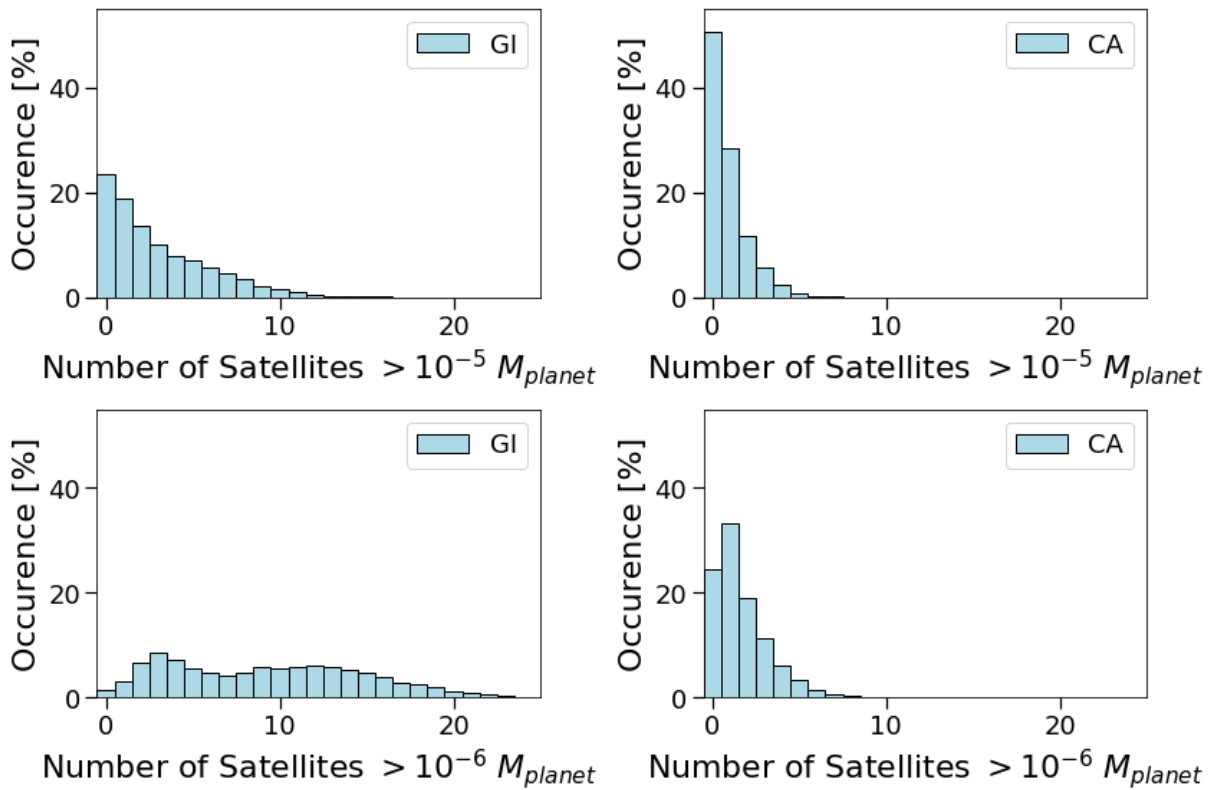


Figure 20: This plot shows the distribution of the number of satellites a given system has. In the GI disk case 1 is more or less an exponentially decaying distribution towards higher numbers, whereas case 2 has two peaks, one narrow one around 4 and a wide one around 10, showing that once you get past around 6 satellites in a system with roughly Europa mass it is very easy to get even more than that. In the CA disk case 1 and 2 are very similar, where the only major difference is that there are less systems with no Europa sized satellites than there are systems with no satellites $> 10^{-5}$ planet masses.

Number of surviving satellites at the end of the simulation

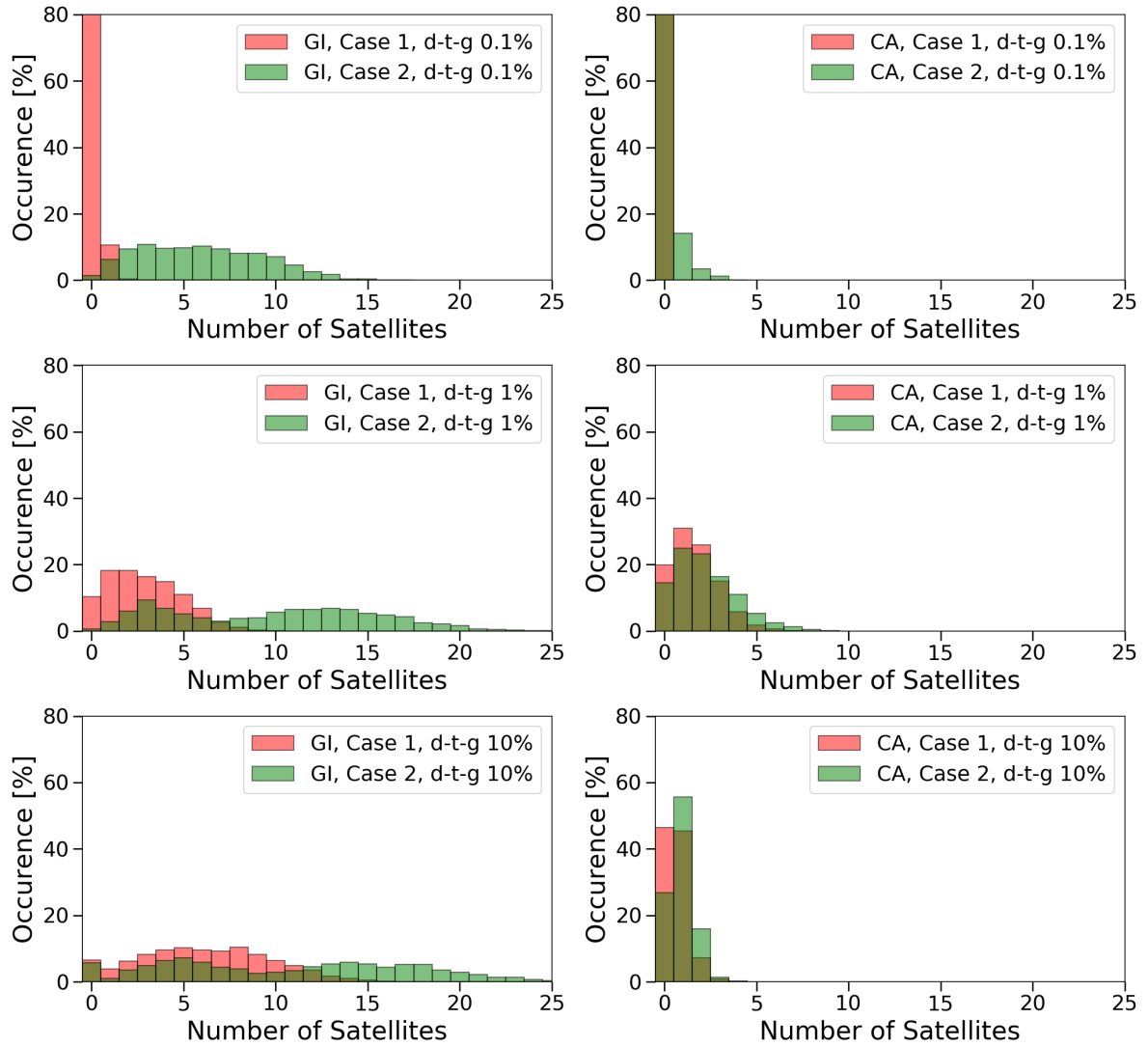


Figure 21: Distribution of number of satellites in a given system, split into the GI and CA case and for simulations where the dust-to-gas ratio was set at different numbers instead of varying them.

Number of surviving satellites at the end of the simulation

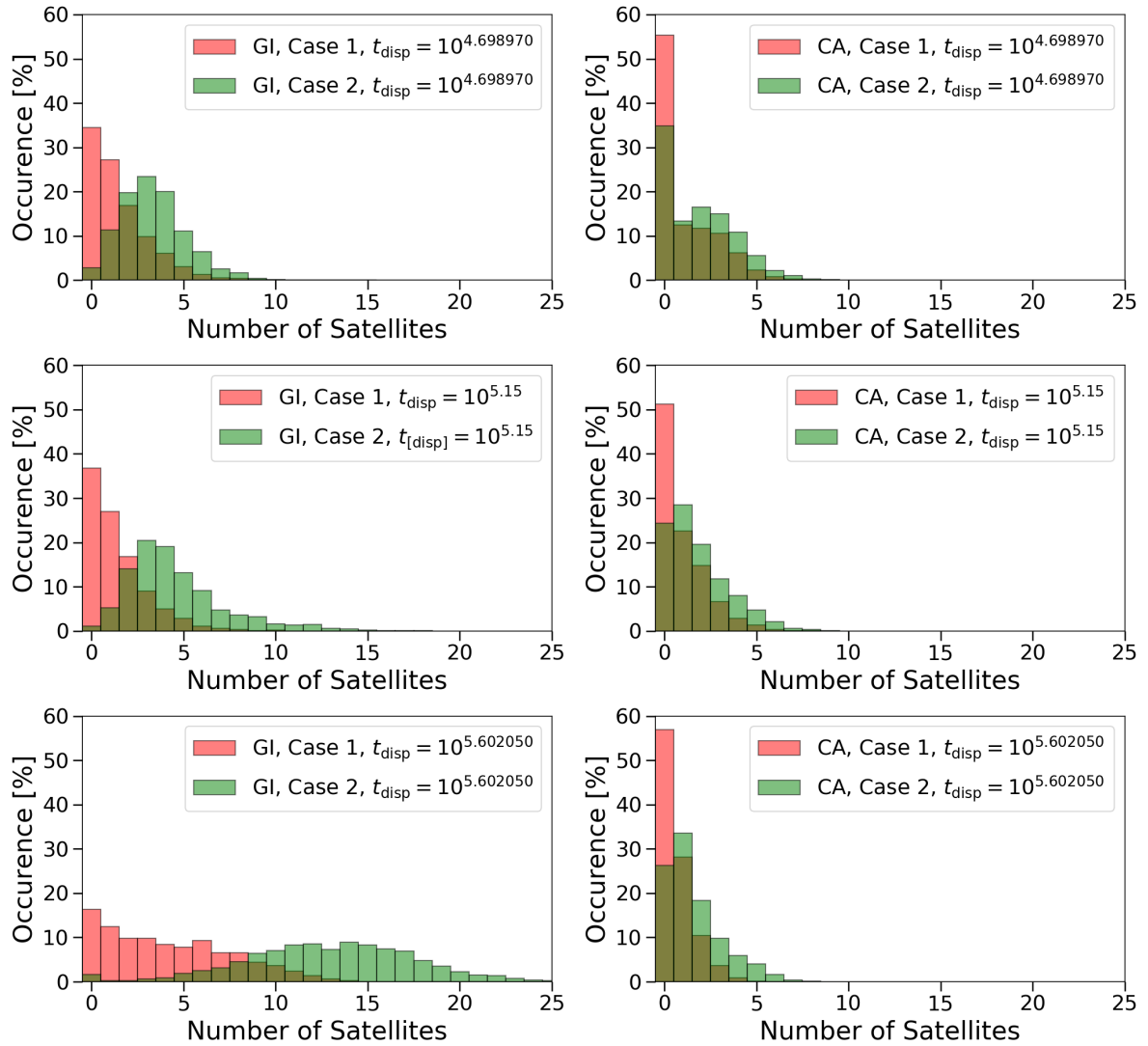


Figure 22: Distribution of number of satellites in a given system, split into the GI and CA case and for simulations where the dispersion timescale was set at different numbers instead of varying them.

Number of surviving satellites at the end of the simulation

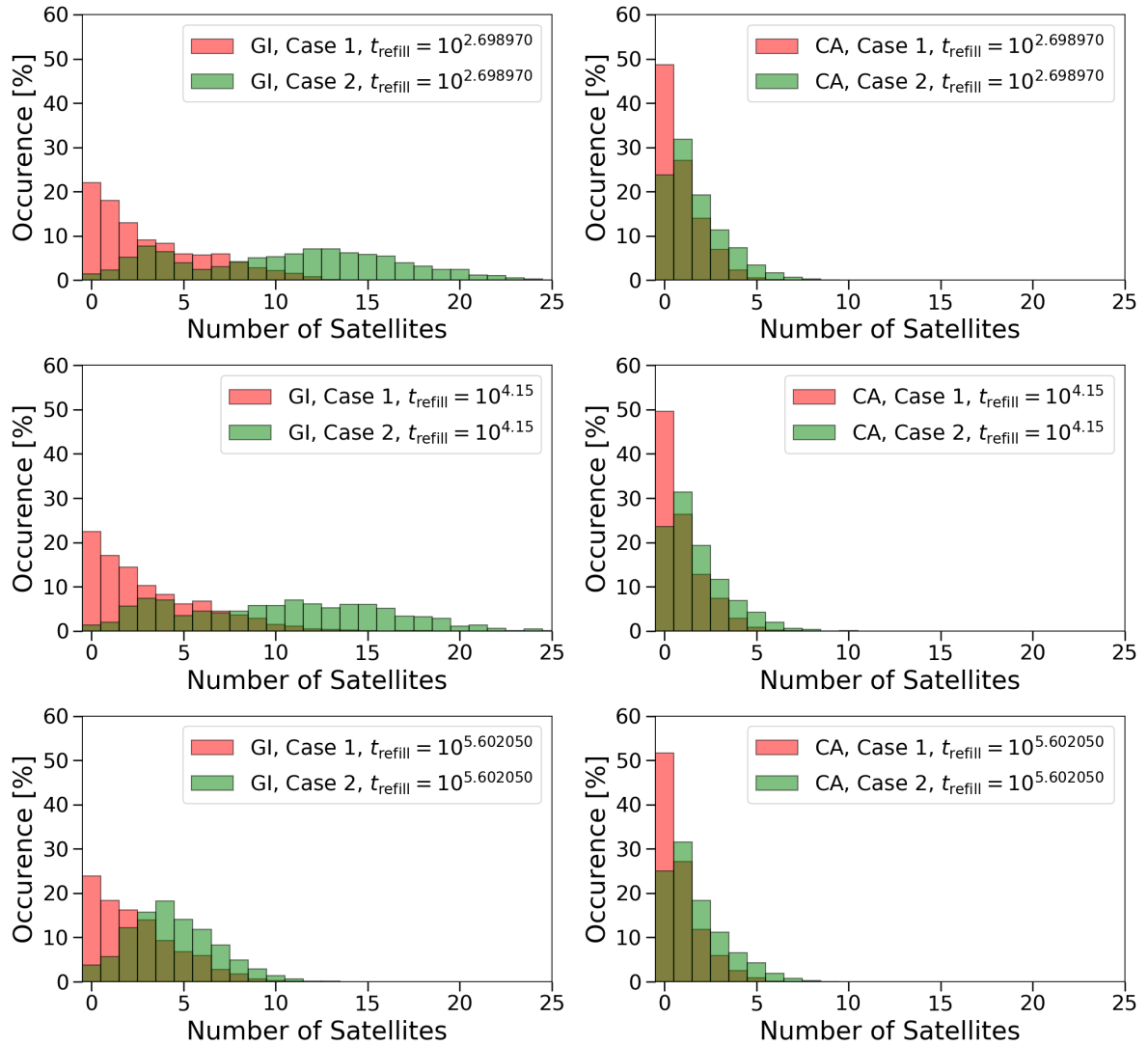


Figure 23: Distribution of number of satellites in a given system, split into the GI and CA case and for simulations where the refilling timescale was set at different numbers instead of varying them.

form, as for more satellites in a system the chances are higher for one of them to migrate into the planet. In case two, low and intermediate refilling look very similar, while for high timescales there are much less systems with more than 10 satellites, but a higher occurrence for systems with around 5 satellites. In the CA disk, the refilling timescale has almost no influence on the number of satellites in both case 1 and 2.

3.3 Positions of orbit

3.3.1 All parameters random

Figure 24 shows the distribution of orbital radii of the satellites remaining at the end of the simulations. In the GI disk there are distinct differences between cases 1 and 2. For case 2, there are 3 regions of clustering: one very close to the planet, with orbits at a handful of times that of the planet radius, one in the mid region (which is very wide) and one far out. Most end up in the second and third region (and those regions are mostly populated by satellites with masses $< 10^{-5} M_{\text{planet}}$) for two reasons: the first is the existence of a "migration barrier", a region at about $4 \cdot 10^{-1}$ disc radii. To migrate past this, due to the low gas densities that far out, an embryo needs to accrete a lot of mass very fast because migration scales with mass and this has to overcome the fact that disk dispersion lowers gas density over time. This usually requires an embryo to be created early in the disk's life, but depending on the available dust can also happen later. So the mid region is made up of satellites that just barely managed to make it past the migration barrier but late enough that the dispersion meant they couldn't migrate much further anymore as well as satellites that were created in this region who didn't manage to migrate far due to either late formation or a low amount of available dust. The outer region is made up of the satellites that are created early but can't make it past the migration barrier and thus they can accrete over a long time over a large region (as this far out the feeding radius will be very big), which still allows them to grow heavy. The inner most peak is a result of feeding radius shrinking the closer a satellite gets to the planet so migration will slow down as accretion essentially stops and the gas disperses.

Case 1 illustrates the connection between mass and migration very well: the distribution is shifted heavily to lower radii. That is because heavy satellites like this will have a much easier time migrating and thus more of them will make it past the migration barrier and past the mid region. There is still a peak far out because, again, if an embryo is created early enough but accretes slowly throughout its life it can still become very heavy.

The CA disk has slightly different behaviour. Due to the on average farther out creation it is much harder for satellites to reach the mid to inner regions. Most don't make it past the migration barrier and most of those that do migrate out of the mid region as well. These satellites are made up of on one hand the first and second generation ones that are created just early enough to get past the migration barrier but but also just late enough to not migrate into the planet. Combined with this disk being less dense the inner peak is also wider. On the other hand they are made up of the mid region satellites that can accrete and migrate enough. This mid region, which in the GI case is at least partially replenished by outer region satellites migrating into it, is depleted in the CA case specifically because it is so much harder for satellites to migrate into it.

Comparing cases 1 and 2 it is also, unlike in the GI disk, apparent that the distributions are very similar. This suggests that mass and the speed of accretion are much less important to where satellites end up as compared to the GI disk, where heavier satellites will end up closer to the planet.

Radial distribution of surviving satellite orbits at the end of the simulation

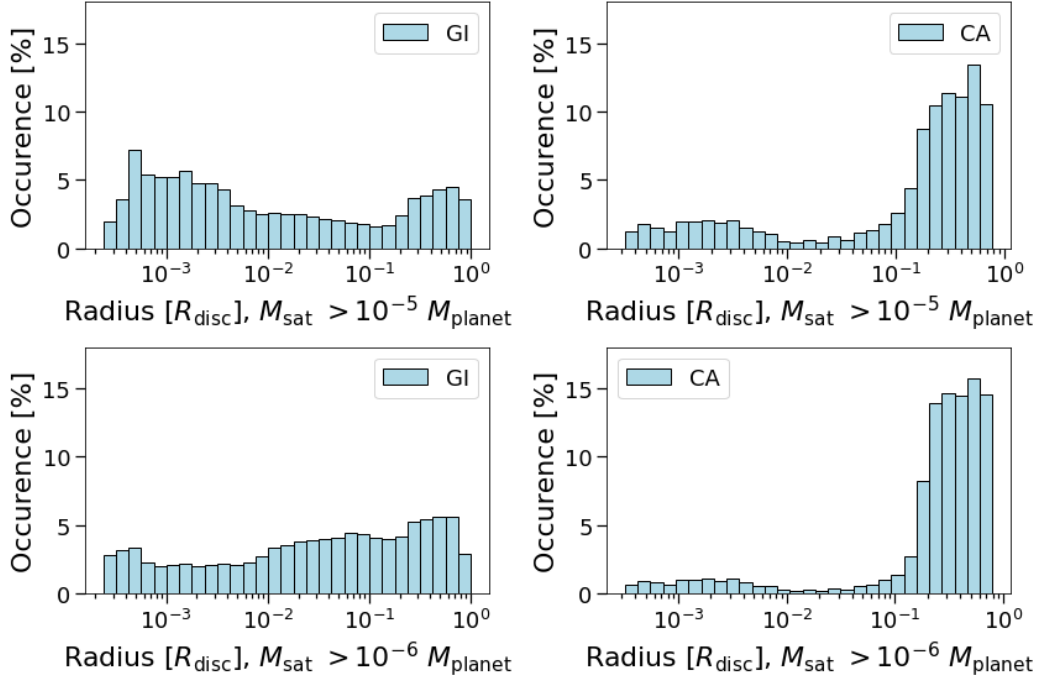


Figure 24: This plot shows the distribution of radial positions of the satellites that survive until the end of the simulation, where the top row is the distribution for satellites with mass $> 10^{-5}$ planet masses and the bottom row with mass $> 10^{-6}$ planet masses. In the GI disk, case 2 has three distinct regions where satellites cluster: an inner one, at about a handful of planet radii, a middle one, between about 1% to 10% of disk radius and an outer one past about 30 % of disk radius. Case 1 on the other hand has two regions of cluster: the inner one that is wider than in case 2 and the outer one that is roughly as wide, illustrating the easier time heavy satellites have in migrating in such a disk. The CA disk distributions look very similar in both cases, with most satellites being in the outer region and a few close to the planet, illustrating that satellites of all sizes have problems migrating and that other factors than mass influence where they end up.

3.3.2 One parameter set

Radial distribution of surviving satellite orbits at the end of the simulation

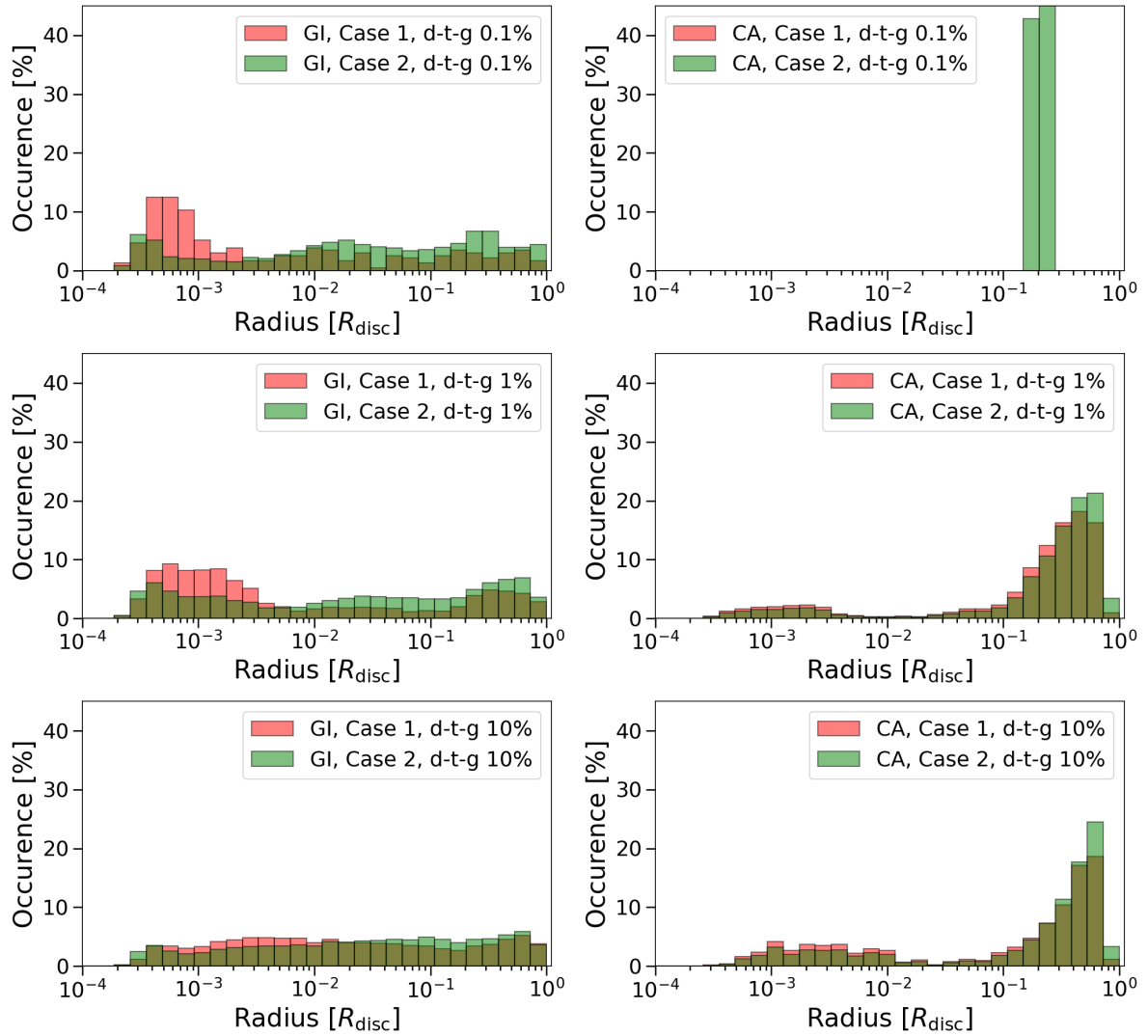


Figure 25: This plot shows the distribution of radial positions of the satellites that survive until the end of the simulation, split into the GI and CA case and for simulations where the dust-to-gas ratio was set at different numbers instead of varying them.

Radial distribution of surviving satellite orbits at the end of the simulation

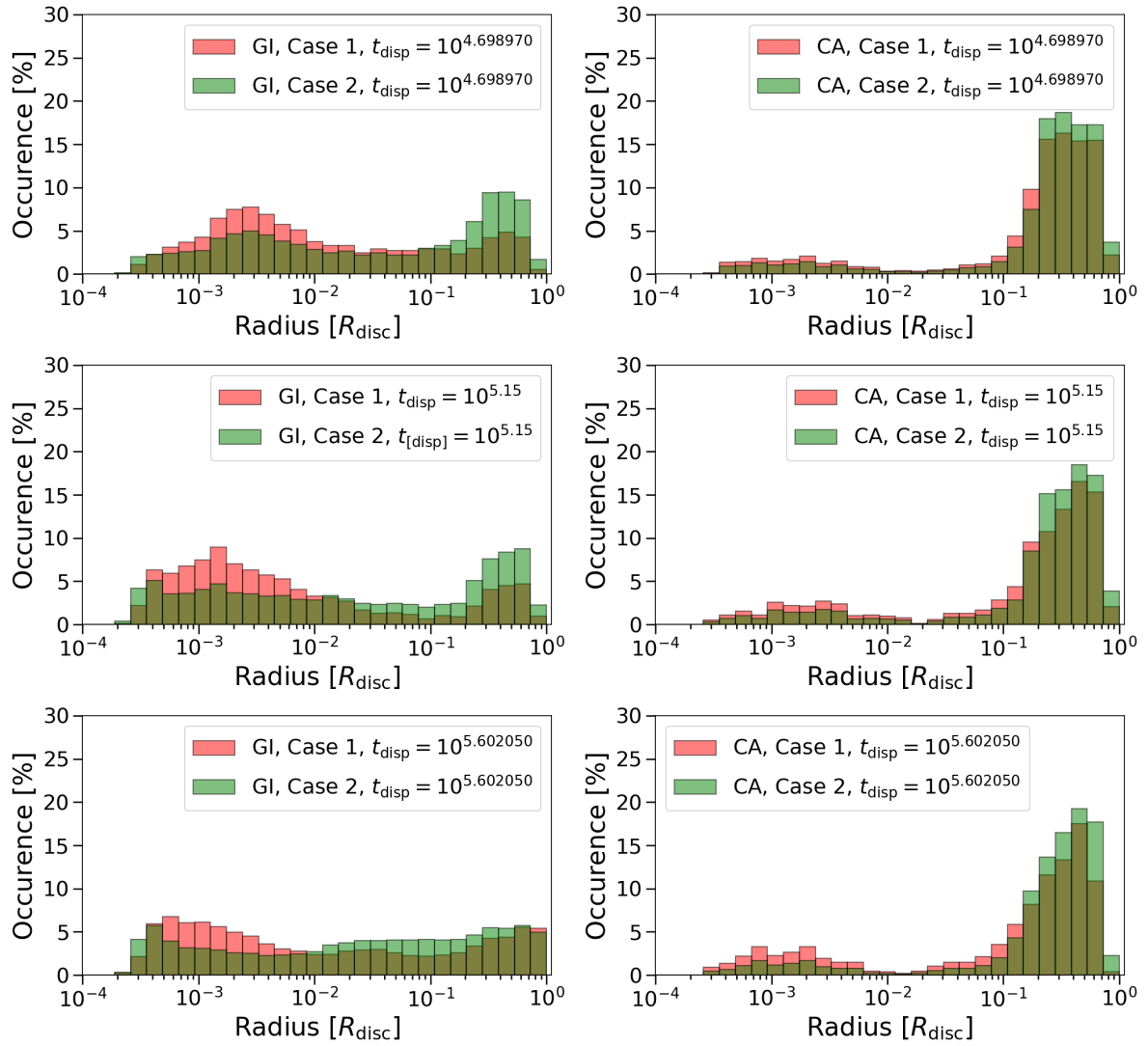


Figure 26: This plot shows the distribution of radial positions of the satellites that survive until the end of the simulation, split into the GI and CA case and for simulations where the dispersion timescale was set at different numbers instead of varying them.

Radial distribution of surviving satellite orbits at the end of the simulation

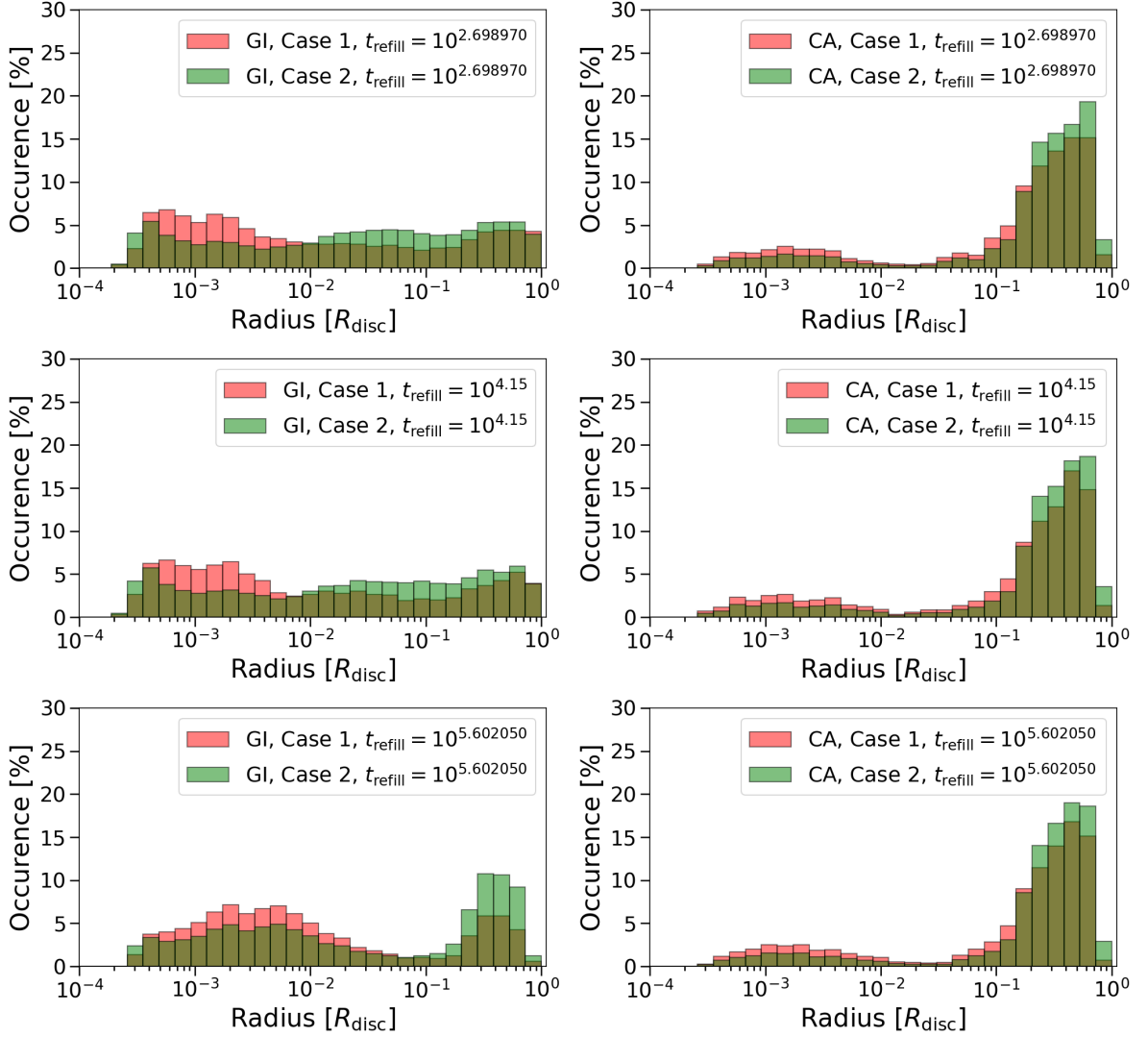


Figure 27: This plot shows the distribution of radial positions of the satellites that survive until the end of the simulation, split into the GI and CA case and for simulations where the refilling timescale was set at different numbers instead of varying them.

The influence of different set parameters on the positions at the end of the simulation shows the following behaviour:

1. Set dust-to-gas ratio (fig. 25): In the GI disk the influence of dust-to-gas ratio works to equalize the distribution. For case 1, the distribution for lowest value is dominated by one peak close to the planet and a relatively equal distribution over the rest of the disk. This inner peak exists because the low dust content means they accrete mass slower and thus also migrate slower, preventing them from falling into the planet. They tend to be old, which is what allows them to accrete this much mass until the end (see also fig. 37). As the ratio increases, some of these heavy ones start to get lost into the planet (leading to more lost mass as seen in fig. 14), but there are more now that can migrate out of the mid region of the disk as well, widening the inner peak. Additionally, now the ones past the migration barrier can accrete more as well, creating a noticeable peak in the outer region. For the highest ratio the distribution mostly equalizes (due to higher numbers of satellites making it past the migration barrier), but the innermost region is slightly depleted now as satellites that migrate that far tend to be heavy enough to fall into the planet. For case 2,

low and intermediate ratios show an opposite distribution: these satellites tend to favour the outer regions and be younger, thus not migrating much and mostly growing in place, although some make it to close orbits. As the ratio increases, the mid region gets slightly depleted as they can now migrate a bit further and there are now two peaks, in the inner and outer region. The highest ratio also equalizes the distribution, showing that if the dust-to-gas ratio is high enough all locations are almost equally as likely to have a satellite end its live there, because overall migration rates are higher. In the CA disk, intermediate and high ratios look very similar for both case 1 and 2, most satellites are in the outer regions due to the higher temperature that makes migration slower. Higher dust-to-gas ratio means more that migrate inwards, but both are dominated by the peak in the outer region. For very low dust-to-gas ratio it is very hard to accrete enough to get past even the case 2 threshold, because the infall is much lower than in the GI case and these will mainly accrete in place.

2. Set Dispersion timescale (fig. 26): The dispersion timescale has little effect on the position distribution in the CA disk. While longer timescales (and this longer disk lifetimes) means more time to accrete and migrate (which shows in an increasing number of satellites in the inner and mid disk and a widening of the outer peak) the distribution stays mostly the same, in both case 1 and 2. In the GI disk the effect is seen by the inner peaks moving towards smaller orbits and the outer peak widening, both effects can be explained by the longer disk lifetimes, which means more time to accrete and migrate.
3. Set refilling timescale (fig. 27): In the GI disk, the distribution for low and intermediate refilling timescales in both case 1 and 2 are very similar, because the refilling is fast enough that all the satellites now move through more or less the same disk, as whatever is depleted by accretion of one satellite is refilled fast enough to look the same to the next satellite that enters a region and now disk mass becomes more important to the masses and thus positions. Case 1 satellites still migrate farther than the case 2 ones and thus both cases dominate different versions of the disk. For the highest refilling timescale (and thus the slowest refilling) both case 1 and case 2 have two peaks around the same locations: a wide inner one and a narrower outer one, where the heavier satellites tend to favour the inner one and the lighter satellites tend to favour the outer one. This difference comes from the fact that, as refilling is low, their mass comes from the disk itself. So all those that migrate have a higher amount of available mass so the heavy satellites favour the inner region because if they can get there they will have accreted more. The opposite is true for the outer regions: migration is low so competition is high and it is harder to accrete a lot without migrating, which is only possible in high dust-to-gas ratio disks. In the CA disk refilling timescale has very little influence on the positions, as infall is lower overall than in the GI case and the smaller migration rate, due to the higher temperatures, means the outer regions (where the first generation tends to be created due to the high temperatures in the inner disk) is where satellites are concentrated and then the infall gets distributed to all of them regardless of speed so it favours neither of the two cases.

3.4 Europa timescales

3.4.1 All parameters random

Table 9: Mean and standard deviations of the distributions.

Disk type and case	Mean	Standard deviation
GI, case 1	$0.599 t_{\text{disp}}$	$0.404 t_{\text{disp}}$
GI, case 2	$0.934 t_{\text{disp}}$	$1.111 t_{\text{disp}}$
CA, case 1	$0.271 t_{\text{disp}}$	$0.134 t_{\text{disp}}$
CA, case 2	$0.402 t_{\text{disp}}$	$0.468 t_{\text{disp}}$

In fig. 28 we can see the distribution of the time it takes for a satellite to reach Europa’s mass.

This mass is used as a measure mainly because it represents (relatively to the planet mass) roughly the mass of the smallest significant satellites we see in the Solar System and because it is a useful comparison as the smallest Jupiter moon. In the GI disk, we can see that in case 2 most satellites form on timescales around or longer than that of a dispersion timescale, with a wide spread, and about half take a fair amount of the disk lifetime to grow this massive. In case 1 they form faster, on average less than a dispersion timescale and in some cases in a few hundred years, owing to favourable combinations of high dust-to-gas ratio and fast dust influx. This shows that for satellites to become significantly more massive than even Jupiter's satellites they have to form very fast, in order to overcome the disk dispersion. Additionally a lot of satellites that are $< 10^{-5}$ planet masses take considerably longer to reach roughly Europa mass, often a significant fraction of the disk lifetime and they are created late enough that they can't accrete mass fast, far enough out to not migrate into the planet or close enough that accretion effectively stops.

In the CA disk, most of the satellites reach Europa mass on timescales lower than a dispersion timescale. In case 2 around 60% form within less than a dispersion time and very few take the whole disk lifetime to do so and they are less spread than in the CA case 2. In the case 1 they form slightly faster than in case 2, which again means they have to form fast enough to overcome disk dispersion. However the ones that form the fastest are still slower in the CA disk than in the GI disk.

We again see the effects of migration: In the GI disk, more first generation satellites (which form the fastest as they have the most disk mass to draw from) are lost so the remaining satellites form slower. Where in the CA disk, because they on average form farther out, less first generation satellites get lost so the remaining ones form faster than in the GI disk. However, as migration and infall is lower there are fewer second generation and later satellites that can reach Europa mass, and as such there are fewer satellites than can reach Europa mass on longer timescales.

Timescales on which satellites reach Europa mass

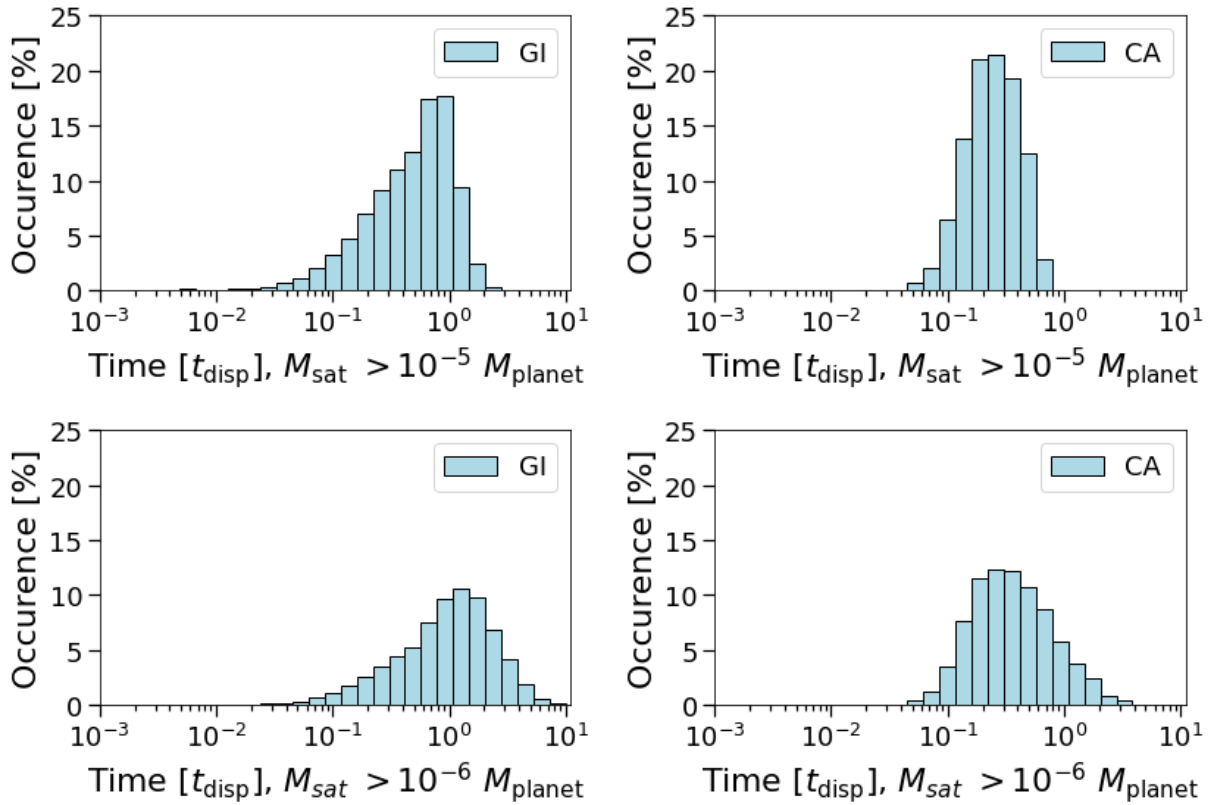


Figure 28: Distribution of timescales after which satellites reach Europa mass. In the GI disk the case 1 satellites reach Europa mass on average much faster, which they have to in order to further increase their mass by about an order of magnitude before the disk dissipates. In the CA disk, the averages are closer but in case 1 the distribution is narrower because if they take long to reach Europa mass it gets harder to grow even more. In the CA disk satellites grow faster than in the GI disk, showing that in the CA disk more satellites are first generation that can grow faster because there is a higher dust density in the disk at that point.

3.4.2 One parameter set

Timescales on which satellites reach Europa mass

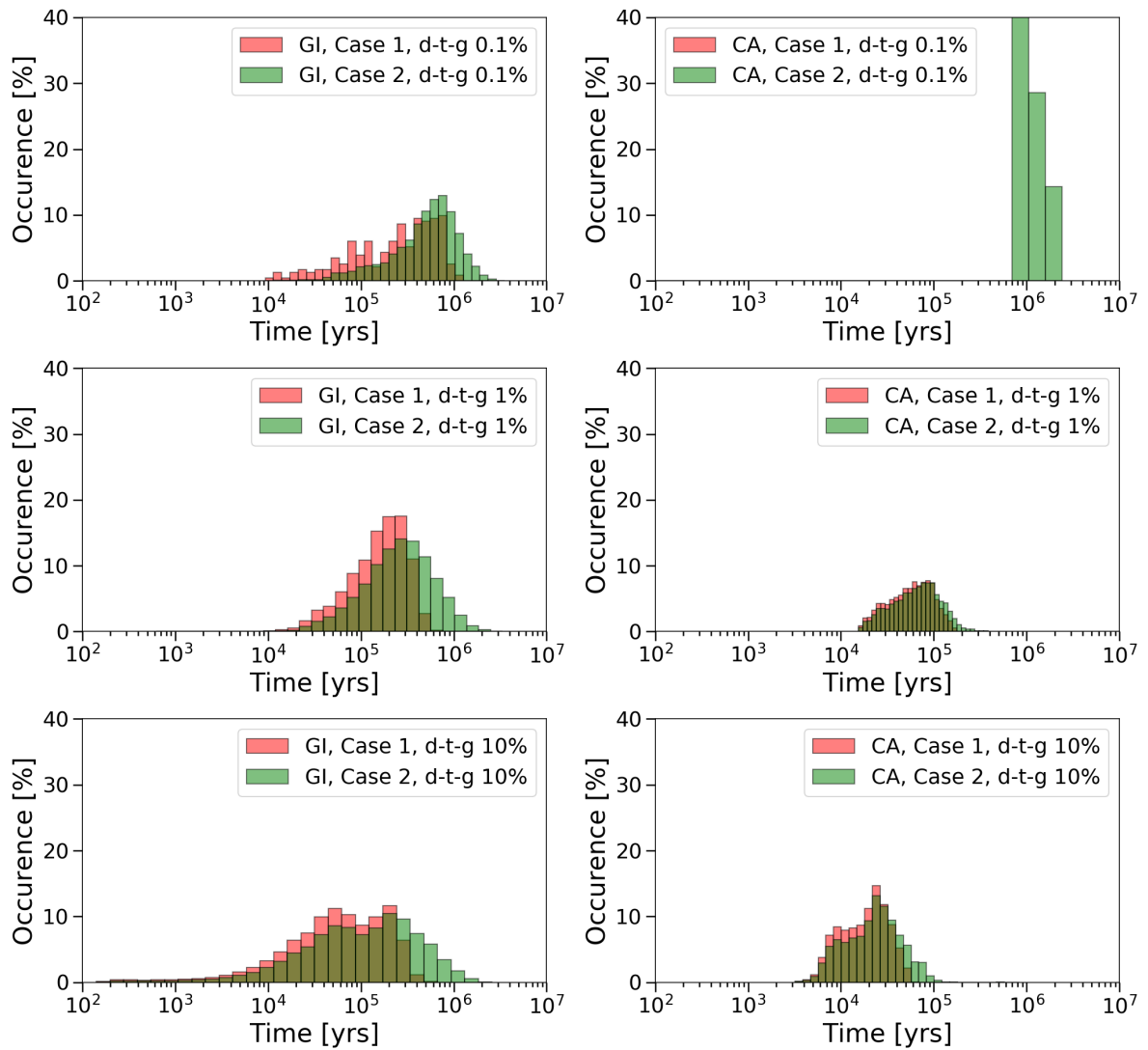


Figure 29: Distribution of timescales after which satellites reach Europa mass, split into the GI and CA case and for simulations where the dust-to-gas ratio was set at different numbers instead of varying them.

Timescales on which satellites reach Europa mass

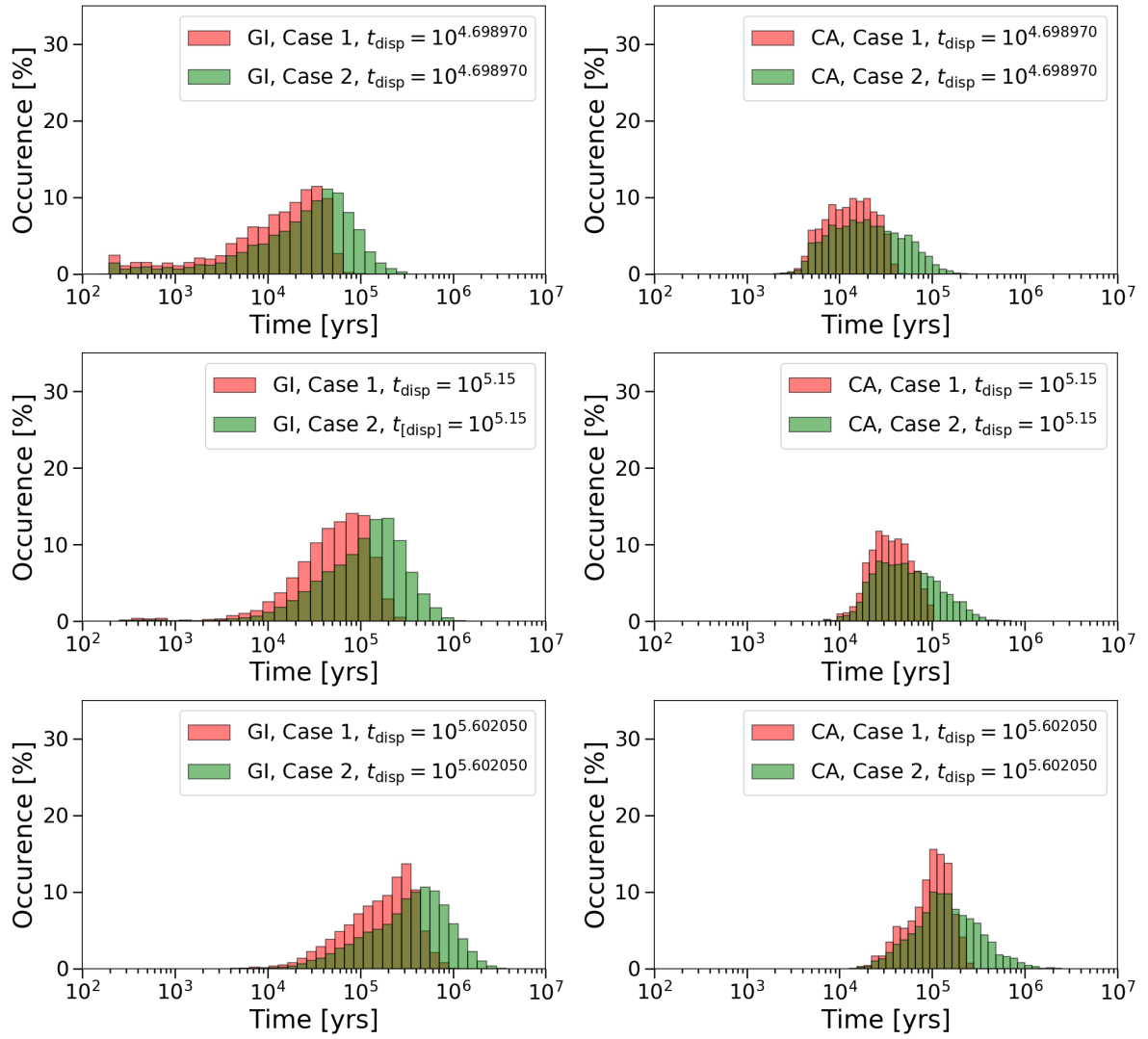


Figure 30: Distribution of timescales after which satellites reach Europa mass, split into the GI and CA case and for simulations where the dispersion timescale was set at different numbers instead of varying them.

Timescales on which satellites reach Europa mass

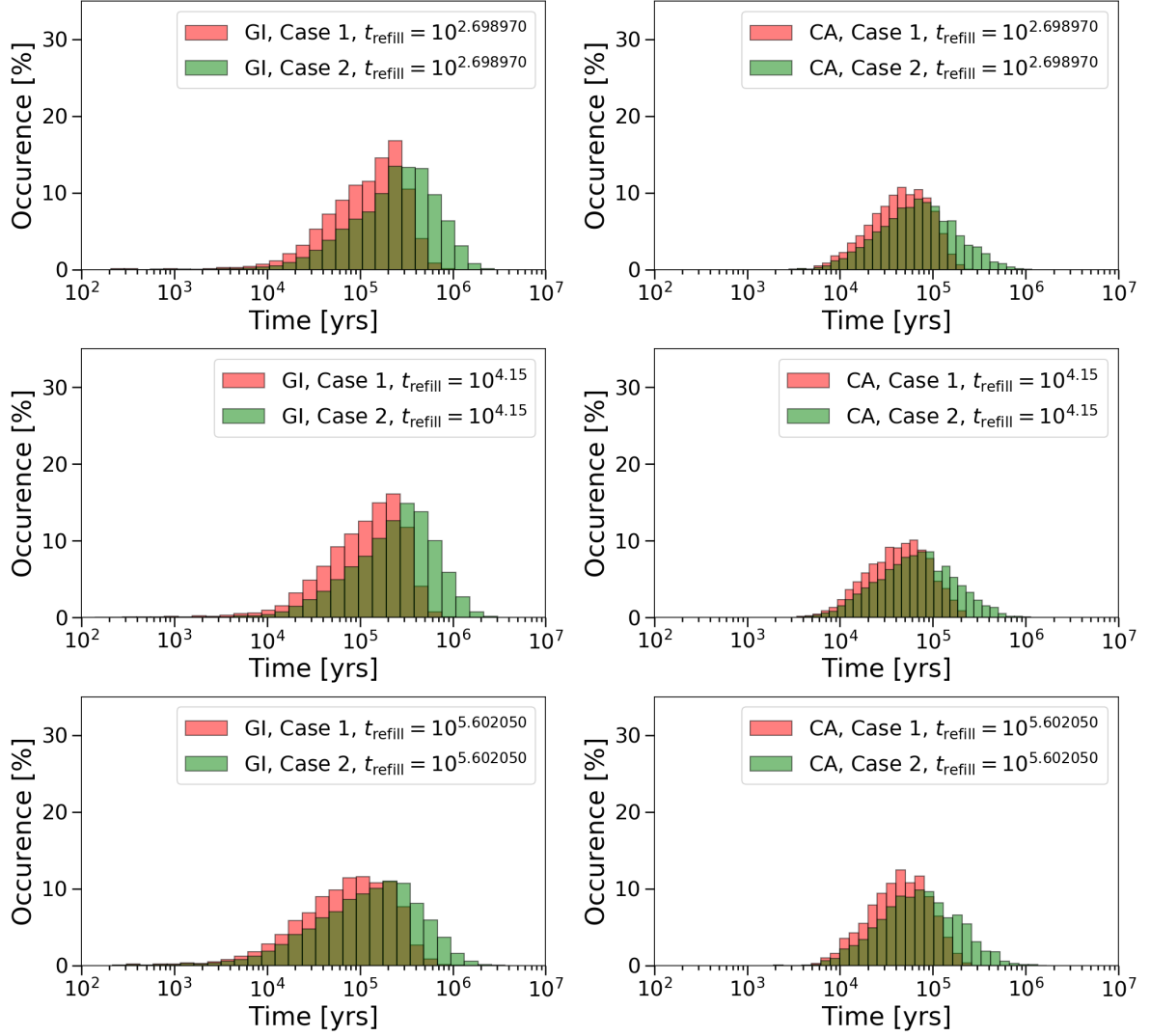


Figure 31: Distribution of timescales after which satellites reach Europa mass, split into the GI and CA case and for simulations where the refilling timescale was set at different numbers instead of varying them.

The influence of different set parameters on the Europa mass timescales shows the following behaviour:

1. Set dust-to-gas ratio (fig. 29): In the GI disk the case 1 satellites favour faster Europa timescales, because for them to then grow another order of magnitude they need the time, while case 2 satellites take longer to reach Europa mass. As the dust-to-gas ratio increases it gets 1) easier for case 1 satellites to form, due to more available mass and 2) in both cases the distributions widen, as it is now easier to have cases of very fast accretion because there is more mass. In the CA disk that is different: for low dust-to-gas ratios it becomes very hard to even reach case 2 mass and those that do take very long. As the ratio increases there are much more that reach case 1 and 2, but the distributions are very similar, where there is only a slight tendency for case 1 satellites to form faster than case 2. For a high ratio, the difference becomes more pronounced, as now more satellites can reach Europa mass overall.
2. Set dispersion timescale (fig. 30): Both the CA and GI disk are very similarly influenced by

the dispersion timescale: in both disks, case 1 satellites tend to form faster than case 2. As the disk lifetime becomes longer, the satellites that form very fast eventually get lost into the planet and more satellites can become heavier, so the whole distribution (in both case 1 and 2) shifts to longer timescales. However, the satellites in the CA disk overall reach threshold masses faster on average, because they are created earlier in the disk and thus have a higher amount of mass they can accrete.

3. Set refilling timescales (fig. 31): In both disks the refilling timescale has little influence on the Europa timescales. In the GI disk that is because (as seen in e.g. fig. 24) the satellites tend to migrate more, so their mass is influenced more by the disk than the infall. On the CA disk, the infall is not high enough to influence the Europa time significantly, as these satellites will reach it mostly due to the initial mass they have at their disposal.

3.5 Formation temperature

3.5.1 All parameters random

Table 10: Mean and standard deviations of the distributions.

Disk type and case	Mean	Standard deviation
GI, case 1	17.59 <i>K</i>	16.22 <i>K</i>
GI, case 2	18.07 <i>K</i>	14.76 <i>K</i>
CA, case 1	655.9 <i>K</i>	239.1 <i>K</i>
CA, case 2	677.9 <i>K</i>	249.9 <i>K</i>

Figure 3.5 shows the distribution of formation temperature, that is the temperature the gas had at the location where the embryo that grew into the satellite was created. The two disks have a vastly different temperature gradient and this can be clearly seen here. The GI disk is even at the beginning below 400 K everywhere and below 180 K (the temperature at which ice forms in a disk) in much of the disk. That means that in both case 1 and 2, all of the satellites will form in a disk where ice can form and thus the expectation will be that they have an icy composition. In case 1, there are a little bit less that form at minimum temperature than in case 2, but by and large the two distributions are very similar. That is partially because the temperature of the disk is so low that it reaches its minimum very fast and that most first and many second generation satellites get lost into the planet, so that the ones that survive tend to be created in very similar temperature environments.

For the CA disk that is different. As it is so much hotter, most of the disk is not a suitable place for embryo creation for a significant part of the disk lifetime. This is reflected in the formation temperatures that are very close to 1500 K, roughly the point where dust sublimates and the temperature after which embryos can start to form. Again cases 1 and 2 do not look all that different because the window for embryo creation is very limited by the temperature, as even once that is low enough for dust to be able to exist, the gas (and thus dust) densities are already lower. So the formation temperatures are high on average because they have to form early enough to be able to accrete a lot of mass, which also shows that many of them will be the first and second generation satellites (few of which migrate into the planet and leading to lower lost mass, see section 3.1). This also means though that almost all of the embryos are created in a disk that is too hot for ice to form. Some might form late enough that they can still accrete appreciable amounts of mass in terms of ice, but even they are likely to be mostly rocky satellites as opposed to the GI case.

Formation temperature of surviving satellites

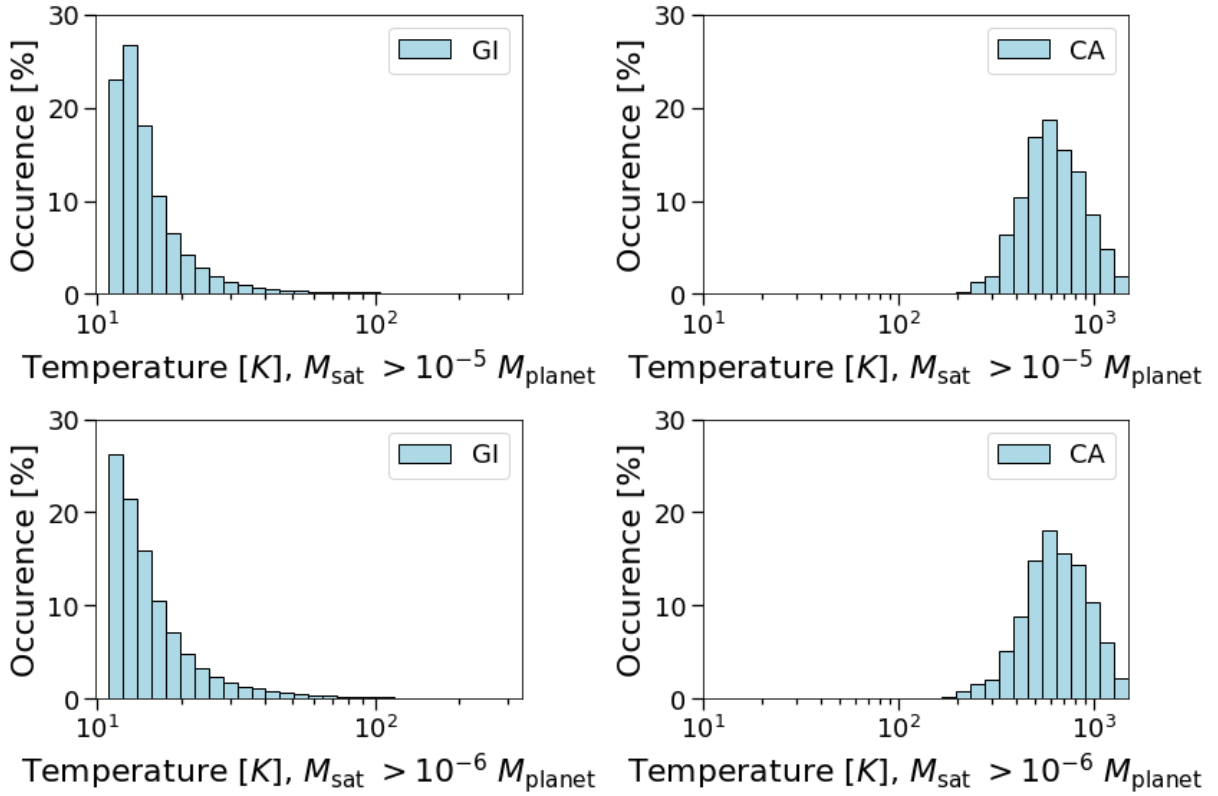


Figure 32: Distribution of formation temperature of satellites. In both disk, the formation temperatures are very similar for both case 1 and 2, so that has very low influence on how heavy a satellite grows. In both case 1 and 2, there is a slight shift to higher temperatures for the case 1 satellites, meaning they were created a little earlier, which makes sense as earlier creation favours more mass, but the shift is minimal.

3.5.2 One parameter set

Formation temperature of surviving satellites

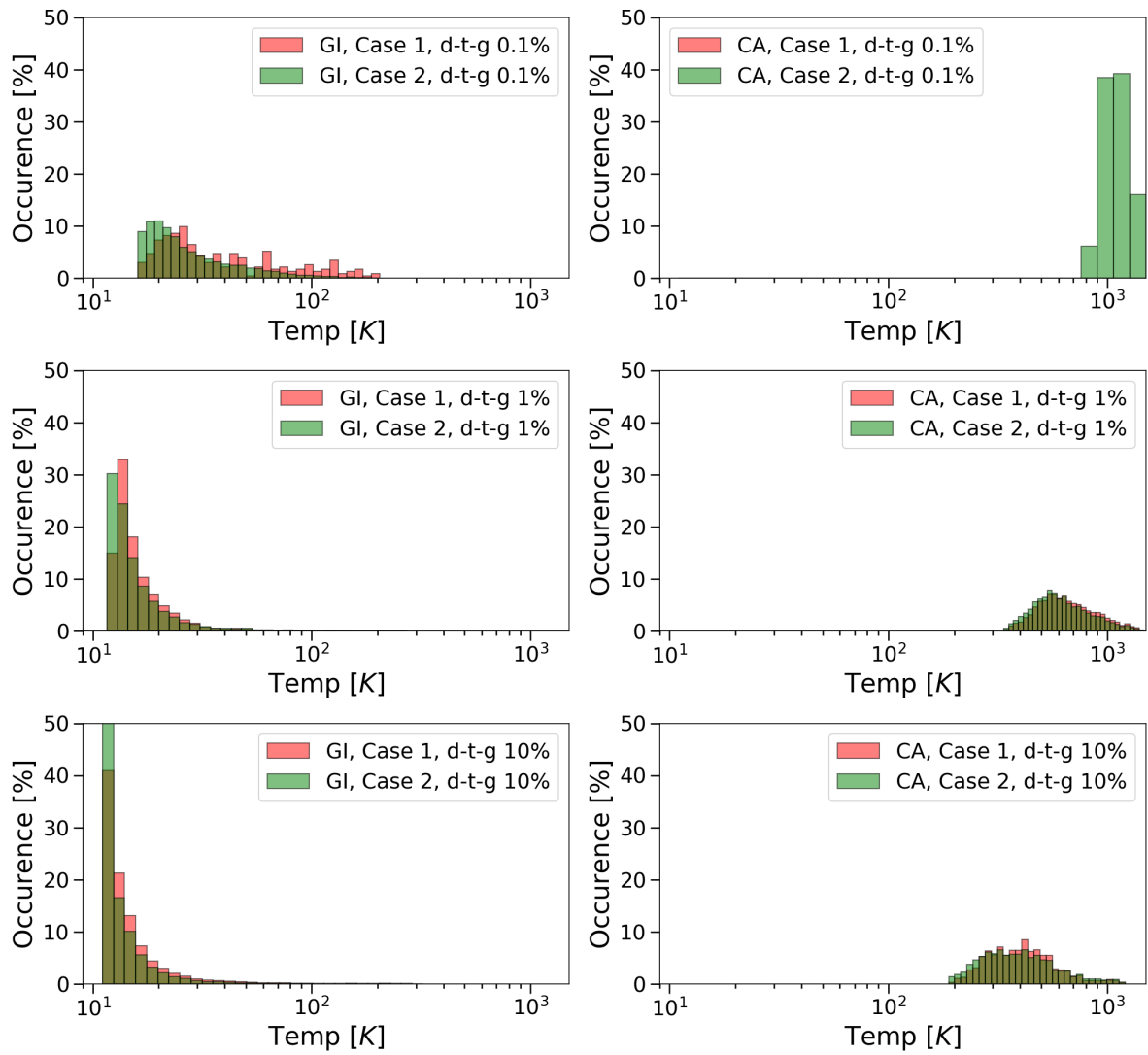


Figure 33: Distribution of formation temperature of satellites, split into the GI and CA case and for simulations where the dust-to-gas ratio was set at different numbers instead of varying them.

Formation temperature of surviving satellites

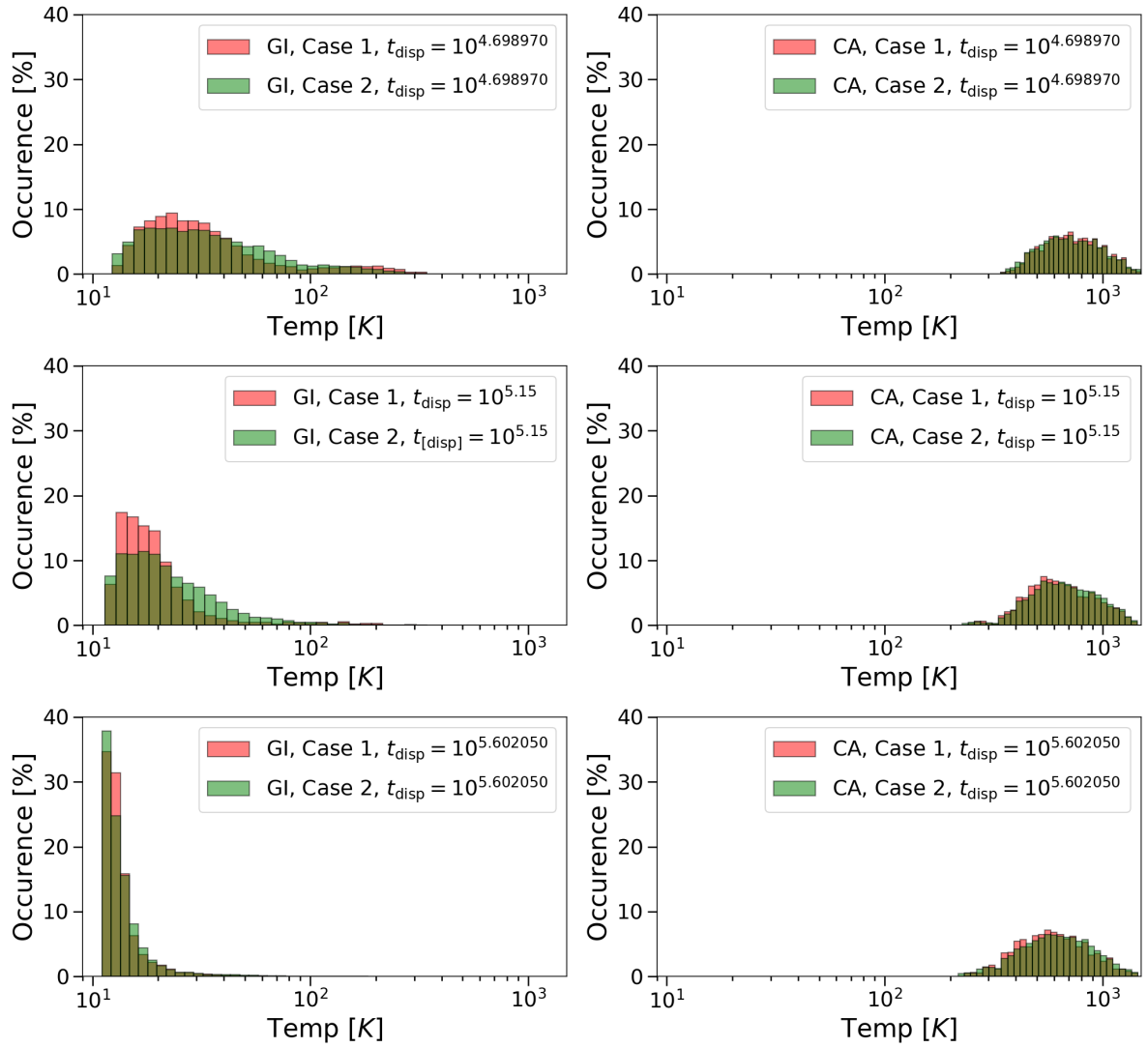


Figure 34: Distribution of formation temperature of satellites, split into the GI and CA case and for simulations where the dispersion timescale was set at different numbers instead of varying them.

Formation temperature of surviving satellites

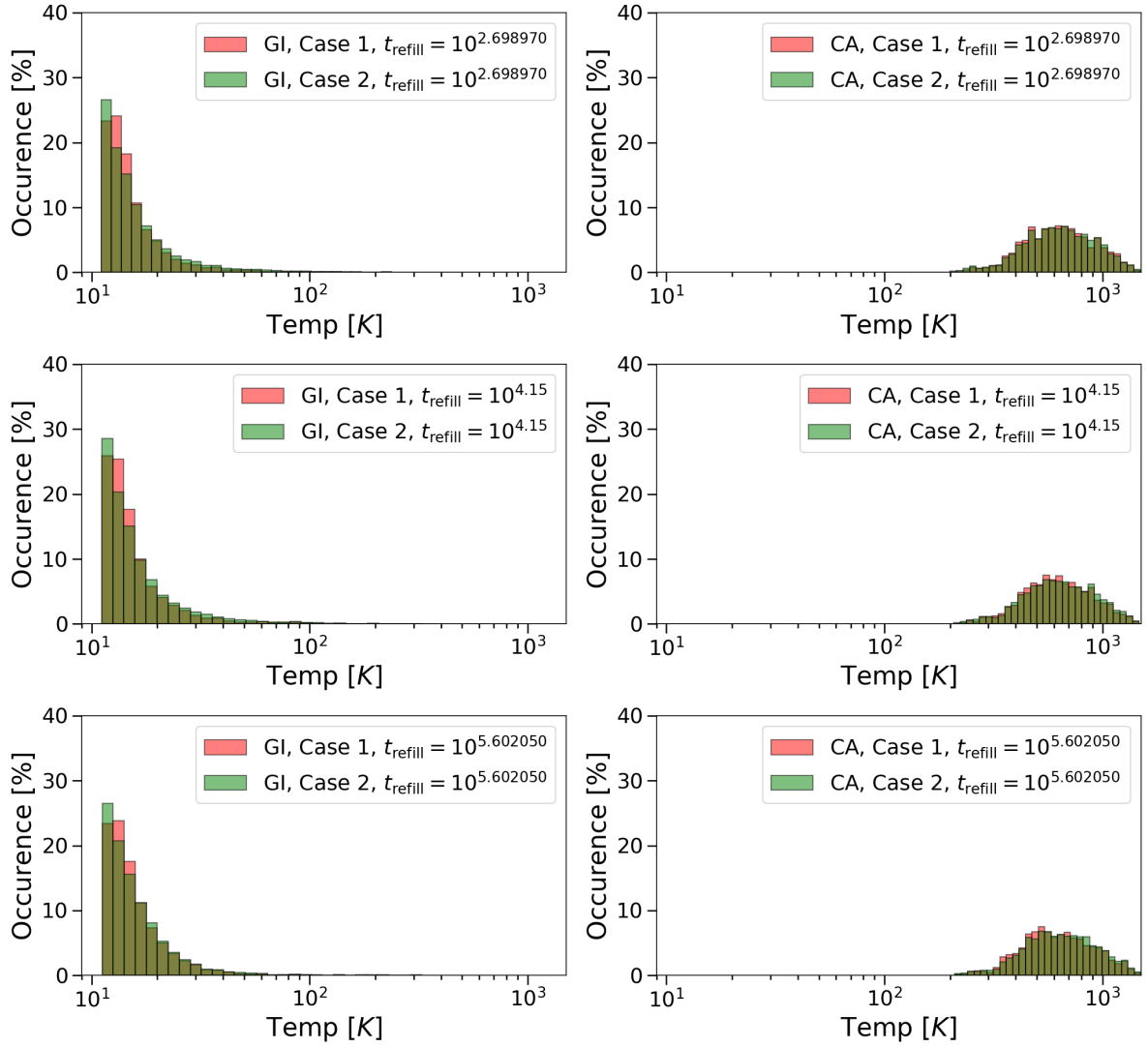


Figure 35: Distribution of formation temperature of satellites, split into the GI and CA case and for simulations where refilling timescale was set at different numbers instead of varying them.

The influence of different set parameters on the formation temperatures shows the following behaviour:

1. Set dust-to-gas ratio (fig. 33): In the CA disk, the formation temperatures are only very slightly influenced by dust-to-gas ratio. As it increases, more of the first generation satellites are lost and the distribution moves towards lower temperatures, but between case 1 and 2 there is not much change, as most of the satellites are still first generation. There are some second generation satellites (which form at lower temperatures), which are more likely to not reach case 2 mass, but they are a minority. In the GI disk there is a distinct tendency for satellites to have formed later the higher the ratio is, due to more and more of earlier generations accreting enough mass to get lost into the planet. So for low ratios, case 1 satellites tend to be older but this tendency becomes less pronounced as the dust-to-gas ratio increases, when more and more of the satellites in both case 1 and 2 were created in an already very cool disk overall.
2. Set dispersion timescale (fig. 34): In the CA disk the influence of the dispersion timescale is mostly felt in that the longer the disk exists, the easier it is for second generation satellites

to form and thus the distribution shifts a little to smaller temperatures, but it is always dominated by first generation satellites, in both case 1 and 2. In the GI disk, as the disk lifetime becomes longer, more and more first generation satellites are lost into the planet and more second or even third generation satellites can form, shifting distributions to lower temperatures. For low and high dispersion timescales, both case 1 and case 2 distributions are very similar, with case 1 slightly favouring higher temperatures than case 2. For intermediate dispersion timescales however, case 1 is much narrower than case 2, as now the disk lifetime is long enough for the case 1 satellites to form later but still short enough for many to not get lost into the planet.

3. Set refilling timescales (fig. 35): In the CA disk the refilling timescale has a very low influence on formation times, because the satellites there are mostly made up of first generation ones and the refilling does not influence their creation. In the GI disk however that is not the case: here, the first generation tends to get lost in any case, as they move fast and thus their mass comes from the disk and not the refilling, so these distributions are made up of second and later generations. As the formation of these satellites is partly tied to the refilling (as the mass to form a satellite has to be in the region where it is form) one would expect the satellites to be younger for fast refilling. However, fast refilling also means a higher chance of losing satellites, leaving the remaining ones to form at similar times as in disks with lower refilling.

3.6 Formation times

3.6.1 All parameters random

Table 11: Mean and standard deviation of the distributions.

Disk type and case	Mean	Standard deviation
GI, case 1	$3.622 t_{\text{disp}}$	$1.441 t_{\text{disp}}$
GI, case 2	$3.813 t_{\text{disp}}$	$1.582 t_{\text{disp}}$
CA, case 1	$0.281 t_{\text{disp}}$	$0.187 t_{\text{disp}}$
CA, case 2	$0.293 t_{\text{disp}}$	$0.205 t_{\text{disp}}$

Figure 36 shows the distribution of the time at which the satellites were created. In the GI disk, most of them were created after 3-4 dispersion timescales, about a third of the total lifetime of the disk, both in case 1 and 2. While there are a few that are from the 1st generation (that is, formed earlier than $0.5 t_{\text{disp}}$) they are very rare, supporting the points made in section 3.1 that they make up most of the lost mass very well. There are again few differences between case 1 and 2. Mainly, in case 2 there are more that were created later in the disk, so the whole distribution is shifted slightly to longer later timescale. That is because for satellites to grow as heavy as in case 1 it is favourable to be created earlier, although the difference is not that pronounced.

In the CA disk it is very clear that something like 90 % of the surviving satellites are first generation. There is an increasing possibility until $0.5 t_{\text{disp}}$, the latest time for a first generation satellite to be formed, and then a clear drop for times past that, where only a few are created at times longer than a dispersion timescale. So one can see that the lost mass in this case is made mostly up of the earliest generated satellites, as they would have been created in the most massive disk with the highest gas density and thus fast migration was possible. In case 2 there are more second generation satellites, but even there they are the minority of cases. This is also partly because of competition, as now the 1st generation satellites survive and they tend not to migrate far (see section 3.3) so they will dominate accretion on account of their mass.

There is a significant difference here between the GI and CA disk in that CA satellites tend to be around for a much larger portion of the disk lifetime. Additionally, as seen in section 3.4, they tend to accrete on faster timescales, and together these two factors could lead to significant differences in internal structure. Fast accretion can help in differentiation as that would generally heat

the satellite much more and thus allow for settling to take place, whereas a long accretion time means that it has more time to cool as dust impacts its surface, working against differentiation.

Time of formation of the satellites at the end of the simulation

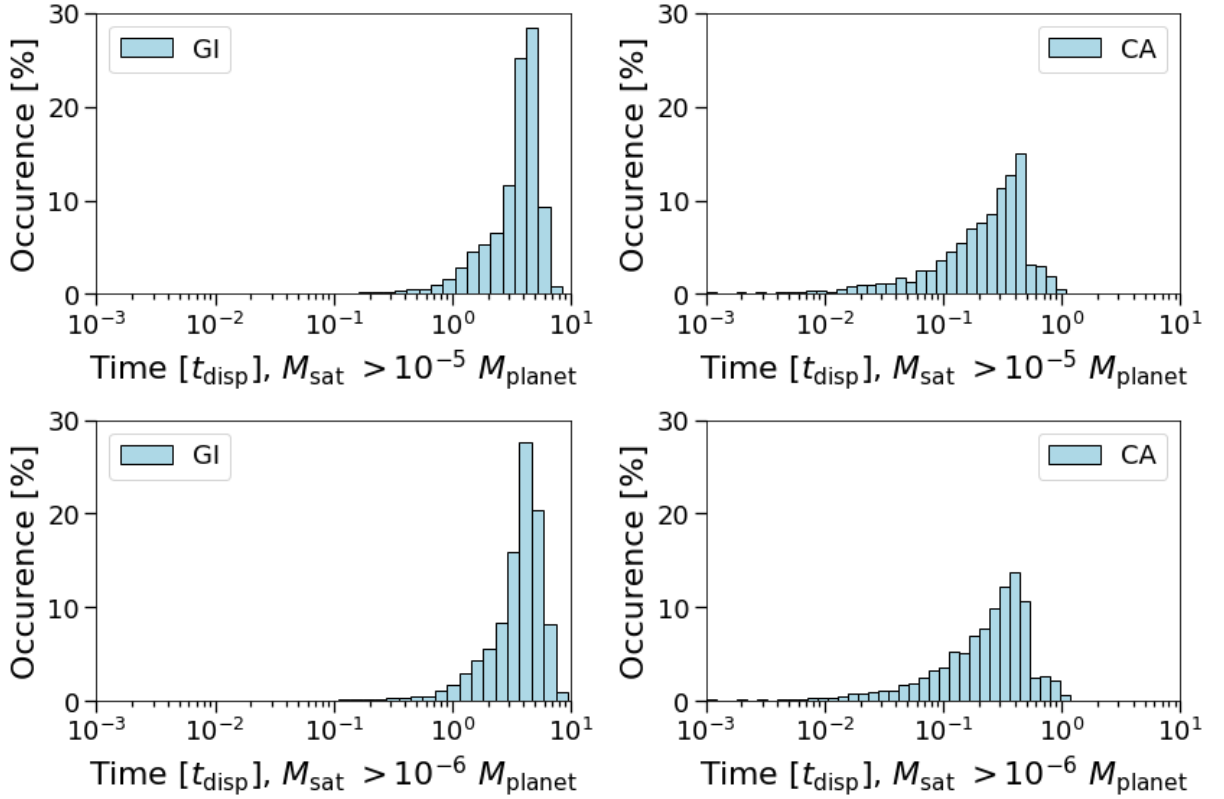


Figure 36: Distribution of formation times of satellites in dispersion timescale. In both disks the difference between case 1 and 2 satellites are very small. In the GI disk most satellites that become this heavy form late in the disk so second generation or older, where the case 1 satellites are all slightly older. In the CA disk most satellites are first and only a few are second generation satellites, where again the case 1 satellites are a bit older. This mirrors the formation temperature results as both these values are connected.

3.6.2 One parameter set

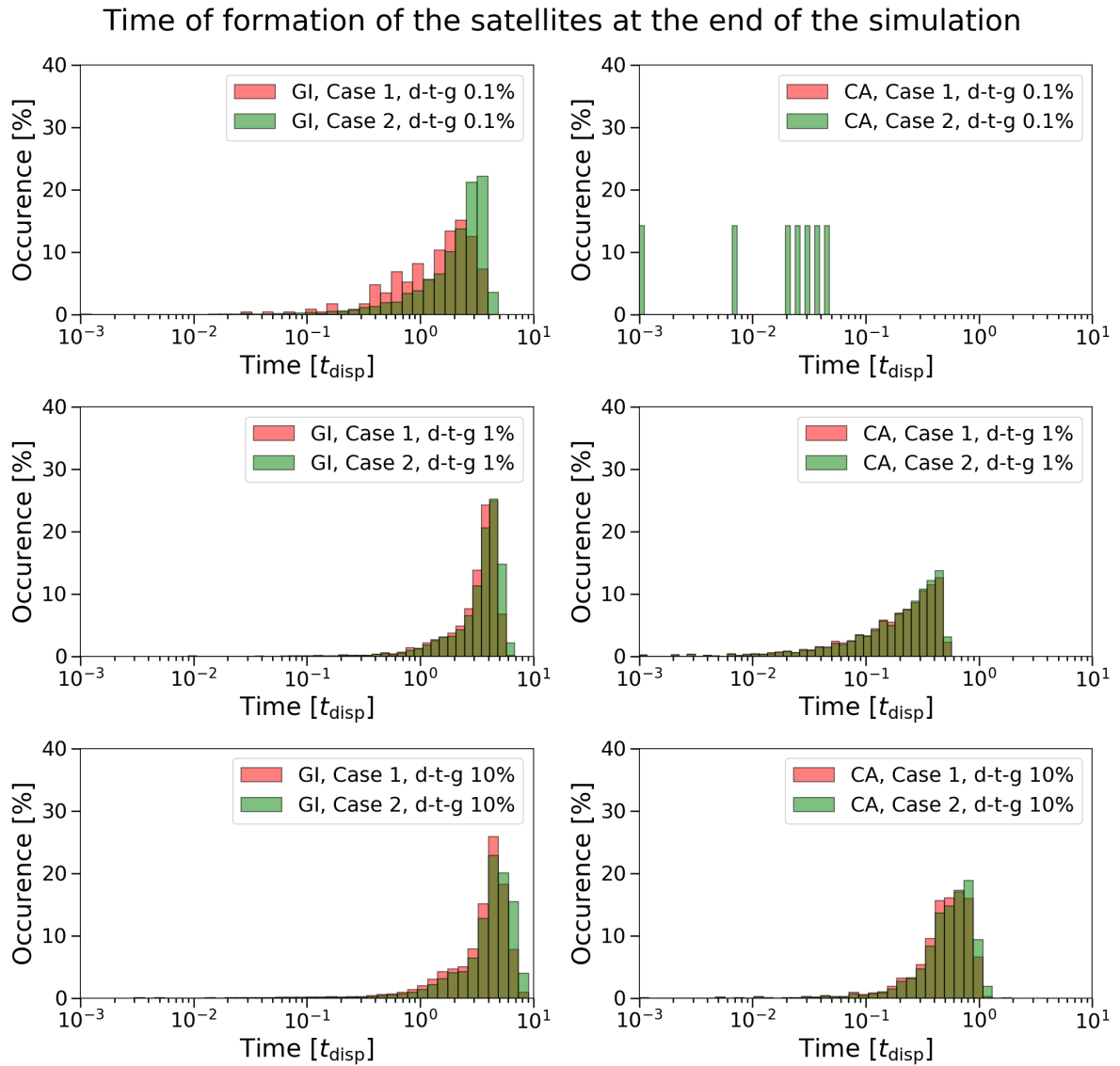


Figure 37: Distribution of formation times of satellites in dispersion timescale, split into the GI and CA case and for simulations where the dust-to-gas ratio was set at different numbers instead of varying them.

Time of formation of the satellites at the end of the simulation

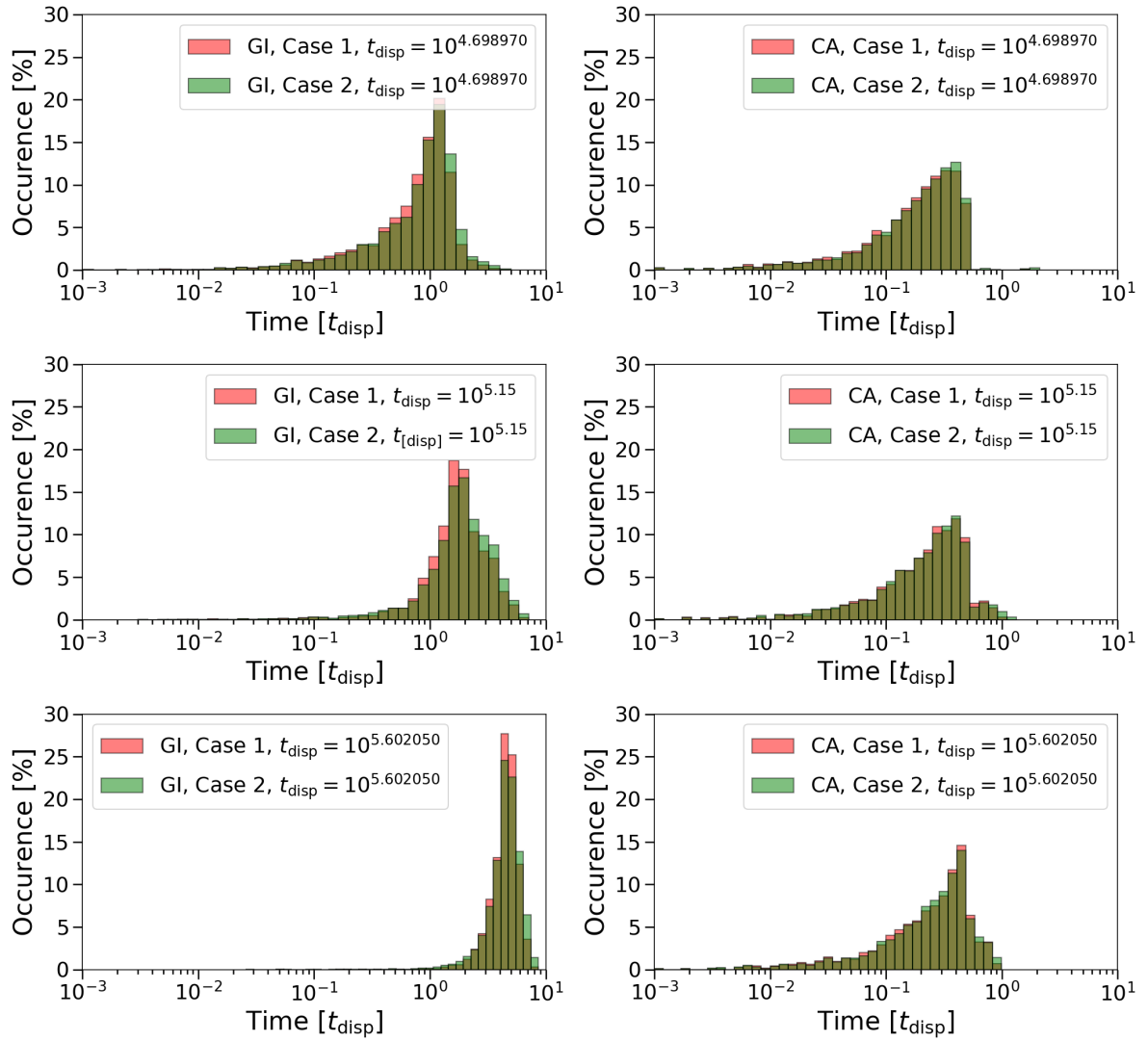


Figure 38: Distribution of formation times of satellites in dispersion timescale, split into the GI and CA case and for simulations where the dispersion timescale was set at different numbers instead of varying them.

Time of formation of the satellites at the end of the simulation

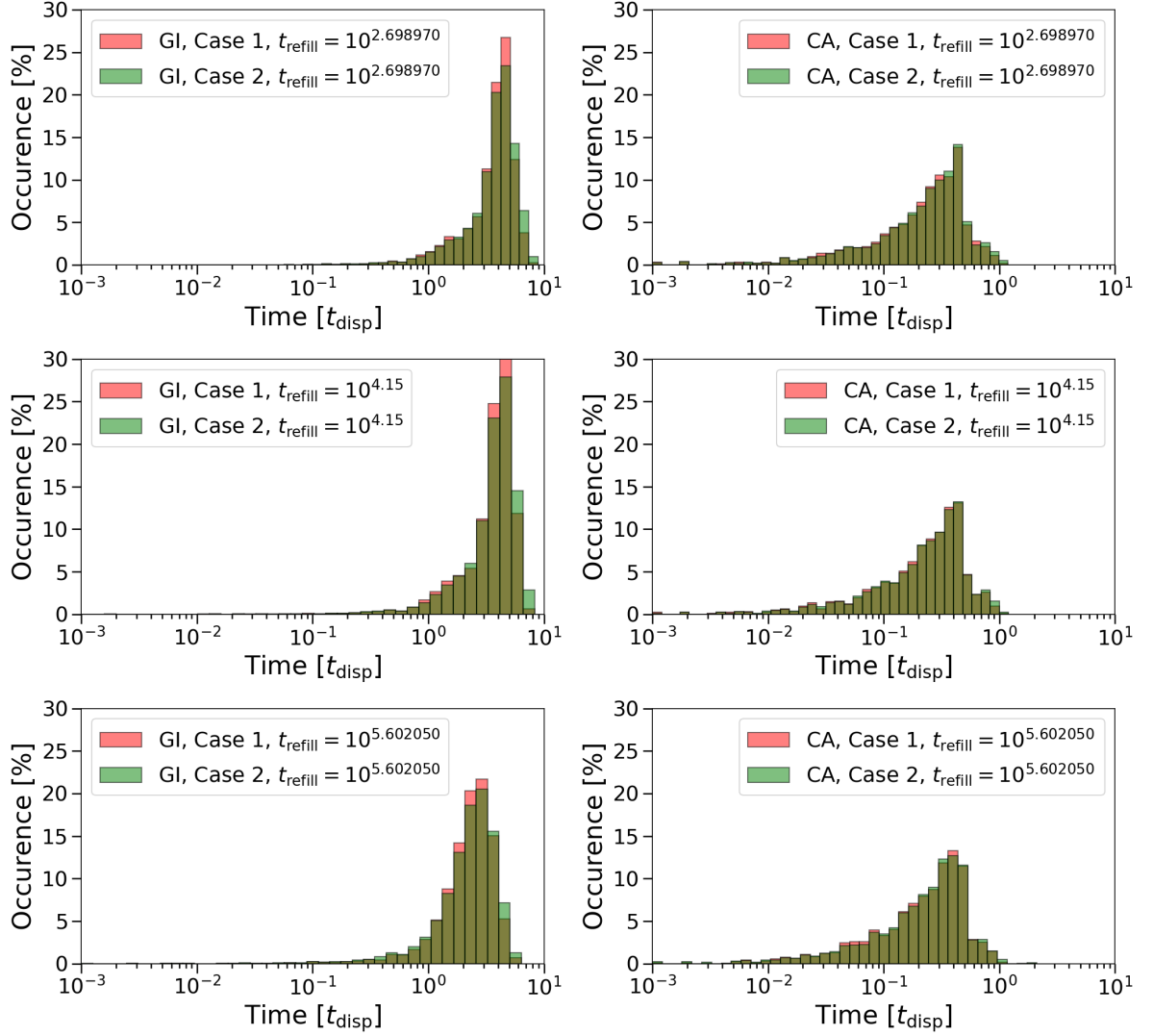


Figure 39: Distribution of formation times of satellites in dispersion timescale, split into the GI and CA case and for simulations the refilling timescale was set at different numbers instead of varying them.

The influence of different set parameters on formation times shows the following behaviour:

1. Set dust-to-gas ratio (fig. 37): In the GI disk, case 1 satellites tend to be older than the case 2 satellites, because that gives them more time to accrete mass. The effect is most pronounced for low dust-to-gas ratio and gets less important towards high ratios because then there is enough dust in the disk where time is less of a factor in the satellites reaching threshold masses. On average the satellites are also formed later in the disk, as with higher dust ratios more of the early satellites, which tend to be the heaviest, are lost in the planet (see also fig. 14). The CA disk has similar behaviour although the difference between case 1 and 2 is smaller for intermediate and high ratios, while for the low ratio it gets almost impossible to get even case 2 satellites, as they tend to be formed farther out in a disk with less mass infall, and those that can grow that much are formed very early in the disk. As the ratio increases, the average formation time does as well and for the highest ratio there is enough dust in the disk for second generation satellites to reach even case 1, while more and more older satellites are lost.

2. Set dispersion timescale (fig. 38): In the CA disk the influence of the dispersion timescale is mainly that the satellites that survived formed later in the disk lifetime, as the longer that is the more satellites have the time to migrate into the planet. In the CA disk this is much the same, only now the longer disk lifetimes means that more second generation satellites can form and accrete a lot of mass.
3. Set refilling timescale (fig. 39): In the GI disk the the refilling timescale affects both case 1 and 2 the same way, the faster the refilling the later in the disk the satellites form, as older satellites accrete mass so fast the get lost into the planet and later generations can grow to these sizes. In the CA disk the refilling timescale has very little influence as the satellites will be dominated by first generation ones where it has no influence on their formation times.

3.7 t-SNE visualization

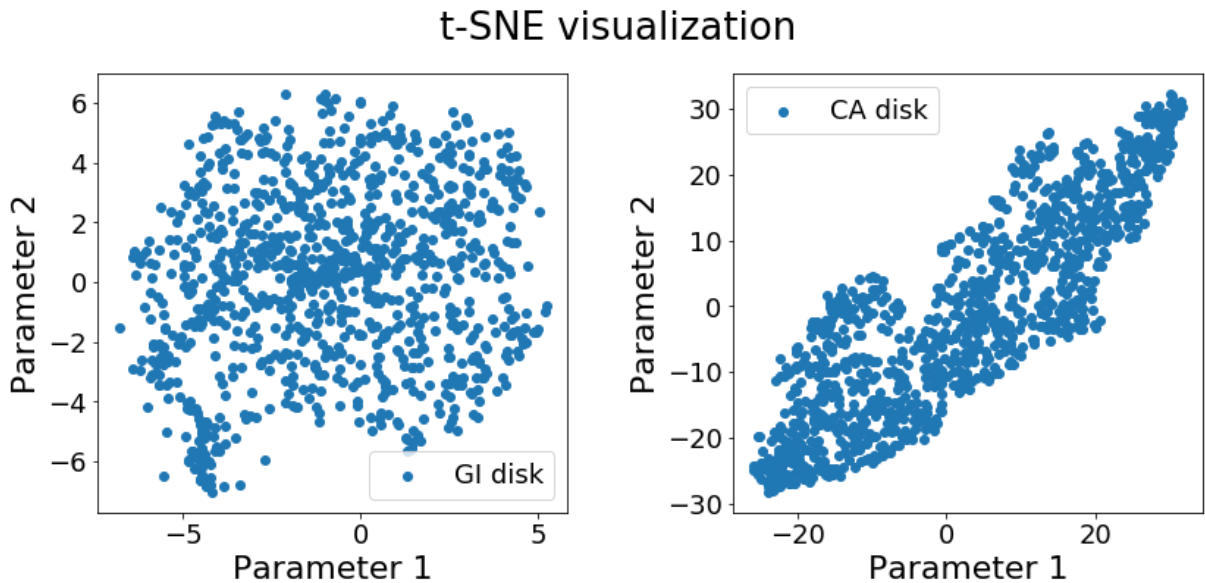


Figure 40: This graphic shows the 2D visualization of a subset of the satellite systems generated with this model. The t-SNE algorithm is meant to reproduce similarities/dissimilarities as points (which represent systems) that are closer/farther apart and to cluster similar ones if possible. In the GI case the spread is very even, with no discernible clusters. In the CA case however the spread is narrow in one direction and very spread in another. This could represent the fact that in the GI disk, both possible positions and masses are very likely over the whole spectrum of possibilities, while in the CA case the positions are much more closer (clustered in the far out part of the disk) while the masses are similar to the GI case. One should however be cautious about these interpretations, as the subset chosen may have influence as well as the specific tuneable parameters. Nevertheless, this seems to represent the different behaviour of the two disks.

Figure 40 shows the visualizations achieved with the t-SNE algorithm. These are not unique outcomes (different runs of the algorithm may produce different results) but were recurring distributions. A perplexity of 50 was chosen, which gave more consistent results. Due to the computational scaling, only a subset of satellites could be analyzed, but they should represent the results nevertheless. The axes parameters are arbitrary numbers assigned by the algorithm and have no special meaning. The algorithm's main purpose is to visualize how close in make-up two satellite systems are by placing them (as represented by points in the plot) closer or farther apart. In this sense, it seems that in the GI disk the visualization says that there is a wide spread of similar/dissimilar systems, as in on average a system is as similar or different to the rest as every other system is. In the CA disk there is more structure, in that it is narrower in one dimension and wider in another. As the underlying distance that measures this similarity is

based on the orbital radii and the masses, this difference could represent the differences in those distributions. As seen in section 3.1, the spread in possible masses is mostly the same (only the CA disk has much more low mass satellites) whereas the possible orbit radii are much closer together in the CA disk than in the GI disk, where the possibilities to land on one radius are very close in the whole disk. So the narrow distribution in the CA disk in fig. 40 could represent this clustering of orbital radii that is not the case in the GI disk, meaning the CA satellite systems are on average more similar to each other because their possible orbital radii are more restricted. However, one has to be cautious with such interpretations of t-SNE visualizations. It is a very good algorithm to see clusters/structures in a certain data set and as the data here doesn't seem to show any of this any interpretation beyond that has to be taken with caution.

4 Discussion

4.1 Model implications

As a population synthesis approach is used, the parameter space of the initial conditions is very important to the results and one has to be aware of the choices made and their implications and limitations.

Dust-to-gas ratio The dust-to-gas ratios that are used here were based on the values observations of the T-Taurus cluster give [Ansdell et al. 2016], where the maximum and minimum values were taken and then for the simulations a log-normal distribution between those two was created and the values chosen from there. The reason for this log-normal distribution is very important: we don't a priori know how these are distributed and if there are constrictions around them and the log-normal distribution means all orders of magnitude are probed equally. As seen in section 3, the dust-to-gas ratio is a very important parameter, very much shaping the properties of the satellites and a better understanding of the origins of the dust ratio is and the occurrence rate of them is very important.

Dispersion timescales The dispersion timescales were estimated by taking the stars' luminosities and CSD parameters to estimate the photoevaporative mass loss rate at 50 AU (where the CPDs are located) using a model by [Picogna et al. 2019] and using that to get a range of dispersion timescales for the CPDs. This is somewhat crude as it ignores that CSDs generally are swept from the inside out in the later stage of their evolution and that evaporation will change over time, but it does give values that are in the range usually adapted for disks like these. For the CA disk this will come into account more in the temperature decay, as the high temperature is the main thing that keeps satellite formation far out, so with a different temperature model the satellites might be created closer, changing their make-up. For the GI disk, longer or shorter dispersion timescales will mainly influence the masses because longer timescales means more time for the satellites to accrete mass, which tends to not be lost because they are created later.

Refilling timescale For the refilling timescales a range is adapted that goes from "not shorter than a time step" to "not longer than the longest dispersion timescale" because this process not only incorporates the influx from the CSD (which is fixed) but also governs the distribution of that across the disk. And as these processes aren't really known and rely on the assumption that the initial state is a steady state the dust wants to return to, the widest possible range is adapted. Thus one has to be aware of the fact that this distribution of incoming dust might look very differently in real life. Simulations have shown that there is a vertical gas influx to the disk (which is where the values adapted in section 2 come from) and further work has shown that at least mm sized particles are a significant part of that infall ([Szulágyi, Binkert & Surville 2021]). It is known that planetesimals pile up at the edge of the gap and as such the later generation's formation could depend very much on the exact form the infall takes.

Initial embryos and sequential formation A major hurdle of any model studying satellite formation is the origin of embryos in the CPD. Here, the disk is seeded at the beginning with a number of satellites and then, by using the accretion timescale of such an embryo to accrete its own mass, embryos are created sequentially. The origin of the first generation can be explained that they were already being built in the CSD and entered the CPD as it formed. The second (and later) generations however suffer from the same difficulties of being formed as planetary embryos in the CSD do (see section 1.3) which are aggravated by the much smaller disk size. The accretion timescale probably represents an upper ceiling on how fast they can form, but how many can form is another question. The disks are certainly big enough and massive enough (with a mass influx to add to this over time) to support a lot of embryos but whether or not so many can be created on such fast timescales is an assumption. However, given that around Jupiter (which would have been a smaller disk due to both mass and position) managed to form 4

satellites which could be second generation (due to the slight metallicity pollution we can observe in its atmosphere) lends a good argument that in these much more massive disks as many as 20 embryos could form.

Initial positions The satellites' initial positions are chosen to be on a range between 1% and 80% of the disk, because this represents a portion of the disk that can mass-wise and in terms of Hill radii, in theory, form an embryo. 80% is very far out compared to other works in Jupiter-like disks, but as these disks are so massive these outer regions have more than enough mass to form embryos, although whether or not there are formation scenarios that allow it is an open question. This has implications on the results, especially in the case of the CA disk, as in these regions many satellites do not migrate very fast (because both migration and accretion are lower due to the low densities). This means that, if the range were to be reduced, this would have profound influence on the results given here. Both this point and the previous one clearly demonstrate that more work on embryo formation in CPDs is needed.

Mass influx The two CPDs have a mass infall rate which is calculated at the time the profiles are taken. It is assumed the CPDs are in equilibrium and that the infall is essentially a set percentage of the CSD mass and decays like the CSD does, which is a reasonable assumption. But as neither disks are evolved with the CPD, that infall could be subject to change. For the CA disk that would be less of a problem, as the satellite properties there are largely independent of the refilling time and the infall at large, but for the GI disk, which has several generations of satellites evolving in it, the infall is what shapes the properties of the later generations, so changes in it would impact it more than the CA disk. Additionally, the CPDs investigated here have different infall rates. This could be because, as they orbit different stars, the CSD masses are different and [Szulágyi et al. 2016a] showed that CPD mass is dependent on CSD mass, so the infall could have a similar relation. It is also possible that CA disks have a smaller infall as part of their nature and as such more disk models might shed some light on this.

N-body interaction Both disks have many satellites simultaneously existing in them and in this model, satellite-satellite interaction is not considered apart from direct collisions. For the GI disk, where the orbits tend to be spread over larger distances and the satellites migrate much more due to gas-satellites interaction, the influence of a proper N-body interaction scheme may be a bit lower, but it might still lead to marked changes in the satellite properties, as now close passes are possible to be modeled, which leads to different dynamics in migration. For the CA disk, where most satellites are clustered in the outer disk, the influence might be much higher, especially since migration due to gas-satellite interaction is much lower. However, extending this model even to 2D would mean reducing the length of the timestep to take full advantage of an N-body interaction, which would make running the simulations much more computationally expensive, but it could be worth investigating.

4.2 Discussion Comparison

As this work is about comparing satellite systems in 2 different planet (and thus disk) creation scenarios it makes sense to discuss if one could possibly distinguish a CA or GI planet by its satellites:

Mass The main difference in mass distributions is that in the CA disk it is more likely for a satellite to grow past 10^{-5} planet masses, but in the GI disk the maximum mass is higher. However, the problem in comparing these is that this model does not include direct satellite-satellite interaction. From N-body simulations of the solar systems, we know that once the disk is dissipated, the remaining planetesimals enter a chaotic phase of impacts before they settle into the "stable" configurations. A similar phase could happen in the case of satellite systems and as such, the mass distribution could look very different if this would be taken into account, so these specific distributions may not be the best indicator.

Lost mass The difference in lost mass is more than an order of magnitude on average and there are a lot of systems where the maximum lost mass in the GI disk is much higher than the maximum lost mass in any CA systems. In principle, this lost mass should lead to an increase in the planets metallicity and then a very high metallicity in a planet could be correlated to a GI disk. However, the lost mass in the GI disk is very high, in the extreme cases coming close to 50 % of planet mass and it is reasonable to be cautious about this result, as it constitutes a massive increase in planet mass which could potentially have influence on disk structure during satellite formation.

Integrated mass As seen in section 3.1, in the GI case in general every system has at least one satellite that manages to grow by 2-3 orders of magnitude. The CA case shows that many systems where this is not the case. So if we were to observe a system with a very low system mass, that would be a potential CA candidate. However, observing such small satellites is another matter entirely and there are other reasons why a planet could end up with such small satellites as well.

Number of satellites The GI disk has, even for the heavy satellites of case 1, a lot of systems with 10 or more satellites in it, whereas for the CA case it is very hard to form that many, even for the lighter ones in case 2. So the number of satellites may be a good way to determine GI planets if they have a system with 10 or more satellites.

Orbital radii While the GI disk does have some orbital radii that are preferred (and does show peaks), it is overall a somewhat equal distribution and satellites can end up in all of the disk, while in the CA disk the outer region is vastly preferred, where only a few satellites make it to the inner system. Given these distributions, the orbits of the satellites can be a good measure to gauge which creation scenario is more likely. However, the lack of satellite-satellite means these distributions have to be looked at with caution, as especially in the CA case, where the satellites are more clustered, an N-body simulation might significantly change the orbits, scattering some of them inwards.

Europa timescale The timescales to form Europa are consistently faster in the CA case than in the GI case. The faster satellites form, the less chance they have to radiate away impact heat and the more likely they are to have a melted crust, which can lead to differentiation of the interior. This is the main influence this timescale has, but there is no easy way really to relate the timescale to differentiation at this point, so we cannot say more than that CA satellites are probably more likely to be fully differentiated. That is not something that we can really observe though only model by using gravimetric data, which we can not gain at a distance.

Formation temperature There is a clear difference in temperature in which the satellite embryos form: GI satellites are created in an environment where ice can form in the disk (< 180 K) and as such they should have a significant portion of their mass be ice as well. In the CA case they are formed in an environment that is mostly too hot for ice to form and even if they can eventually accrete some ice, their mass is likely to be made up by mostly rock. This could be a very good way to distinguish formation scenarios, provided the temperature differences in a CA and GI disk are consistently this different. Like in the case of the Europa timescale, this is not a thing that we can observe from far away though so it is of little help.

Formation times The formation times of satellites is also very different between the GI and CA case, where in the former satellites are consistently much older than in the later. While this can have a various impact on that structure, it is not something that we can determine from far away and as such, even though there is a clear difference, not something we can use to determine planet origin.

All together, there are significant differences in the distributions between the two disks in regards to orbital positions, number of satellites, Europa mass timescale, formation times, formation temperatures and lost as well as retained mass, while some distributions show minor differences like the masses and the integrated masses. Unfortunately, many of the differences are not of the type that we could observe from afar, such as the formation temperature or the Europa mass time (which would be indirect measurements through composition). The only things that we could directly observe through various means would be the orbital positions and the number of satellites, both of which can be subject to bias though, for example if we observe them by transit that would make close orbits harder to detect.

5 Conclusion

In this work, the satellite formation in two different circumplanetary disks was investigated, one that formed as a result of a giant planet forming via the core accretion scenario, the other as a result of the gravitational instability scenario. A semi-analytical model was used, in which satellite embryos are produced in a sequential matter, which can then accrete mass, migrate and potentially enter a resonant configuration or collide. A population synthesis approach was then taken, where many simulation runs were done with varying initial parameters: the dust-to-gas ratio, the dispersion timescale, the refilling timescale and the number and position of initial seeds. The resulting distribution of satellites and systems as a whole were then analyzed and compared.

The mass distribution shows that in a gravitational instability disk a higher percentage of created embryos can accrete significant masses, most between 2 and 4 orders of magnitude, where some reach very high masses. In the core accretion case there are many more embryos that barely accrete mass, so a smaller percentage manage to grow 2 or more orders of magnitude. However, they are on average more massive than the gravitational instability ones, although the maximum mass is lower.

For the lost masses one can see that in the gravitational instability disk many more satellites (or more massive ones) are lost, where the average is more than one order of magnitude higher than in the core accretion disk. This also connects to the masses: The gravitational instability disk loses many of its high mass satellites in the disk, which is not the case for the core accretion one.

The distribution of integrated mass shows in both disks a peak around 10^{-4} planet masses, which is the value we consistently observe in the Solar System. The gravitational instability distribution is much narrower and it shows that the majority of systems have at least one embryo that accreted 2-3 orders of magnitude in mass. In the core accretion case the distribution is much broader, where now there are many systems that consist of a few satellitesimals that barely accreted any mass (hence a second peak that sits at a couple of embryo masses).

As there is no defined minimum mass for moons, two different thresholds were investigated: Case 2, which looks at every satellite $> 10^{-6}$ planet masses, which is close to Europa's mass ($\simeq 2.5 \cdot 10^{-5}$ Jupiter masses) and case 1, which looks at every satellite $> 10^{-5}$ planet masses. The lower threshold was chosen because it represents relatively the smallest significant satellites we can observe in the Solar system and is at the same time a useful metric as it is effectively close to Europa's mass, the smallest Galilean satellite.

For the number of satellites there is a clear difference in that the gravitational instability disk has on average satellite systems that contain more satellites. In case 1 the effect is a bit less pronounced, but it is very clear in case 2 where the gravitational instability disk can have more than twice as many satellites as a maximum and the core accretion disk stays under 10 satellites per system for the majority of cases.

The orbital radii in the end of the simulations also show a clear difference. In the gravitational instability case orbital radii are somewhat equally distributed. Case 1 satellites favour the inner system, while case 2 favours the outer system, but they can end up anywhere in the disk in significant numbers. In the core accretion case however the satellites heavily favour the outer system, where only very few make it to the inner system and the mid section is depleted.

The timescales on which the satellites reach Europa mass was also investigated. This timescale is used as a measure of how fast satellites grow, where Europa mass was chosen because it is useful metric as the smallest Jupiter satellites. In the gravitational instability disk, case 1 satellites on average accrete mass faster than the case 2 satellites, often shorter than a dispersion timescale. In the core accretion disk the difference between case 1 and 2 is similar, but compared to the gravitational instability disk they reach Europa mass much faster.

The temperature of the disk at the position where the embryo forms is a useful measure to see whether ice can be part of the satellites make-up and how big the percentage could be. The

difference between case 1 and 2 is minimal in both disks, but there is a huge difference between the gravitational instability and the core accretion disk. The gravitational instability disk is very cold to begin with, so almost every satellites is created in a disk that has significant amounts of mass in ice, whereas in the core accretion disk all are created in a disk that is made up mostly of rocks. This could mean that gravitational instability satellites are a combination of ice-rock and CA satellites are mostly rock.

The formation times of the satellites that survive are also very different between the gravitational instability and core accretion disk: the gravitational instability satellites are mostly second generation and later, where case 1 satellites are slightly older on average, while the core accretion satellites are mostly made up of first generation satellites.

Of these results, the two that are potentially observable from afar are the number of satellites as well as their orbital positions, although the observation of either of which would not be an easy feat to accomplish. Nevertheless they represent, in the case of the two disks used here, the best option to distinguish between the two formation scenarios.

5.1 Outlook

There are a few ways these results could be improved in future work:

1. The code could be expanded to include N-body interaction, which would not only make collisions more accurate and close passes possible but also let orbits be more than just circular and co-planar. Especially in the case of the core accretion disk, where satellites are clustered in the outer disk, this could have significant influence. This would make the simulations much more computationally expensive though and a possible way to split the difference might be to run this model until the disk dissipates and then switch to an N-body simulation for the surviving satellites, under the assumption that as long as the disk is there satellite-disk interaction dominates.
2. This work only looks at one core accretion disk and one gravitational instability disk. As sample sizes go this is very small and more disks could shed some light on how much of an influence the formation scenario actually has, i.e. how different are mass influx, temperature and density for different disks with a given formation scenario. So the population synthesis could be expanded to include more disks as well.
3. In this model embryos are formed by taking the time it would take for an already existing embryo to accrete its own mass. While this has the benefit of tying formation to disk parameters such as the dust-to-gas ratio and the dust density, the fact is that the accretion rate is based on an existing body gravitationally capturing and colliding with much smaller particles, which is going to be different than the actual processes that lead to embryo formation. Ideally one could find a way to create embryos that is much closer to reality, where the fact of the matter is however that there are still open questions as to how exactly this process happens.
4. Both gas density and temperature evolution are approximated by an exponential decay over a certain timescale, in this case the dispersion timescale. A more detailed evolution of these two parameters, say with a radiative transfer model for the temperature, may change some of the outcomes as well. Particularly, the gas density (and thus the dust density, as we say they are coupled) might create a structure of over- and underdensities, which could provide locations for the streaming instability to work.

Acknowledgements

First and foremost, I would like to thank Prof. Dr. Judit Szulágyi from ETH Zurich who supervised this work. I'm grateful for the opportunity to do this work as part of her group and her encouragement in both successes and failures as well as any advice given to me were a tremendous help to drive this thesis to a successful end.

I would also like to thank Prof. Dr. Aurel Schneider for taking on the role of administrative supervisor on the University of Zurich's side.

Further I would also like to thank Dr. Marco Cilibrasi from the University of Zurich, who was always prepared to respond to any questions that I had and provided useful comments on parts of this thesis.

References

- [Agnor & Hamilton 2006] Agnor, C. B. & Hamilton, D. P. (2006) "Neptune's capture of its moon Triton in a binary-planet gravitational encounter". *Nature*. 441: 192
- [Alexander & Armitage 2007] Alexander, R. D. & Armitage, P. J. (2007) "Dust dynamics during protoplanetary disc clearing". *MNRAS*. 375: 500
- [Alexander et al. 2014] Alexander, R. (2014) "The Dispersal of Protoplanetary Disks". Chapter in *Protostars and Planets VI*. University of Arizona Press.
- [Alibert 2019] Alibert Y. (2019) "A new metric to quantify the similarity between planetary systems - application to dimensionality reduction using T-SNE". *A&A*. 624: A45
- [Anderson et al 1996] Anderson, J. D. et al. (1996) "Galileo Gravity Results and the Internal Structure of Io". *Science*. 272: 709
- [Ansdell et al. 2016] Ansdell, M. et al. (2016) "ALMA survey of Lupus protoplanetary disks. I. Dust and gas masses". *ApJ*. 828: 46
- [Armitage 2017] Armitage, P. J. (2017) "Lecture notes on the formation and early evolution of planetary systems". *arXiv:astro-ph/0701485*
- [Bai et al. 2016] Bai, X. N. et al. (2016) "Magneto-thermal Disk Winds from Protoplanetary Disks". *ApJ*. 818: 152
- [Balbus & Hawley 1998] Balbus S. A. & Hawley J. F. (1998) "Instability, turbulence, and enhanced transport in accretion disks". *Reviews of Modern Physics*. 70: 1
- [Balsara 1995] Balsara, D. S. (1995) "von Neumann stability analysis of smoothed particle hydrodynamics—suggestions for optimal algorithms". *J. Comput. Phys*. 121: 357
- [Bargel & Sommeria 1995] Barge, P., & Sommeria, J. (1995) "Did planet formation begin inside persistent gaseous vortices?". *A&A*. 295: L1
- [Baruteau et al. 2014] Baruteau, C., et al. (2014) "Protostars & Planets VI". University of Arizona Press. Tucson: p. 667
- [Bell & Lin 1994] Bell, K. R. & Lin, D. N. C. (1994) "Using FU Orionis Outbursts to Constrain Self-regulated Protostellar Disk Models". *ApJ*. 427: 987
- [Benítez-Llambay et al. 2015] Benítez-Llambay, P. et al (2015) "Planet heating prevents inward migration of planetary cores". *Nature*. 520: 63
- [Bergstralh, Miner & Matthews 1991] Bergstralh, J. T., Miner, E. E. & Matthews, M. (1991). "Uranus" University of Arizona Press. pp. 485–486
- [Bhatia & Sahijpal 2017] Bhatia, G.K. & Sahijpal, S. (2017) "Thermal evolution of trans-Neptunian objects, icy satellites, and minor icy planets in the early solar system". *Meteoritics & Planetary Science*. 52: 2470
- [Birnstiel, Fang & Johansen 2016] Birnstiel, T., Fang, M. & Johansen, A. (2016) "Dust Evolution and the Formation of Planetesimals". *Space Science Reviews*. 205: 41
- [Bland, Showman & Tobie 2007] Bland, M. T., Showman, A.P. & Tobie, G. (2007) "Ganymede's orbital and thermal evolution and its effect on magnetic field generation" *Lunar and Planetary Society Conference*. 38: 1338
- [Bodenheimer & Pollack 1986] Bodenheimer, P. & Pollack, J. B. (1986) "Calculations of the accretion and evolution of giant planets: The effects of solid cores". *Icarus*. 67: 391
- [Bolton 2017a] Bolton, S. J. et al (2017a) "The Juno Mission". *Space Science Reviews*. 213: 5

- [Bolton 2017b] Bolton, S.J. et al (2017b) "Jupiter's interior and deep atmosphere: The initial pole-to-pole passes with the Juno spacecraft". *Science*. 356: 821
- [Bonnell et al. 2001] Bonnell, I. A. et al. (2001) "Competitive accretion in embedded stellar clusters". *MNRAS*. 323: 785
- [Bressert et al. 2010] Bressert, E. et al. (2010) "The spatial distribution of star formation in the solar neighbourhood: do all stars form in dense clusters?". *MNRAS*. 409: L54
- [Brown et al. 2006] Brown, R. H. et al. (2006) "Composition and Physical Properties of Enceladus' Surface". *Science*. 311: 1425
- [Brown et al. 2009] Brown, R. et al. (2009) "Titan from Cassini-Huygens". Springer Science & Business Media. p. 69
- [Cameron 1978] Cameron, A. G. W. (1978) "Physics of the Primitive Solar Accretion Disk". *Moon and the Planets*. 18: 5
- [Canup & Ward 2002] Canup, Robin M. & Ward, William R. (2002) "Formation of the Galilean Satellites: Conditions of Accretion" *ApJ*. 124: 3404
- [Canup 2014] Canup, R.M. (2014) "Lunar-forming impacts: processes and alternatives". *Philosophical Transactions of the Royal Society of London. Series A* 372: 20130175-20130175
- [Carrera et al. 2017] Carrera, D. et al. (2017) "Planetesimal Formation by the Streaming Instability in a Photoevaporating Disk". *ApJ*. 839: 16
- [Charnoz et al. 2009a] Charnoz, S. et al. (2009a) "Saturn from Cassini-Huygens" Springer Science. p. 537-575
- [Charnoz et al 2009b] Charnoz, S. et al. (2009b) "Did Saturn's rings form during the Late Heavy Bombardment?" *Icarus*. 199: 413
- [Chevance et al. 2020] Chevance, M. et al. (2020) "The lifecycle of molecular clouds in nearby star-forming disc galaxies". *MNRAS*. 493: 2872
- [Cilibrasi et al. 2018] Cilibrasi, M. et al. (2018) "Satellites form fast & late: a population synthesis for the Galilean moons". *MNRAS*. 480: 4355
- [Commerçon et al 2011] Commerçon, B. et al. (2011) "Radiation hydrodynamics with adaptive mesh refinement and application to prestellar core collapse". *A&A*. 529: A35
- [Crida et al. 2006] Crida, A., Morbidelli, A. & Masset, F. (2006) "On the width and shape of gaps in protoplanetary disks". *Icarus*. 181: 587
- [Cruikshank 2004] Cruikshank, Dale P. (2004) "Triton, Pluto, Centaurs, and Trans-Neptunian Bodies" *Space Science Reviews*. 116: 421
- [D'Allesio et al. 1997] D'Allesio, P., Calvet, N. & Hartmann, L. (1997) "The Structure and Emission of Accretion Disks Irradiated by Infalling Envelopes". *ApJ*. 474: 397
- [D'Allesio et al. 2001] D'Allesio, P., Calvet, N. & Hartmann, L. (2001) "Accretion Disks around Young Objects. III. Grain Growth". *ApJ*: 553: 321
- [Delitsky & Lane 1998] Delitsky, M. L. & Lane, A. L. (1998) "Ice chemistry of Galilean satellites". *J. Geophys. Res.* 103: 31, 391-31, 403
- [de Val-Borro et al 2006] de Val-Borro, M. et al. (2006) "A comparative study of disc-planet interaction". *MNRAS*. 370: 529
- [Dones, Agnor & Asphaug 2007] Dones L., Agnor C. B. & Asphaug E. (2007) "Formation of Saturn's rings by tidal disruption of a Centaur". *BAAS* 38: 420
- [Draine 2010] Draine B. T. (2010) "Physics of the Interstellar and Intergalactic Medium". Princeton University Press

- [Drazkowska, Alibert & Moore 2016] Drazkowska, J., Alibert, Y. & Moore, B. (2016) "Close-in planetesimal formation by pile-up of drifting pebbles". *A&A*. 594: A105
- [Durisen et al. 2006] Durisen, R. et al. (2006). "Gravitational Instabilities in Gaseous Protoplanetary Disks and Implications for Giant Planet Formation". Chapter in "Protostars and Planets V" published by University of Arizona Press.
- [Esposito, O'Callaghan & West 1983] Esposito L.W., O'Callaghan M. & West R.A. (1983) "The structure of Saturn's rings - Implications from the Voyager stellar occultation". *Icarus*. 56: 439
- [Faure & Mensing 2007] Faure, G. & Mensing, T. (2007) "Uranus: What Happened Here?" Introduction to Planetary Science. Springer Netherlands. pp. 369–384
- [Fedele et al. 2010] Fedele, D. et al. (2010) "Timescale of mass accretion in pre-main-sequence stars". *A&A*. 510: 72
- [Federrath et al. 2014] Federrath, C. et al. (2014) "Modeling Jet and Outflow Feedback during Star Cluster Formation". *ApJ*. 790: 128
- [Figueredo & Greeley 2004] Figueredo, P. H. & Greeley, R. (2004) "Resurfacing history of Europa from pole-to-pole geological mapping". *Icarus*. 167: 287
- [Fletcher et al. 2009] Fletcher, L. N. et al. (2009) "Methane and its isotopologues on Saturn from Cassini/CIRS observations". *Icarus* 199: 351
- [Fortes 2000] Fortes, A. D. (2000). "Exobiological implications of a possible ammonia-water ocean inside Titan". *Icarus*. 146: 444
- [French et al. 2019] French, R. G. et al. (2019) "Kronoseismology III: Waves in Saturn's inner C ring". *Icarus* 319: 599
- [Fuller 2014] Fuller, J. (2014) "Saturn ring seismology: Evidence for stable stratification in the deep interior of Saturn". *Icarus* 242: 283
- [Galilei 1610] Galilei, Galileo; Sidereus Nuncius, Thomam Baglionum (Tommaso Baglioni), Venice (March 1610), pp. 17-28 (q.v.)
- [Geissler et al. 1998] Geissler, P.E. et al. (1998) "Evolution of Lineaments on Europa: Clues from Galileo Multispectral Imaging Observations". *Icarus*. 135, 107
- [Greenberg et al. 1978] Greenberg, R. et al. (1978) "Planetesimals to planets - Numerical simulation of collisional evolution". *Icarus*. 35: 1
- [Greenberg et al. 1991] Greenberg, R. et al. (1991) "Planetary accretion rates: Analytical derivation". *Icarus*. 94: 98
- [Greenberg 2005] Greenberg, R. (2005) "Europa: The Ocean Moon: Search for an Alien Biosphere". Springer Praxis Books. Springer + Praxis. pp. 7 ff
- [Goldreich & Ward 1973] Goldreich, P., & Ward, W. R. (1973) "The Formation of Planetesimals". *ApJ*. 183: 1051
- [Goldreich & Ward 1979] Goldreich, P. & Tremaine, S. (1979) "The excitation of density waves at the Lindblad and corotation resonances by an external potential". *ApJ*. 233: 857
- [Guillot et al. 2004] Guillot, T. et al. (2004) "Chapter 3: The Interior of Jupiter". In Bagenal, F. et al. "Jupiter: The Planet, Satellites and Magnetosphere". Cambridge University Press
- [Guillot 2019] Guillot, T. (2019). "Signs that Jupiter was mixed by a giant impact". *Nature*. 572: 315
- [Herbert et al 1987] Herbert, F. et al (1987). "The Upper Atmosphere of Uranus: EUV Occultations Observed by Voyager 2" *Journal of Geophysical Research*. 92: 15, 093–15, 109

- [Hurford, Sarid & Greenberg 2007] Hurford, T.A., Sarid, A.R. & Greenberg, R. (2007) "Cycloidal cracks on Europa: Improved modeling and non-synchronous rotation implications". *Icarus*. 186: 218
- [Hansen 2009] Hansen, B.M.S. (2009) "Formation of the Terrestrial Planets from a Narrow Annulus". *ApJ*. 703: 1131
- [Hansen et al. 2012] Hansen, C. E. et al. (2012) "Feedback Effects on Low-mass Star Formation". *ApJ* 747: 22
- [Hauck, Aurnou & Dombard 2006] Hauck, S. A., Aurnou, J. M. & Dombard, A. J. (2006) "Sulfur's impact on core evolution and magnetic field generation on Ganymede". *J. Geophys. Res.* 111: E09008.
- [Hedman, Nicholson & French 2019] Hedman, M. M., Nicholson, P. D. & French, R. G. (2019) "Kronoseismology IV: Six Previously Unidentified Waves in Saturn's Middle C Ring". *ApJ*. 157: 18
- [Herschel 1787] Herschel, W. (1787) "Account of a Comet. By Mr. Herschel, F. R. S.; communicated by Dr. Watson, Jun. of Bath, F. R. S.". *Philosophical Transactions of the Royal Society of London*. 71: 492
- [Hubbard 1997] Hubbard, W.B. (1997) "Neptune's Deep Chemistry". *Science*. 275: 1279
- [Hubickyj, Bodenheimer & Lissauer 2005] Hubickyj, O., Bodenheimer, P. & Lissauer, J. J. (2005) "Accretion of the gaseous envelope of Jupiter around a 5-10 Earth-mass core". *Icarus*. 179: 415
- [IAU 2006] International Astronomical Union, General Assembly 2006. Resolution 5A: "Definition of 'planet'". <https://www.iau.org/static/archives/releases/doc/iau0603.doc>
- [Ida & Guillot 2016] Ida, S. & Guillot, T. (2016) "Formation of dust-rich planetesimals from sublimated pebbles inside of the snow line". *A&A*. 596: L3
- [Ida & Lin 2010] Ida, S. & Lin, D. N. C. (2010) "Toward a Deterministic Model of Planetary Formation. VI. Dynamical Interaction and Coagulation of Multiple Rocky Embryos and Super-Earth Systems around Solar-type Stars". *ApJ*. 719: 810
- [Iess et al 2012] Iess, L. et al. (2012) "The Tides of Titan". *Science*. 337: 457
- [Iess et al 2014] Iess, L. et al. (2014) "The Gravity Field and Interior Structure of Enceladus". *Science*. 344: 78
- [Jetley et al. 2008] Jetley, P. et al. (2008) "Massively parallel cosmological simulations with ChaNGa". *Proc. IEEE Int. Parallel and Distributed Processing Symp.* p. 1
- [Jia et al. 2018] Jia, X. et al. (2018) "Evidence of a plume on Europa from Galileo magnetic and plasma wave signatures". *Nature Astronomy*. 2: 459
- [Johansen et al. 2007] Johansen, A. et al. (2007) "Rapid planetesimal formation in turbulent circumstellar disks". *Nature*. 448: 1022
- [Johansen et al. 2015] Johansen, A. et al. (2015) "Growth of asteroids, planetary embryos, and Kuiper belt objects by chondrule accretion". *Science Advances*. 1: 1500109
- [JPL 1996] "Europa, a Continuing Story of Discovery". Project Galileo. NASA, Jet Propulsion Laboratory. Archived in 1997 under <https://web.archive.org/web/19970105180851/http://www.jpl.nasa.gov/galileo/europa/>
- [JPL 2001] "Europa: Another Water World?". Project Galileo: Moons and Rings of Jupiter. NASA, Jet Propulsion Laboratory. 2001. Archived in 2011 under <https://web.archive.org/web/20110721210346/http://teachspacescience.org/cgi-bin/search.plex?catid=10000304&mode=full>

- [Kargel et al 2000] Kargel, J. S. et al. (2000) "Europa's Crust and Ocean: Origin, Composition, and the Prospects for Life". *Icarus*. 148: 226
- [Kerr 2010] Kerr, R. A. (2010) "Magnetics Point to Magma 'Ocean' at Io". *Science*. 327: 408
- [Kivelson et al. 2000] Kivelson, M. G. et al. (2000) "Galileo Magnetometer Measurements: A Stronger Case for a Subsurface Ocean at Europa". *Science*. 289: 1340
- [Kivelson et al. 2002] Kivelson, M.G. et al. (2002) "The Permanent and Inductive Magnetic Moments of Ganymede" *Icarus*. 157: 507
- [Kokubo & Ida 1998] Kokubo, E. & Ida, S. (1998) "Oligarchic Growth of Protoplanets". *Icarus*. 131: 171
- [Kokubo & Ida 2000] Kokubo, E. & Ida, S. (2000) "Formation of Protoplanets from Planetesimals in the Solar Nebula". *Icarus*. 143: 15
- [Kruijssen 2012] Kruijssen, J. M. D. (2012) "On the fraction of star formation occurring in bound stellar clusters". *MNRAS*. 426: 3008
- [Kruijssen et al. 2019] Kruijssen, J. M. D. et al. (2019) "Fast and inefficient star formation due to short-lived molecular clouds and rapid feedback". *Nature*. 569: 519
- [Krumholz, Mckee & Bland 2019] Krumholz, M. R., McKee, C. F. & Bland, H. J. (2019) "Star Clusters Across Cosmic Time". *ARA&A*. 57: 227
- [Kuiper 1951] Kuiper, G. P. (1951) "On the Origin of the Solar System". *Proc. Natl. Acad. Sci*. 37: 1
- [Kuskov, Kronrod & Zhidikova 2005] Kuskov, O.L., Kronrod, V.A. & Zhidikova, A.P. (2005) "Internal Structure of Icy Satellites of Jupiter" *Geophysical Research Abstracts*. 7: 1892
- [Kuskov & Kronrod 2005] Kuskov, O.L. & Kronrod, V.A. (2005) "Internal structure of Europa and Callisto". *Icarus*. 177: 550
- [Lada & Lada 2003] Lada, C. J. and Lada, E.A. (2003) "Embedded Clusters in Molecular Clouds". *ARA&A*. 41: 57
- [Lambrechts & Johansen 2012] Lambrechts, M. & Johansen, A. (2012) "Rapid growth of gas-giant cores by pebble accretion". *A&A*. 544: A32.
- [Lambrechts & Johansen 2014] Lambrechts, M. & Johansen, A. (2014) "Forming the cores of giant planets from the radial pebble flux in protoplanetary discs". *A&A*. 572: A107.
- [Liu et al. 2019] Liu, S. F. et al. (2019) "The formation of Jupiter's diluted core by a giant impact". *Nature*. 572: 355
- [Longmore et al. 2014] Longmore, S. N. et al. (2014) "The Formation and Early Evolution of Young Massive Clusters". *Protostars and Planets VI*. University of Arizona Press. 291-314
- [Lopes et al. 2004] Lopes, R. M. C. et al. (2004) "Lava lakes on Io: Observations of Io's volcanic activity from Galileo NIMS during the 2001 fly-by". *Icarus*. 169: 140
- [Lorentz et al 2008] Lorentz, R. D. et al. (2008) "Titan's Rotation Reveals an Internal Ocean and Changing Zonal Winds". *Science*. 319: 1649
- [Malik et al. 2015] Malik, M. et al. (2015) "On the gap-opening criterion of migrating planets in protoplanetary disks" *ApJ*. 802: 56
- [Mankovich et al. 2019] Mankovich, C. et al. (2019) "Cassini Ring Seismology as a Probe of Saturn's Interior. I. Rigid Rotation". *ApJ* 871: 1
- [Mankovich & Fuller 2021] Mankovich, C.R. & Fuller, J. (2021) "A diffuse core in Saturn revealed by ring seismology". *Nature Astronomy*

- [McKinnon & Kirk 2014] McKinnon, W. B. & Kirk, R. L. (2014) "Triton". Encyclopedia of the Solar System (3rd ed.). Amsterdam; Boston: Elsevier. pp. 861–882
- [Menon et al. 2015] Menon, H. et al. (2015) "Adaptive techniques for clustered N-body cosmological simulations". *Comput. Astrophys. Cosmol.* 2: 1
- [Miguel & Ida 2015] Miguel, Y. & Ida, S. (2015) "A semi-analytical model for exploring Galilean satellites formation from a massive disk". *Icarus*: 266: 1
- [Millholland & Batygin 2019] Millholland, S. & Batygin, K. (2019) "Excitation of Planetary Obliquities through Planet–Disk Interactions". *ApJ* 876: 119
- [Miville-Deschênes, Murray & Lee 2017] Miville-Deschênes, M. A., Murray, N. & Lee E. J. (2017) "Physical Properties of Molecular Clouds for the Entire Milky Way Disk". *ApJ*. 834: 57
- [Mizuno 1980] Mizuno, H. (1980) "Formation of the Giant Planets". *Progress of Theoretical Physics*. 64: 544
- [Mueller et al. 2018] Mueller, S., Helled, R. & Mayer, L. (2018) "On the Diversity in Mass and Orbital Radius of Giant Planets Formed via Disk Instability". *ApJ*. 854: 112
- [Monteux et al. 2014] Monteux, J. et al. (2014) "Can large icy moons accrete undifferentiated?" *Icarus*. 237: 377
- [Movshovitz et al 2010] Movshovitz, N. et al. (2010) "Formation of Jupiter using opacities based on detailed grain physics". *Icarus*. 209: 616
- [Nelson et al. 1998] Nelson, A. F. et al. (1998) "Dynamics of Circumstellar Disks" *ApJ*. 502: 342
- [Nicholson et al. 2008] Nicholson, P.D. et al. (2008) "A close look at Saturn's rings with Cassini VIMS". *Icarus*. 193: 182
- [Null et al. 1981] Null G.W. et al. (1981) "Saturn gravity results obtained from Pioneer 11 tracking data and earth-based Saturn satellite data". *ApJ*. 86: 456
- [Offner & Chaban 2017] Offner, S. S. R. & Chaban, J. (2017) "Impact of Protostellar Outflows on Turbulence and Star Formation Efficiency in Magnetized Dense Cores". *ApJ*. 847: 104
- [Okuzumi et al. 2012] Okuzumi, S. et al. (2012) "Rapid Coagulation of Porous Dust Aggregates outside the Snow Line: A Pathway to Successful Icy Planetesimal Formation". *ApJ*. 752: 106
- [Ormel et al 2009] Ormel, C. W. et al. (2009) "Dust coagulation and fragmentation in molecular clouds I". *A&A*. 502: 845
- [Ormel & Klahr 2010] Ormel, C.W. & Klahr, H.H. (2010) "The effect of gas drag on the growth of protoplanets. Analytical expressions for the accretion of small bodies in laminar disks". *A&A* 520: A43
- [Ormel et al 2011] Ormel, C. W. et al. (2011) "Dust coagulation and fragmentation in molecular clouds II". *A&A*. 532: A43
- [Ormel, Vazan & Brouwers 2021] Ormel, C., Vazan, A. & Brouwers, M. (2021) "How planets grow by pebble accretion. III. Emergence of an interior composition gradient". *A&A* 647: A175
- [Paardekooper et al. 2010] Paardekooper, S.-j. et al. (2010) "A torque formula for non-isothermal type I planetary migration – I. Unsaturated horseshoe drag". *MNRAS*. 401: 1950
- [Paardekooper et al. 2011] Paardekooper, S.-j. et al. (2011) "A torque formula for non-isothermal Type I planetary migration – II. Effects of diffusion". *MNRAS*. 410: 293
- [Papaloizou & Lin, 1984] Papaloizou, J. & Lin, D. N. C. (1984) "On the tidal interaction between protoplanets and the primordial solar nebula. I - Linear calculation of the role of angular momentum exchange". *ApJ*. 285: 2

- [Peale, Cassenand & Reynolds 1979] Peale, S. J., Cassenand, P. & Reynolds, R. T. (1979) "Melting of Io by Tidal Dissipation". *Science*. 203: 892
- [Pedregosa et al. 2011] Pedregosa, F. et al. (2011) "Scikit-learn: Machine Learning in Python". *Journal of Machine Learning Research*. 12: 2825
- [Perry et al. 2016] Perry, M. E. et al. (2016) "Direct Measurement of the Velocity of the Enceladus Vapor Plumes". 47th Lunar and Planetary Science Conference. The Woodlands, Texas. p. 2846
- [Piazzi 1846] Piazzi, G. (1846) "Account of the Discovery of the Planet of Le Verrier at Berlin". *MNRAS*. 7: 153
- [Picogna et al. 2019] Picogna, G. et al. (2019) "The dispersal of protoplanetary discs I: A new generation of X-ray photoevaporation models". *MNRAS*. 487: 1
- [Pollack et al 1976] Pollack, J. B. et al. (1976) "The formation of Saturn's satellites and rings as influenced by Saturn's contraction history". *Icarus* 29: 35
- [Pollack et al 1996] Pollack, J. B. et al. (1996) "Formation of the Giant Planets by Concurrent Accretion of Solids and Gas". *Icarus*. 124: 62
- [Porco et al. 2006] Porco, C. C. et al. (2006) "Cassini Observes the Active South Pole of Enceladus" *Science*. 311: 1393
- [Rothery 1999] Rothery, D. A. (1999) "Satellites of the Outer Planets: Worlds in their own right". Oxford University Press.
- [Sachs 1974] Sachs, Abraham J. (1974). "Babylonian Observational Astronomy". *Philosophical Transactions of the Royal Society of London*. Royal Society of London. 276 (1257): 43-50 [45 & 48-9].
- [Salmeron et al. 2011] Salmeron R. et al. (2011) "Wind-driving protostellar accretion discs – II. Numerical method and illustrative solutions". *MNRAS*. 412: 1162
- [Saumon & Guillot 2004] Saumon, D. & Guillot, T. (2004) "Shock Compression of Deuterium and the Interiors of Jupiter and Saturn". *ApJ* 609: 1170
- [Saur et al 2015] Saur, J. et al. (2015) "The Search for a Subsurface Ocean in Ganymede with Hubble Space Telescope Observations of its Auroral Ovals". *Journal of Geophysical Research: Space Physics*. 120: 1715
- [Saxton 2016] Saxton, B. (2016) "Process of star formation". Published on the ESO Supernova website under: https://supernova.eso.org/exhibition/images/0408_F_Clump-core_med-CCfinal/
- [Schäfer, Yang & Johansen 2017] Schäfer, U., Yang, C.-C. & Johansen, A. (2017) "Initial mass function of planetesimals formed by the streaming instability". *A&A*. 597: A69
- [Schoonenberg & Ormel 2017] Schoonenberg, D. & Ormel, C.W. (2017) "Planetesimal formation near the snowline: in or out?". *A&A*. 602: A21
- [Shakura & Sunyaev 1973] Shakura, N. I. & Sunyaev, R. A. (1973) "Black holes in binary systems. Observational appearance". *A&A*. 24: 337
- [Sheppard 2018] Sheppard, S. S. (2018). "A Dozen New Moons of Jupiter Discovered, Including One "Oddball"". Carnegie Institution for Science.
- [Sheppard 2019] Sheppard, S. S. (2019) "New Saturn Moons". Published on Carnegie Science website: <https://carnegiescience.edu/news/saturn-surpasses-jupiter-after-discovery-20-new-moons-and-you-can-help-name-them>
- [Showman & Malhotra 1999] Showman, A. P. & Malhotra, R. (1999) "The Galilean Satellites". *Science*. 286: 77

- [Shu et al. 2007] Shu F. H. et al. (2007) "Mean Field Magnetohydrodynamics of Accretion Disks". *ApJ*. 665: 535
- [Simon & Armitage 2014] Simon, J. B. & Armitage, P. J. (2014) "Efficiency of Particle Trapping in the Outer Regions of Protoplanetary Disks". *ApJ*, 784: 15
- [Simon et al 2016] Simon, J.B. et al. (2016) "The Mass and Size Distribution of Planetesimals Formed by the Streaming Instability. I. The Role of Self-gravity". *ApJ*. 822: 55
- [Smith et al 1979] Smith, B. A., et al. (1979) "The Jupiter system through the eyes of Voyager 1". *Science*. 204: 951
- [Smoluchowski 1971] Smoluchowski, R. (1971) "Metallic interiors and magnetic fields of Jupiter and Saturn". *ApJ*. 166: 435
- [Spohn & Schubert 2003] Spohn, T. & Schubert, G. (2003) "Oceans in the icy Galilean satellites of Jupiter?" *Icarus*. 161: 456
- [Stofan et al 2007] Stofan, E. R. et al. (2007) "The lakes of Titan". *Nature*. 445: 61
- [Strom et al 1979] Strom, R. G.; et al. (1979) "Volcanic eruption plumes on Io". *Nature*. 280, 733
- [Suzuki et al. 2010] Suzuki T. K. et al. (2010) "Protoplanetary disk winds via magnetorotational instability: formation of an inner hole and a crucial assist for planet formation". *ApJ*. 718: 1289
- [Syer & Clarke 1995] Syer, D. & Clarke, C. J. (1995) "Satellites in discs: regulating the accretion luminosity". *MNRAS*. 277: 758
- [Szulágyi et al. 2014] Szulágyi, J. et al. (2014) "Accretion of Jupiter-mass planets in the limit of vanishing viscosity". *ApJ*. 782: 65
- [Szulágyi et al. 2015] Szulágyi, J., 2015, PhD thesis, Univ. Nice Sophia, Antipolis
- [Szulágyi et al. 2016a] Szulágyi, J., Mayer, L. & Quinn, T. (2016a). "Circumplanetary disks around young giant planets: a comparison between core-accretion and disk instability". *MNRAS*. 464: 3158
- [Szulágyi et al. 2016b] Szulágyi, J. et al. (2016b) "Circumplanetary disc or circumplanetary envelope?". *MNRAS*. 460: 2853
- [Szulágyi, Binkert & Surville 2021] Szulágyi, J., Binkert, F. & Surville, C. (2021) "Meridional Circulation of Dust and Gas in the Circumstellar Disk: Delivery of Solids onto the Circumplanetary Region". arxiv e-print:2103.12128
- [Tanaka et al. 2002] Tanaka, H., Takeuchi, T., & Ward, W. R. (2002) *ApJ*. 565: 1257
- [Tanaka, Tan & Zhang 2017] Tanaka, K. E. I., Tan, J. C. & Zhang, Y. (2017) "The Impact of Feedback During Massive Star Formation by Core Accretion". *ApJ*. 835: 32
- [Teachey & Kipping 2021] Teachey, A. & Kipping, D. (2021) "Identifying Potential Exomoon Signals with Convolutional Neural Networks" pre-print arXiv:2109.10503
- [Thomas et al 2016] Thomas, P. C. et al. (2016) "Enceladus's measured physical libration requires a global subsurface ocean". *Icarus*. 264: 37
- [Thompson 2017] Thompson, J. R. (2017) "Hydrothermal Activity". Cassini Solstice Mission Team. JPL/NASA. Published on the Nasa website under: <https://solarsystem.nasa.gov/missions/cassini/science/enceladus/>
- [Throop & Bally 2005] Throop, H. B., & Bally, J. (2005) "Can Photoevaporation Trigger Planetesimal Formation?". *ApJ*. 623: L149

- [Tobie et al. 2005] Tobie, G. et al. (2005) "Titan's internal structure inferred from a coupled thermal-orbital model". *Icarus*. 175: 496
- [Tombaugh 1946] Tombaugh, C. W. (1946) "The Search for the Ninth Planet, Pluto". *Astronomical Society of the Pacific Leaflets*. 5: 73
- [Vance et al 2014] Vance, S. et al. (2014) "Ganymede's internal structure including thermodynamics of magnesium sulfate oceans in contact with ice". *Planetary and Space Science*. 96: 62
- [Vanderburg et al. 2018] Vanderburg, A., Rappaport, S. & Mayo, A. W. (2018). "Detecting Exomoons Via Doppler Monitoring of Directly Imaged Exoplanets." *ApJ*. 156: 184
- [Van der Maaten & Hinton 2008] van der Maaten L. & Hinton G. (2008) "Visualizing Data using t-SNE". *Journal of Machine Learning Research*. 9: 2579
- [Van der Maaten 2014] van der Maaten L. (2014) "Accelerating t-SNE using Tree-Based Algorithms". *Journal of Machine Learning Research*. 15: 3221
- [Walsh et al. 2011] Walsh, K.J. et al. (2011) "A low mass for Mars from Jupiter's early gas-driven migration". *Nature*. 475: 206
- [Ward, Kruijssen & Rix 2020] Ward, J. L., Kruijssen J. M. D. & Rix, H. W. (2020) "Not all stars form in clusters - Gaia-DR2 uncovers the origin of OB associations". *MNRAS*. 49: 663
- [Weidenschilling 1980] Weidenschilling, S.J. (1980) "Dust to planetesimals - Settling and coagulation in the solar nebula". *Icarus*. 44: 172
- [Wetherill & Stewart 1989] Wetherill, G.W. & Stewart, G.R. (1989) "Accumulation of a swarm of small planetesimals". *Icarus*. 77: 330
- [Williams 1995] Williams, D.R (1995) "Jovian Satellite Fact Sheet". Published on the Nasa website under: <https://nssdc.gsfc.nasa.gov/planetary/factsheet/joviansatfact.html> (last updated in 2018)
- [Williams 1995] Williams, D.R. (1995) "Saturn Fact Sheet". Published on the Nasa website under: <https://nssdc.gsfc.nasa.gov/planetary/factsheet/saturnfact.html>
- [Windmark et al. 2012] Windmark, F. et al. (2012) "Planetesimal formation by sweep-up: how the bouncing barrier can be beneficial to growth". *A&A*. 540: A73
- [Wolszczan 1992] Wolszczan, A. & Frail, D. A. (1992). "A planetary system around the millisecond pulsar PSR1257 + 12". *Nature*. 355: 145
- [Woo et al. 2021] Woo, J. M. Y. et al "Did Uranus' regular moons form via a rocky giant impactor?". arxiv pre-print: 2105.13663
- [Yang, Johansen & Carrera 2016] Yang, C.C., Johansen, A. & Carrera, D. (2016) "Concentrating small particles in protoplanetary disks through the streaming instability". *A&A*. 606: A80
- [Yoder 1979] Yoder, C. (1979) "How tidal heating in Io drives the galilean orbital resonance locks". *Nature*. 279: 767
- [Youdin & Goodman 2005] Youdin, A.N. & Goodman, J. (2005) "Streaming Instabilities in Protoplanetary Disks". *ApJ*. 620: 459
- [Zahnle, Dones & Levison 1998] Zahnle, K., Dones, L. & Levison, H. F. (1998) "Cratering Rates on the Galilean Satellites" *Icarus*. 136: 202
- [Zebker et al 1985] Zebker, H.A. et al. (1985) "Saturn's rings - Particle size distributions for thin layer model". *Icarus*. 64: 531

[Zimmer, Khurana & Kivelson 2000] Zimmer, C., Khurana, K. K. & Kivelson, M. G. (2000)
"Subsurface Oceans on Europa and Callisto: Constraints from Galileo Magnetometer Observations" *Icarus*. 147: 329